

**MCAT Institute  
Progress Report  
95-04**

---

## **TURBULENCE MODELING**

---

**Jorge E. Bardina**

---



**February 1995**

**NCC2-585**

**MCAT Institute  
3933 Blue Gum Drive  
San Jose, CA 95127**

(NASA-CR-197751) TURBULENCE  
MODELING Final Annual Report (MCAT  
Inst.) 74 p

N95-26665

Unclass

G3/34 0048499



**ORIGINAL . CONTAINS  
COLOR ILLUSTRATIONS**

NCC 2 - 585 - 95-04  
ANNUAL REPORT

	Page
Technical Proposal	1
Work Statement	3
Work Accomplished	4
Acknowledgments	10
Appendix	11



**NCC 2-585**  
**ANNUAL REPORT**

**Technical Proposal**

The objective of this work is to develop, verify and incorporate the baseline two-equation turbulence models which account for the effects of compressibility into the three-dimensional Reynolds averaged Navier-Stokes (**RANS**) code and to provide documented descriptions of the models and their numerical procedures so that they can be implemented into 3-D CFD codes for engineering applications.

Computational Fluid Dynamics (**CFD**) is recognized as a significant engineering design tool in modern engineering projects. The design of airplanes and aerospace vehicles is a highly complex process. One of the critical tasks involved in such a process is the ability of the turbulence model to predict boundary layer separation, shock-wave/turbulent boundary layer interactions, viscous/inviscid interactions, transition, adverse pressure gradient flows, rotation and streamline curvature effects, mixing problems, and a range of other turbulence phenomena.

Turbulence models are developed on the basis of insight gained from experimental and theoretical research. The complexity of turbulence requires that the mathematical models be guided by the flow physics in a rational and practical approach. Test and validation of new models with data of recognized quality is an essential step toward model acceptability. A database with a detailed experimental information on turbulent flows is necessary as a benchmark for testing and validation of model modifications. The simulations of complex turbulent flows with the new

turbulence models complement and assist the design of the data base for turbulence modeling validation.

A major consideration throughout the research effort is the development of improved corrections to the turbulence models and the identification of models which are superior in their predictive capabilities.

### Work Statement

The work statement for this period is:

1. Prepare material and documentation for AIAA paper 94-1905 to be presented in the 1994 Applied Aerodynamics conference. to be held June 20-23 in Colorado Springs, Colorado.
2. Supervise and deliver information needed to implement compressible two-equation turbulence models into 3-D codes. Prepare material and documentation for AIAA paper 94-2950 to be presented in the 30th AIAA/ASME/SAE/ASEE Joint Propulsion Conference to be held June 27-29 in Indianapolis, Indiana.
3. Study and continue analysis of 3-D turbulence model corrections with numerical simulations of 3-D intersecting shock-waves/ turbulent boundary layer interaction (SWBLI) flows at Mach 8.3 and 4.
4. Prepare material and documentation of the numerical simulations of the 3-D Reynolds Averaged Navier-Stokes equations of the 3-D Intersecting Shock Wave - Turbulent Boundary layer Interactions (ISWBLI) at Mach 8.3 and 4.

## Work Accomplished

The work accomplished is presented with a general description of the present general capabilities and the achievements in this performance period. These achievements are published in AIAA papers whose general descriptions are shown below.

### 1. Present General Capabilities.

The RANS 3-D Reynolds Averaged Navier-Stokes code has presently the capability to predict turbulent flows with the following models:

- Wilcox  $k - \omega$  model (baseline model)
- Menter BSL  $k - \omega / k - \epsilon$  model
- Menter SST  $k - \omega / k - \epsilon$  model
- Jones-Launder  $k - \epsilon$  model
- Launder-Sharma  $k - \epsilon$  model (baseline model)
- Chien  $k - \epsilon$  model
- Baldwin-Lomax algebraic mixing-length model

Four important model modifications are optional in the baseline models:

- A length scale modification in order to decrease the heat transfer rate in flow reattachment zones (all models).
- A rapid compression modification to increase the size of the flow separation zone in high speed flows (all models).
- A rotation or vortex stretching length scale modification to decrease the level of turbulent dissipation in flow recirculating zones (all models).
- A turbulence transition modification to simulate flow transition and complex surfaces with both laminar and turbulent compress-

ible flow zones ( $k - \omega$  model).

The validation of the different models and modifications have been accomplish with comparisons against theoretical correlations, other numerical codes, and different experimental data. Flows included in the validation are:

- Mach 14 laminar boundary layer on a  $24^\circ$  compression ramp (code validation).
- Mach 5 flat plate turbulent boundary layer (turbulence modeling validation).
- Mach 3 separated turbulent boundary layer on a  $24^\circ$  compression ramp (turbulent flow separation validation).
- Mach 8 shock wave / turbulent boundary layer interaction generated with a  $15^\circ$  and a  $10^\circ$  fin mounted on a cooled flat plate with  $T_{wall}/T_\infty = 0.3$  and  $Re_\infty = 5 \cdot 10^6$  (complex 3-D SWBLI with crossflow separation).
- Mach 8 and 4 intersecting shock waves / turbulent boundary layer interaction generated with two  $15^\circ$  fins mounted on a flat plate (complex 3-D SWBLI with completely crossflow separation).

## 2. AIAA 94-1905 Paper (see appendix).

“Three-Dimensional Navier-Stokes Simulations with Two-Equation Turbulence Models of Intersecting Shock-Waves/ Turbulent Boundary layer at Mach 8.3,” has been written and presented in the 12th AIAA Applied Aerodynamics Conference held in June 20-23, 1994, at Colorado Springs, Colorado. This paper is co-authored with Dr. T.J. Coakley.

This publication shows the validation and comparison of the baseline  $k-\omega$  two-equation model with and without different combinations of model corrections, the SST two-equation model, and the Baldwin-Lomax algebraic mixing-length model. It demonstrate the ability to predict accurately surface pressure, heat transfer rates, flow yaw angles and Pitot pressures. The model corrections give improved heat transfer predictions in the reattachment zones. A very important result is the influence of the fin boundary layer on the flat plate distributions. The flow structures are well capture and superior results.

3. AIAA 94-2950 Paper (see appendix).

“Three-Dimensional Navier-Stokes Method with Two-Equation Turbulence Models for Efficient Numerical Simulation of Hypersonic Flows,” has been written and presented in the 30th AIAA/ ASME/ SAE/ ASEE Joint Propulsion Conference and Exhibit held in June 27-29, 1994, at Indianapolis, Indiana.

This publication shows the 3-D method used to predict the turbulent flows, and the necessary information to implement the two-equation turbulence models into 3-D CFD codes. The method is very efficient and allows the simulation of different turbulence models in complex 3-D flows in less computational time than other well-known methods. This research has shown that the presence of oblique shock waves introduce errors in the upwind methods that propagate downstream and have a significant effects in the performance of the model equations. A limiter has been designed and tested to avoid this numerical error. The use of implicit and coupled treatment of the model equations provide a fast convergence in complex flows, including separa-

tion and reattachment of boundary layers. This paper provides the basic documentation and delivers the information on their numerical procedures needed to implement the baseline turbulence models into 3-D CFD codes.

4. NASA TM 108827 (see appendix).

The final report of the GWP-18 in the Modeling and Experimental Validation Branch was written together with Tom Coakley. This report has been published as NASA TM 108827, "Turbulence Compressibility Corrections," and includes the database, recommended models, and model equations for hypersonic flows.

5. AIAA 95-2215 Paper (to be published).

"The Structure of Intersecting Shock-Waves/ Turbulent Boundary layer Flow," will be presented in the 26th AIAA Fluid Dynamics Conference, to be held June 19-22, 1995, in San Diego, California. This paper is co-authored with Dr. T.J. Coakley.

This paper study the interactions of the shock-waves and the turbulence structures and the effects of the turbulence models at Mach 8 in high resolution numerical simulations with over 1.5 million grid-points. This structures are currently not well understood, and their modeling requires a higher-level knowledge of their physics. This simulations provides the best description of this flow and a very valuable database. Researchers in this area have already expressed their interest in this data set. The implicit boundary approximations of the models have been tested and improved. The length-scale model correction show improvements in the prediction of peak surface pressure and heat transfer rate. The rapid-compression model

correction show increased secondary separation under the main vortical structures. These simulations study the effects and capabilities of different two-equation turbulence models in their predictions of complex turbulence.

6. AIAA 95 Paper (to be published).

The study of the validation of the different turbulence models with the intersecting shock-waves/turbulent boundary layer interaction flow at Mach 4 will be presented in an AIAA meeting to be held later this year. The organization of this meeting begun in 1994, the session chairman is J. Marvin and the final information will be soon available. This experimental database of the Garrison and Settles experiment provides surface pressure and skin friction distributions, and flowfield Pitot pressure. The numerical simulations have been carried out with a  $91 \times 61 \times 61$  3-D grid and the baseline two-equation turbulence model with and without corrections. The few other simulations available have consistently shown poor agreement with the experimental data in the skin friction coefficient (and heat transfer rate). The models also show significant differences in the flow streamline patterns. This meeting provides the mean to effective validation of models and methods in a complex turbulent flow.

7. As part of a collaborative effort, several tests of the shock-tunnel inlet simulation have been run. Velocity profiles, temperature profiles, skin friction and heat transfer coefficient have been compared under different Reynolds numbers, Mach numbers, ratio of specific heat-transfer coefficients, and Prandtl numbers.

## 8. NASA Peer Review

A Peer Review of Turbulence Modeling work at NASA was held in September. The review team consisted of Managers of aerospace companies and university Professors. The presentations showed the research work in progress at Ames (including CTR), Lewis, and Langley. A set of slides was prepared for this meeting with comparisons between models and experiment in 3-D shock-wave/ turbulent boundary layer interactions (flat plate/  $10^\circ$  single fin, flat plate/  $15^\circ$  single fin, and flat plate/  $15^\circ$  double fin). The results show the effects of turbulence compressibility corrections in two-equation turbulence models in the prediction of surface pressure, heat transfer, skin friction, yaw angles, and Pitot pressure measurements. This work was presented by Joseph Marvin. The review team found the research being excellent. However, they found a lack of general management of the whole NASA program. Their main recommendation was that turbulence research done at NASA is a fundamental need of the American industries, otherwise, the future technology will be lost to European or Japanese companies. Their recommendations include the appointment of a general manager of the turbulence and transition programs with authority and outstanding expertise; creation of a board with members of industry and universities to guide this program; creation of a technical board to supervise the research; and a general coordination of all these NASA Center research activities.

### Acknowledgments

The principal investigator wishes to thank Dr. T.J. Coakley for his guidance and insightful discussions throughout this work, and J.G. Marvin for his general guidance. This research was performed at NASA Ames Research Center and supported by the grant NCC 2-585.

---

# **Turbulence Compressibility Corrections**

---

T. J. Coakley, C. C. Horstman, J. G. Marvin,  
J. R. Viegas, J. E. Bardina, P. G. Huang,  
and M. I. Kussoy

---

May 1994



---

# Turbulence Compressibility Corrections

---

T. J. Coakley, C. C. Horstman, J. G. Marvin, J. R. Viegas, J. E. Bardina, P. G. Huang, and M. I. Kussoy, Ames Research Center, Moffett Field, California

May 1994



National Aeronautics and  
Space Administration

**Ames Research Center**  
Moffett Field, California 94035-1000



## Summary

The basic objective of this research was to identify, develop and recommend turbulence models which could be incorporated into CFD codes used in the design of the NASP vehicles. To accomplish this goal, a combined effort consisting of experimental and theoretical phases was undertaken. The experimental phase consisted of a literature survey to collect and assess a database of well documented experimental flows, with emphasis on high speed or hypersonic flows, which could be used to validate turbulence models. Since it was anticipated that this database would be incomplete and would need supplementing, additional experiments in the NASA Ames 3.5' hypersonic wind tunnel (HWT) were also undertaken. The theoretical phase consisted of identifying promising turbulence models through applications to simple flows, and then investigating more promising models in applications to complex flows. The complex flows were selected from the database developed in the first phase of the study. For these flows it was anticipated that model performance would not be entirely satisfactory so that model improvements or corrections would be required. The primary goals of the investigation were essentially achieved. A large database of flows was collected and assessed, a number of additional hypersonic experiments were conducted in the Ames HWT, and two turbulence models ( $k$ - $\epsilon$  and  $k$ - $\omega$  models with corrections) were determined which gave superior performances for most of the flows studied and are now recommended for NASP applications.

## Introduction

With the advent of the hypersonic airplane, hypersonic flows are receiving special attention from researchers in computational fluid dynamics. Complex flow phenomena such as shock-wave boundary layer interactions, separation and combustion are of particular interest because of their importance to the successful design of structural, propulsive and thermal protection systems. Rapid advances in CFD in recent years have resulted in its increased use as a design tool for aeronautical systems and have lead to reductions in the time and costs of wind tunnel testing. A major obstacle to the use of CFD as a design tool is its dependence on turbulence modeling for accurate prediction of complex flows. Although recent advances have been made in turbulence modeling, many more will be required before CFD can be applied with confidence to a wide range of flow problems. This is especially true at hypersonic speeds where high temperatures and pressures

create additional difficulties for turbulence modeling and where wind tunnel experiments which can be used to validate models are sparse.

The overall goal of this research is to identify, develop and recommend turbulence models which can be incorporated into the CFD codes used in the design of the NASP vehicle. To accomplish this objective, a combined and joint effort consisting of experimental and theoretical phases was undertaken. The objective of the experimental phase was to conduct a literature survey to identify and assess a database of well documented experimental flows which could be used to validate turbulence models. Since it was anticipated that this database would be incomplete, it was also decided to perform additional experiments in the NASA Ames 3.5' hypersonic wind tunnel (HWT) to supplement the database.

The objective of the theoretical phase was to identify promising turbulence models through applications to simple flows, such as flat plate flows, and to then investigate the more promising models in applications to more complex flows. The complex flows were to be selected from the database developed in the first phase of the study. For these flows it was anticipated that model performance would not be entirely satisfactory so that model improvements or corrections would be required. The flows of interest were restricted to ideal gas flows because of the sparsity of high quality experimental validation data and viable turbulence models for real gas flows.

The schedule of tasks and milestones for the completion of the research on Government Work Package 18 is shown in fig. 1. With this report the work is essentially complete with the exception of the compressible shear layer experiment in the Ames 3.5' HWT. Completion of this experiment was halted due to the lack of funds caused by funding reductions in the NASP project.

The report is organized into 7 sections. Following the introduction, two sections on the experimental phase of the study will be presented including one on the database collection and assessment and another on the experiments conducted in the Ames 3.5' HWT. Next, sections describing the theoretical phase of the study will be presented. These include sections on recommended baseline turbulence models, compressibility corrections recommended for improved predictions of complex flows and representative results of numerical predictions using the baseline and corrected models. Finally, the report con-

cludes with a summary of basic results and recommendations including topics for future study.

## Database Collection and Assessment

As stated in the introduction, the purpose of the database collection and assessment activity was to provide a base of reliable and well documented wind tunnel experiments by means of which turbulence models could be validated. These experiments, for the most part, involve relatively simple geometric shapes which may be viewed as separate elements of an overall vehicle. The results of this activity are reported by Settles and Dodson (1991, 1993a and 1993b) and will be summarized here.

Settles and Dodson (1991 and 1993b) provide a survey and assessment of experiments involving two and three dimensional shock-wave boundary-layer interaction flows. Eight hundred experiments were initially identified for further review. Of these, 112 distinct experiments were found involving flows at Mach 3 and above. The acceptance criteria applied to these included: 1) Measurements of surface pressures, skin friction and/or heat transfer, and velocity, temperature, or pitot pressure profiles at selected locations, 2) well defined experimental boundary conditions, 3) well defined error bounds, 4) adequate spatial resolution of measurements and 5) full documentation of tabulated data. For hypersonic conditions, i.e.  $M > 5$ , only 7 studies passed the acceptance criteria and only three were three dimensional. An additional 11 experiments passed the criteria at supersonic speeds.

The survey and assessment of attached boundary layer and free shear flow experiments is given by Settles and Dodson (1993a). The acceptance criteria applied to these cases was identical to that applied to the shock-wave boundary-layer interaction experiments. For the boundary layer experiments, 153 candidate cases were identified for further review. Of these 39 were subjected to the acceptance criteria. No hypersonic and only 9 supersonic cases passed. For the free shear layer experiments, 1137 candidate cases were identified for further review. Of these, 45 were subjected to the acceptance criteria and only 3 passed.

# **Experiments in the NASA Ames 3.5' Hypersonic Wind Tunnel**

The experiments were conducted in the Ames 3.5' hypersonic wind tunnel and were done with relatively simple generic shapes such as cones, cylinders, plates and wedges. These shapes were chosen to typify locations on a high speed vehicle where turbulence modeling was expected to be a critical issue. The experiments were run at nominal Mach numbers ranging from 7 to 8.3 and unit Reynolds numbers (per meter) from 4.9 to 5.8 million. Boundary-layers approaching the interaction region were relatively large, with thicknesses on the order of 2.5 to 3.7 cm, which allowed detailed flow field surveys to be easily made. In most of the experiments, both surface measurements and flow field (profile) measurements were made including initial boundary conditions required to start numerical computations. With two minor exceptions, the experiments passed the acceptance criteria described in the previous section. In addition, an analysis of measurement errors was made and documented. The results of these experiments are described in detail by Kussoy et al (1989; 1991a,b; 1992; 1993a,b,c) and Horstman and Kussoy (1989) and the data have been made available on floppy disks.

## **M = 7 Hypersonic Cylinder-Flare and Fin flows**

The test bed employed in this experiment consisted of an ogive-cylinder at zero angle of attack with a series of removable symmetric flares or sharp fins (see figs. (2a and 2b)). Both flare and fin angles were varied, producing shock waves of various strengths, and resulting in both attached and separated flow fields. Detailed measurements verified a fully developed turbulent boundary-layer on the cylinder ahead of the interaction region. The resulting flows were axisymmetric with and without separation for the flare case, and three dimensional with separation for the fin case. Surface pressures and heat transfer rates were measured on both configurations, and flow field surveys were done on the flare configuration. The results are reported in Kussoy and Horstman (1989) and Horstman and Kussoy (1989).

## **M = 8.2 2-D Wedge and 3-D Vertical Fin Flows**

A flat plate arrangement was used for this experimental series and is shown in fig.(3). It was of a hollow modular construction, enabling both test bodies and instrumen-

tation to be easily manipulated and changed. The full length of the wind tunnel test section was utilized in the design and because of this a well developed equilibrium turbulent boundary-layer was present at the shock interaction zone. Two configurations were tested; the first consisted of a sharp wedge supported over the width of the test section, the second was a sharp vertical fin attached to the plate surface. These are both illustrated in fig.(3). Both the wedge and fin angles were varied, producing shock-wave boundary-layer interactions of varying strength with a maximum wall-pressure ratio of  $p/p_\infty = 21.5$  and 6.4, respectively. This resulted in both attached and separated flow fields for the wedge flows, and swept three dimensional vortical flow fields for the fin flows. Detailed surveys verified a fully developed hypersonic turbulent boundary-layer on the flat plate ahead of the interaction zone.

For the wedge configuration, only surface conditions were measured. For the fin configuration, however, mean flow profile surveys were also taken - both in the undisturbed and interaction regions - and from them pitot pressure contours and boundary-layer thickness parameters were obtained. We believe this is the first fully three dimensional shock-wave boundary-layer interaction flow to be so documented at hypersonic speeds. Results for both configurations are reported in Kussoy et al (1991a,b;1992). Experimental and computational results for the  $10^\circ$  and  $15^\circ$  vertical fin flows are discussed in the section on Model Validation-Representative Results.

### **M = 8.3 Crossing Shock Flow**

For the third series of experiments, a configuration was chosen to reflect several key elements of a generic hypersonic inlet. These included a thick turbulent boundary-layer approaching two vertical fins of varying wedge angle, a crossing shock pattern produced by the fins, boundary-layer vortices, large pressure gradients, and separation zones. The test body for this series of experiments is shown in fig.(4).

Streamwise and transverse surface pressure and heat transfer distributions were measured as well as flow field surveys of pitot pressure and flow angle. One important result of these measurements should be mentioned here. This was the persistence of an extensive low pressure region far downstream of the fin leading edges. This low pressure region implied that the generic inlet tested here would not be a very efficient pressure diffusing device. The experimental results for this configuration are given in Kussoy et al

(1993a,b,c). experimental and computational results for the 15° fin-angle case are discussed in the section on Model Validation-Representative Results.

## **Recommended Baseline Turbulence Models**

The baseline turbulence models recommended for use in NASP applications will be described in this section. A variety of turbulence models have been investigated in varying degrees throughout the course of the study. They include 0-eq, 1-eq, and 2-eq eddy viscosity models, and Reynolds stress transport models. For NASP applications, the primary emphasis has been placed on 2-eq models and these models will be the only ones described in detail here. Descriptions of other models used in the course of the study, and results obtained with them, are given in Coakley and Huang (1992) and Coakley and Marvin (1993), Horstman (1991,1992), and Huang and Coakley (1993a,b).

The models investigated and recommended here are those that utilize no slip boundary conditions at solid walls and involve the use of wall damping functions (in most cases). This is in contrast to conventional practice with two equation models in which wall functions and essentially slip type boundary conditions are used. This choice was made because at the very high speeds of hypersonic flight, the effective Reynolds numbers of the flows can be quite low, in some cases involving transition and relaminarization. In these cases, the thickness of the laminar sublayer becomes an appreciable fraction of the overall boundary layer thickness and the wall function approach becomes inapplicable or ineffective. In addition, the wall function approach gives questionable results for separated flows. For these reasons it was decided to use the wall damping function approach.

Two equation models have been emphasized since these are viewed as the simplest and most practical models available which have sufficient generality to be applied to the complex flows of interest in NASP applications. Although numerous two equation models have been investigated, descriptions of only two of these will be given here since these are the baseline models of our final recommendation. In Coakley and Huang (1992) a detailed investigation of the performance of a variety two equation models was presented for flat plate boundary layers over a wide range of Mach and Reynolds numbers. The results of that study showed that most of the models gave reasonably good predictions of skin friction, heat transfer and velocity profiles with little clear preference of one model over the other. For this reason only two models were selected for further study, and it is

believed that these models are representative of most two equation models currently in use. The baseline models are the  $k$ - $\epsilon$  model of Jones and Launder (1972), as modified by Launder and Sharma (1973), and the  $k$ - $\omega$  model of Wilcox (1984). These models are used with the (mass weighted) Reynolds averaged compressible Navier-Stokes equations which, in cartesian tensor form, are given below.

### Reynolds Averaged Compressible Navier-Stokes Equations

$$\begin{aligned}\frac{\partial}{\partial t}(\rho) + \frac{\partial}{\partial x_j}(\rho u_j) &= 0 \\ \frac{\partial}{\partial t}(\rho u_i) + \frac{\partial}{\partial x_j}(\rho u_i u_j + \sigma_{ij}) &= 0 \\ \frac{\partial}{\partial t}(\rho E) + \frac{\partial}{\partial x_j}(\rho E u_j + u_i \sigma_{ij} + q_j) &= 0\end{aligned}$$

where;  $\rho$  is the density;  $u_i$  are the cartesian velocity components;  $E = e + 0.5 u_i u_i + k$  is the total specific energy;  $e = c_v T$  is the specific internal energy;  $k = 0.5 \overline{\rho u_i' u_i'}$  is the turbulent kinetic energy;  $T$  is the temperature;  $p = (\gamma - 1) \rho e$  is the equation of state; and  $p$  is the pressure;  $\gamma = c_p / c_v$  is the ratio of specific heats, and  $c_p$  and  $c_v$  are the specific heats at constant pressure and volume respectively. The variables  $\sigma_{ij}$  and  $q_j$  are the total stress tensor and heat flux vector, respectively, which include both molecular and (Reynolds averaged) turbulent contributions. Using the Boussinesq approximation, these variables are represented in terms of an eddy viscosity by

$$\begin{aligned}\sigma_{ij} &= \delta_{ij} \left( p + \frac{2}{3} \rho k \right) - (\mu + \mu_T) \left( \frac{\partial u_i}{\partial x_j} + \frac{\partial u_j}{\partial x_i} - \frac{2}{3} \delta_{ij} \frac{\partial u_k}{\partial x_k} \right) \\ q_j &= -\gamma \left( \frac{\mu}{\sigma} + \frac{\mu_T}{\sigma_T} \right) c_v \frac{\partial T}{\partial x_j} - \left( \mu + \frac{\mu_T}{\sigma_k} \right) \frac{\partial k}{\partial x_j}\end{aligned}$$

where  $\mu$  and  $\mu_T$  are the molecular and turbulent (eddy) viscosities  $\sigma$  and  $\sigma_T$  are molecular and turbulent Prandtl numbers with  $\sigma = c_p \mu / \kappa$  (assuming air)  $\sigma_T = 0.9$  and  $\sigma_k$  depending on the model used. The turbulent eddy viscosity is expressed in terms of the turbulent kinetic energy,  $k$ , and either the dissipation rate,  $\epsilon$ , or the specific dissipation rate  $\omega$

depending on the model. This expression is

$$\mu_T = C_\mu f_\mu \rho \sqrt{k} l = C_\mu f_\mu \rho \frac{k^2}{\varepsilon} = C_\mu f_\mu \rho \frac{k}{\omega} \quad , \quad \omega = \frac{\varepsilon}{k}$$

where  $\sqrt{k}$  is the turbulent velocity scale,  $l = \sqrt{k^3/\varepsilon} = \sqrt{k}/\omega$  is the length scale,  $C_\mu$  is a modeling constant, and  $f_\mu$  is a damping function depending on the specific model used. For applications to complex flows, the governing equations were expressed in terms of curvilinear coordinates and solved using the finite volume method, Viegas and Rubesin (1991), and Huang and Coakley (1992b) or the finite difference method, Bardina (1994).

The recommended baseline  $k$ - $\varepsilon$  and  $k$ - $\omega$  turbulence models are expressed by the formulas given below.

$$\begin{aligned} \frac{\partial}{\partial t}(\rho k) + \frac{\partial}{\partial x_j}(\rho k u_j - \mu_k \frac{\partial k}{\partial x_j}) &= (P_k (\frac{S}{\omega})^2 - \frac{2}{3} \frac{D}{\omega} - D_k) \rho \omega k \\ \frac{\partial}{\partial t}(\rho s) + \frac{\partial}{\partial x_j}(\rho s u_j - \mu_s \frac{\partial s}{\partial x_j}) &= (P_s (\frac{S}{\omega})^2 - \alpha_s \frac{D}{\omega} - D_s) \rho \omega s \\ S &= \left( \frac{\partial u_i}{\partial x_j} + \frac{\partial u_j}{\partial x_i} \right) \frac{\partial u_i}{\partial x_j} - \frac{2}{3} \left( \frac{\partial u_k}{\partial x_k} \right)^2 \quad , \quad D = \frac{\partial u_k}{\partial x_k} \end{aligned}$$

In these equations and in the following Tables, variable “s” and subscript “s” are replaced with  $\varepsilon$  for the  $k$ - $\varepsilon$  model or  $\omega$  for the  $k$ - $\omega$  model, respectively.

The model parameters are defined in Tables 1, 2 and 3

**Table 1: Model Parameters**

$C_\mu = 9/100$	$\mu_k = \mu + \mu_T / \sigma_k$	$\mu_s = \mu + \mu_T / \sigma_s$
$R_T = k^2 / \nu \varepsilon = k / \nu \omega$	$P_k = C_\mu f_\mu$	$P_s = C_{s1} P_k$
$\alpha_s = 2/3 C_{s1}$	$\nu = \mu / \rho$	$\nu_T = \mu_T / \rho$

**Table 2: Launder-Sharma  $k$ - $\epsilon$  Model,  $s \equiv \epsilon = \omega k$**

$\sigma_k = 1$	$\sigma_\epsilon = 1.3$
$C_{\epsilon 1} = 1.45$	$C_{\epsilon 2} = 1.92$
$f_\mu = \exp(-3.4/(1.0 + R_T^2/50))$	$f_2 = 1 - 0.3 \exp(-R_T^2)$
$D_k = 1 + (2\nu/\epsilon) (\partial k^{1/2}/\partial x_k)^2$	$D_\epsilon = C_{\epsilon 2} f_2 - (2\nu \nu_T/\epsilon^2) (\partial^2(u_k u_k)^{1/2}/\partial x_k \partial x_k)^2$

**Table 3: Wilcox  $k$ - $\omega$  Model,  $s \equiv \omega = \epsilon/k$**

$\sigma_k = 1/2$	$\sigma_\omega = 1/2$	$C_{\omega 1} = 5/9$	$C_{\omega 2} = 5/6$	$f_\mu = 1$	$D_k = 1$	$D_\omega = C_{\omega 2}$
------------------	-----------------------	----------------------	----------------------	-------------	-----------	---------------------------

For the Launder-Sharma model, the thin layer approximation was normally used to compute the derivatives in the  $D_k$  and  $D_\epsilon$  terms.

An important consideration in using the Wilcox  $k$ - $\omega$  model, which is not necessary with the  $k$ - $\epsilon$  model, is the value of  $\omega$  in the free stream (just outside the boundary-layer edge) where it cannot be too small. In all of the applications of this study, it was possible to choose values of  $\omega$  at the inflow boundary which insured that the values of  $\omega$  in the free stream would not be too small. (It must be chosen such that  $\omega_\infty > 10 U_\infty/L$  where  $U_\infty$  is the free stream velocity and  $L$  is the length of run of the boundary layer and  $\omega_\infty$  is the free stream value of  $\omega$  at the start of the boundary layer). It may be that in future applications it will not be feasible to control the free stream  $\omega_\infty$  in this manner, and other measures will be necessary. One alternative would be to use the  $k$ - $\omega$  model of F. Menter (1992), which uses a blending of the  $k$ - $\omega$  and  $k$ - $\epsilon$  models to circumvent the problem. This model will be discussed more fully in the next section.

## Recommended Model Corrections for Complex Flows

The baseline models described above are generally not adequate to accurately predict complex flow problems and must be corrected to deal with these cases. The types of modeling corrections that have been found useful in practice and which are recommended for NASP applications are summarized below. Other model corrections which have been tried in the course of the study but which are not recommended for applications are described in Coakley and Huang (1992).

## Length Scale Correction

The first correction is addressed to difficulties encountered in predicting heat transfer in the reattachment or shock impingement zone of shock-wave boundary-layer interaction flows. In these zones, all 2-eq models dramatically overpredict heat transfer and must be corrected. The correction involves the use of an algebraic length scale which limits the slope of the length scale predicted by the two equation model, which otherwise would become very large in these regions. The formulas defining the length scale correction for the  $k$ - $\epsilon$  and  $k$ - $\omega$  models are given below,

$$l = \min\{2.5y, \sqrt{k^3/\epsilon}\} = \min\{2.5y, \sqrt{k/\omega}\}$$

in these formulas,  $l$  is the turbulent length scale which is taken to be the smaller of an algebraic expression ( $\kappa C_\mu^{-3/4} y = 2.5 y$ , based on a von Karman constant of  $\kappa = 0.41$ ) and the conventional length scale given by the two equation model. Having computed this parameter, the value of  $\epsilon$  or  $\omega$  is recomputed and reset to be consistent with this value, e.g.  $\epsilon = \sqrt{k^3/l}$  or  $\omega = \sqrt{k/l}$ .

## Rapid Compression Correction

The second correction to be described is called the rapid compression correction and is used to improve predictions of separation in shock-wave turbulent boundary-layer interactions. The correction involves changing the coefficient of the dilatation or velocity divergence in the  $\epsilon$  and  $\omega$  equations, i.e.  $\alpha_\epsilon$  or  $\alpha_\omega$ . The net effect of this correction is to increase the production of epsilon or omega in regions of rapid compression, or shock in waves, which reduces the eddy viscosity and enhances separation. The corrected values of the dilatation coefficient for each model are

$$\alpha_\epsilon = 2 \quad or \quad \alpha_\omega = 4/3$$

as opposed to the Launder-Sharma coefficient  $\alpha_\epsilon = (2/3) C_{\epsilon 1} = 0.97$  and the Wilcox coefficient  $\alpha_\omega = (2/3) C_{\omega 1} = 0.37$  shown in Tables 1, 2, and 3. The development of this correction is discussed more fully in Coakley and Huang (1992).

## Compressible Dissipation Correction

The third and final correction recommended for NASP applications is applicable to free shear flows (e.g. mixing layers, wakes and jets). In these types of flows, it is well known that shear layer spreading rates decrease as Mach numbers increase compared with spreading rates at zero Mach number. The correction recommended to improve predictions of these flows was developed originally by Zeman (1990), and is closely related to similar corrections developed by Sarkar (1991), and Wilcox (1992). The correction is listed below,

$$\begin{aligned} D_k &\rightarrow D_k + \phi_k \\ D_\omega &\rightarrow D_\omega - \phi_k \\ \phi_k &= a_0 (1 - \exp(-( \max(0, a_1 M_T - a_2) / a_3 )^2)) \end{aligned}$$

$D_\epsilon$  is unchanged,  $M_T = \sqrt{k}/c$ ,  $c$  is the local sound speed,  $a_0 = 3/4$ ,  $a_1 = \sqrt{\gamma+1}$ ,  $a_2 = 1/10$ , and  $a_3 = 6/10$ .

For applications involving boundary layers, or solid walls, this correction has been found to underpredict skin friction especially at high free stream Mach numbers. It is recommended, therefore, that this correction only be used in free shear flow applications. The correction of Wilcox (1992), which is similar to that of Zeman, has been found to work well in boundary layers as well as free shear flows and Wilcox recommends its use without reservation. Since we have not investigated this model under the wide range of conditions investigated using other model corrections, we chose not to recommend the model at this time.

## Other Corrections and Models of Interest

Although the above models and corrections constitute our final recommendations for NASP applications, it is important to note that these models only constitute an improvement over previous models and may very well give poor predictions for flow situations which have not yet been investigated and validated. In this regard we draw attention to the  $k-\omega$  model of F. Menter (1993), which has proven quite successful in incompressible and transonic flow applications. This model was designed to overcome certain defi-

ciencies of the Wilcox  $k$ - $\omega$  model and has certain features which might prove useful in hypersonic applications. One feature of the model is the so called shear stress transport or rapid strain feature which enables the model to give improved predictions of adverse pressure gradient boundary-layers and separation. This feature is similar to the rapid compression correction discussed above and enhances separation by reducing the eddy viscosity in non-equilibrium regions where the flow is changing rapidly. This feature was also tried with the baseline models and gave results very similar to those obtained with the rapid compression correction. It is believed that some combination of the two corrections may ultimately prove more accurate and reliable in future applications. It must be stated, however, that we did apply Menter's model to most of the flows described in this study and obtained no improvement over the recommended models. In some cases it did not perform as well. Since the model is considerably more complicated than the other models studied we decided not to include it in the list of recommended models.

## **Model Validation - Representative Results**

Representative results of calculations and comparisons of model predictions with experimental measurements will be given in this section. The flows discussed include free shear (mixing layer) flows, 3 two dimensional shock-wave boundary- layer interaction flows, and 2 three dimensional shock-wave boundary-layer interactions. The turbulence models used include the recommended baseline and corrected  $k$ - $\epsilon$  and  $k$ - $\omega$  models.

### **Compressible Mixing layer**

The first series of flows to be discussed consists of high speed mixing layers which are of considerable importance in the design of propulsive exhaust nozzles for the NASP vehicle. The comparisons of computations with experimental measurements is shown in fig.(5). The figure shows predictions of spreading rate divided by spreading rate at zero Mach number compared with experimental measurements over a range of convective Mach numbers. The data include the Bogdanoff (1993) compilation of the Langley data, and the measurements of Samimy and Elliot (1990). The calculations were done by Viegas and Rubesin (1992), who used the baseline  $k$ - $\epsilon$  model with the compressible dissipation corrections of Zeman and Sarkar. Although not shown, results obtained with the  $k$ - $\omega$  model give similar results. Examination of the comparisons indicates that the baseline model significantly overpredicts the spreading rate while the model corrections improve

the predictions. Of the two model corrections, the Zeman correction gives the best overall result.

## Two-Dimensional Shock-Wave Boundary-Layer Interaction Flows

The second series of model validation studies to be discussed consists of two dimensional (planar and axisymmetric) shock-wave boundary-layer interactions. The flows are the Mach 7 ogive-cylinder-flare flow of Kussoy and Horstman (1989) ( $35^\circ$  flare angle), the Mach 9 planar compression ramp flow of Coleman and Stollery (1972) ( $34^\circ$  ramp angle), and the Mach 7 axisymmetric impinging shock flow of Kussoy and Horstman (1975) ( $15^\circ$  generator angle). In all cases, the walls were highly cooled with wall-to-adiabatic wall temperature ratios on the order of 0.3 to 0.4. The test configurations for these cases are shown in figs.(6a,b,c).

All calculations were done using the code developed by Huang and Coakley (1992). The inlet flow conditions just ahead of the shock interaction zones were obtained by calculating the flow over a flat plate and matching measured and computed displacement thicknesses. The value of  $y^+$  at the first grid point off the wall was maintained to be less than 0.5 and the grid was expanded exponentially from the wall to the free stream. This gave between 60 to 80 grid cells in the boundary-layer and 140 cells overall in the cross stream direction. Computations with fewer cells inside the boundary-layer (i.e. 40 cells) were made and no significant differences were observed. In the streamwise direction a grid of 140 cells was used except in the impinging shock case where 200 cells were used. The comparisons of computations with measurements are shown in figs.(7-9). They include measured and computed surface pressures and heat transfer distributions (and skin friction for the impinging shock case) and were done with the baseline and corrected  $k-\epsilon$  and  $k-\omega$  models. The pressure and heat transfer measurements are normalized by the measured values in the region ahead of the interaction. Zeman's compressible dissipation correction designed for shear layers was not used as explained in the section on model corrections. It is clear from these results that the baseline models significantly under predict the extent of separation and over predict the heat transfer in the interaction region. The corrected models both give results in much better agreement with experiment.

## Three-Dimensional Shock-Wave Boundary-Layer Interaction flows

The Ames experiments on 3-D shock-wave boundary-layer interactions described in this report were used here to test the compressible turbulence models and the model corrections. The experiments and the data are also described in Settles and Dodson [1993a and 1993b] and Kussoy and Horstman [1991,1992,1993]. The calculations were done with the code of Bardina (1994)

### 3-D Vertical Fin Shock Interaction Flows

This experiment investigates the interaction of a hypersonic shock wave with a thick turbulent boundary layer [Kussoy and Horstman, 1991 and 1993b]. A  $10^\circ$  and a  $15^\circ$  vertical fins mounted on top of a flat plate were used to generate oblique shock waves. The free-stream Mach number was  $M_\infty = 8.2$ , the temperature was  $T_\infty = 81^\circ \text{ K}$ , and the Reynolds number was  $Re_\infty = 5 \cdot 10^6$  per meter. The wall temperature was fixed at  $300^\circ \text{ K}$ . The interaction of the shock wave with the turbulent boundary layer generates a crossflow vortex separation with a “quasi conical” shape [Settles and Lu, 1985; Knight, Horstman, and Monson, 1992]. Peak wall pressure, skin friction, and heat transfer rates were observed in the re-attachment zone behind the crossflow vortex.

The numerical computations were made with  $61 \times 41 \times 61$  and  $31 \times 21 \times 31$  meshes [Bardina, Coakley, and Marvin, 1992]. Only small differences between the solutions were observed, and the fine mesh solutions are considered accurate for engineering purposes. The inflow conditions were obtained from the Navier-Stokes code solution matching the experimental displacement thickness.

A few comparisons of experiment and simulation with the finer mesh are described below. Figures 10a and 10b show the surface pressure and skin friction distributions, respectively, for the  $10^\circ$  fin flow on the flat plate surface at the crossed section located at  $x=0.1819 \text{ m}$  downstream of the fin leading edge. Figure 10c shows the comparison of the wall heat transfer distribution on the flat surface at  $x=0.1645 \text{ m}$  downstream of the fin leading edge. Comparable results for the  $15^\circ$  fin case are shown in fig.(11a,b,c). The symbols in the figures show the experimental data points, the solid lines show the solution with the baseline  $k-\omega$  model, and the dash lines show the solution with the  $k-\omega$  model with both model corrections (length-scale and rapid compression corrections). Both

simulations show good agreement with the experimental data. The peak values observed in the re-attachment zone are also well predicted. The simulations fail to predict the small plateau observed in the wall heat transfer rate distributions upstream of the shock wave. Comparison of baseline and corrected model predictions show only small differences. This is probably due to the fact that, compared with the 2-D results, the pressure rise through the shock wave is relatively weak and separation is relieved by three dimensional effects.

### 3-D Crossing Shock Interaction Flow

This experiment studies the interactions of two intersecting hypersonic shock waves with a thick turbulent boundary layer [Kussoy and Horstman, 1992]. Two  $15^\circ$  fins mounted on top of a flat plate were used to generate intersecting oblique shock waves (see fig. 4). The free-stream Mach number was  $M_\infty = 8.3$ , the temperature was  $T_\infty = 80^\circ \text{ K}$ , and the Reynolds number was  $Re_\infty = 5.3 \cdot 10^6$  per meter. The wall temperature was fixed at  $300^\circ \text{ K}$ . The intersection of both crossflow vortices generates different complex flow structures with high static pressures and surface heat transfer rates. The intersection of the two “quasi conical” vortical structures uplifts the flow and induces a wave structure in the symmetry plane [Gaitonde and Shang, 1993].

The numerical simulations were made with a  $231 \times 81 \times 81$  mesh [Bardina and Coakley, 1994; Bardina, 1994]. Simulations studies with  $101 \times 61 \times 41$  and  $31 \times 21 \times 31$  grid points were also done to analyze grid effects. Small differences between the solutions were observed in the surface pressure and heat transfer distributions, but significant differences were observed in flow structure. The fine mesh solutions provided the best resolution of the turbulence structures and are considered accurate for engineering purposes. The inflow conditions were obtained from the Navier-Stokes code solution matching the experimental displacement thickness.

Figures 12a and 12b show the pressure and heat transfer distributions, respectively, on the plate surface along the symmetry plane located between the two fins. The symbols show the experimental data, the solid lines show the solution with the baseline  $k-\omega$  model, and the dash lines show the solution with the  $k-\omega$  model with both model corrections (length-scale and rapid compression corrections). Predictions of both surface pressure and heat transfer show good agreement, within the experimental uncertainty, except

near the outflow zone. The small plateau at the beginning of the interaction is also not predicted by either model. The peak pressure and heat transfer rate are very well predicted. As in the single fin cases, both the baseline and corrected model predictions show only small differences.

Figures 13a and 13b show the pressure distributions on the plate surface at two cross-sections, one located at  $x/\delta_\infty = 5.60$  and the other located at  $x/\delta_\infty = 6.92$  downstream of the fin leading edge. The first distribution is upstream of the peak surface pressure, and the second distribution is downstream of the peak surface pressure generated by the flow re-attachment. Both simulations show good agreement within the experimental uncertainty of the data, and both models give similar predictions.

Figures 13c and 13d show the comparison of heat transfer rate profiles on the plate surface in the crossed sections located at  $x/\delta_\infty = 5.08$  and  $x/\delta_\infty = 6.40$ , respectively, upstream and downstream of the peak heat transfer rate observed in the symmetry plane. Both simulations agree in general with the experimental data. The model corrections show improved heat transfer rate predictions in the downstream zone.

Figure 14 shows experimental pitot pressure contours compared with computational contours obtained with the corrected  $k-\omega$  model. Three locations are shown,  $x/\delta_\infty = 5.60$ ,  $6.9$ , and  $8.3$ , respectively. The resolution of the numerical data is  $81 \times 81$  grid points while the resolution of the experimental data is  $5 \times 24$ ,  $4 \times 24$ , and  $4 \times 24$  respectively. The agreement with the experimental data is very good.

## Summary and Conclusions

In this section we summarize the work performed under GWP 18, give our principal results and recommendations, and discuss plans for future work. We feel that, overall, the results produced in the course of the work were of a very high caliber and will be of considerable use to modelers and designers of hypersonic flight vehicles. The research was divided into two distinct phases; one experimental and the other theoretical. The experimental phase consisted of the collection and assessment of a database of high speed wind tunnel experiments gathered from sources around the world and the conduct of additional experiments in the NASA Ames 3.5' hypersonic wind tunnel which would add to the database. The primary aim of this effort was to produce a database of reliable and rele-

vant flow measurements which could be used to validate turbulence models for NASP CFD design codes. Out of a total of over 2000 experiments that were initially studied, the list of acceptable experiments was reduced a total of 30 using a set of strict acceptance criteria. The kinds of flows analyzed and recommended as legitimate candidates for inclusion in the database included two- and three-dimensional shock-wave boundary-layer interaction flows, attached boundary layers flows and free shear flows.

The theoretical phase of the work consisted of identifying, testing, and recommending turbulence models which would be of practical use in the CFD design codes. A large number of baseline models were initially tested on flat plate flows and this number was then reduced to two for further testing on more complex flows. The baseline models selected were the Launder-Sharma version of the  $k$ - $\epsilon$  model, and the Wilcox  $k$ - $\omega$  model. These models were tested on free shear flows and two- and three-dimensional shock-wave boundary-layer interaction flows. Some of the results of these calculations have been discussed in this report. It was found that the baseline models did not perform satisfactorily with regard to separation and heat transfer predictions especially for the 2-D shock-wave boundary-layer interaction flows, and did not accurately predict the spreading rate of free shear layers. To improve model performance for these complex flows, a series of compressibility corrections was investigated. The more promising of these corrections were then selected to be the final model recommendations for incorporation in to the NASP CFD codes. Representative results using the corrected models were discussed in this report. It was shown that for the flows investigated, the model corrections give substantially improved predictions.

Although the work performed in the course of this research has led to the identification of useful flows for model validation and the development of improved turbulence models for hypersonic flight, much work remains to be done. Not all of the flows included in the database of recommended flows have been investigated computationally, and these need to be investigated. More complicated flows not included in the database also need to be investigated. Flows that fall into this latter category include flows with chemical reactions such as those occurring in SCRAM jet combustion and propulsion, and flows that include transitional phenomena just to mention two. Interest in these and other areas of turbulence modeling research is very high and the work goes on.

## References

- Bardina, J. E. (1992), "Two-Equation Turbulence Modeling for Hypersonic Flight," NCC 2-585, NASA-CR-190313, NASA Ames Research Center, PR-92-010, MCAT Inst., CA.
- Bardina, J., Coakley T., and Marvin, J. (1992), "Two-Equation Turbulence Modeling for 3-D Hypersonic Flows," AIAA Paper 92-5064, 4th International Aerospace Planes Conference, Orlando, FL.
- Bardina, J. E. (1993), "Two-Equation Turbulence Modeling for Hypersonic Flight," NCC 2-585, NASA Ames Research Center, PR-93-07, MCAT Inst., CA, Feb.
- Bardina, J. E., and Coakley, T. J. (1994), "Three-Dimensional Navier-Stokes Simulation with Two-Equation Turbulence Models of Intersecting Shock-Waves/Turbulent Boundary Layer at Mach 8.3," AIAA Paper 94-1905, Colorado Springs, CO.
- Bardina, J. E. (1994), "Three-Dimensional Navier-Stokes Method with Two-Equation Turbulence Models for Efficient Numerical Simulation of Hypersonic Flows," AIAA Paper 94-2950, Indianapolis, IN.
- Bogdanoff, D.W. (1983), "Compressibility Effects in Turbulent Shear Layers," *AIAA J.*, Vol. 21, No. 6, pp. 926-927.
- Coakley, T. J., and Marvin, J. G. (1986), "Numerical Implementation and Performance of Turbulence Models for Compressible Flow Simulations," paper presented at First World Congress on Computational Mechanics, University of Texas, Arlington, TX.
- Coakley, T. J., and Huang, P. G. (1990), "Evaluation of Turbulence Models for Hypersonic Flows," 8th National Aero-Space Plane Technology Symposium, Paper No. 24, Monterey, CA.
- Coakley, T. J., Viegas, J. R., Huang, P. G., and Rubesin, M. W. (1990), "An assessment and Application of Turbulence Models for Hypersonic Flows," 9th National Aero-Space Plane Technology Symposium, Paper No. 106, Orlando, FL.
- Coakley, T. J., and Huang, P. G. (1991), "Modeling for Compressible High Speed Flows," Tenth National Aero-Space Plane Technology Symposium, Paper No. 210, Monterey, CA.
- Coakley, T. J., and Huang, P. G. (1992), "Turbulence Modeling for High Speed Flows," AIAA Paper 92-04366, Reno, NV.

- Coakley, T. J., and Marvin, J. G. (1993), "Compressibility connections for Hypersonic Flow Turbulence Modeling," 1993 National Aero-Space Plane Technology Review, Monterey, CA.
- Coakley, T. J., Huang, P. G., Bardina, J. E., and Viegas, J. R. (1993), "Modeling of Turbulence for Complex High Speed Flows," paper presented at Second National Congress on Computational Mechanics, Washington, D. C.
- Coleman, G.T., and Stollery, J.L. (1972), "Heat Transfer from Hypersonic Turbulent Flow at a Wedge Compression Corner," *J. of Fluid Mech.*, Vol. 56, pp. 741-752.
- Horstman, C. C., and Kussoy, M. I. (1989), "2- and 3-Dimensional Hypersonic Shock-Wave Turbulent-Boundary Layer Interaction Flows - Experiment and Computation," 6th NASP Symp., Monterey, CA.
- Horstman, C. C. (1990), "Turbulence Modeling for Sharp-Fin-Induced Shock Wave/Turbulent Boundary-Layer Interactions," IUTAM Symp. on Separated Flows and Jets, Novosibirsk, USSR, Jul. 1990; also NASA TM 102828.
- Horstman, C. C. (1991), "Hypersonic Shock-Wave Turbulent-Boundary-Layer Interaction Flows: Experiment and Computation (U)," 10th NASP Symp., Monterey, CA.
- Horstman, C. C., Settles, G. S., and Dodson, L. J. (1991), "Hypersonic Shock-Wave Turbulent-Boundary-Layer Interaction Flows: Experiment and Computation," 10th NASP Symp., Monterey, CA.
- Horstman, C. C. (1992), "Hypersonic Shock-Wave Turbulent-Boundary-Layer Interaction Flows," *AIAA J.*, Vol. 30, No. 6, pp. 1480-1481; also in AIAA Paper 91-1760, Honolulu, HI.
- Huang, P. G., Bradshaw, P., and Coakley, T. J. (1992), "Assessment of Closure Coefficients for Compressible Flow Turbulence Models," NASA TM-103882.
- Huang, P. G., and Coakley, T. J. (1992), "An Implicit Navier-Stokes Code for Turbulence Flow Modeling," AIAA Paper 92-0547, Reno, NV.
- Huang, P. G., and Coakley, T. J. (1993), "Modeling Hypersonic Boundary-layer Flows with Second-moment Closure," present at the International Conference on Near Wall Turbulent Flows, Tempe, AZ.
- Huang, P. G., and Coakley, T. J. (1993), "Calculations of Supersonic and Hypersonic Flows Using Compressible Wall Functions," presented at the 2nd International Symposium on Engineering Turbulence Modeling and Measurements, Florence, Italy.

- Huang, P. G., and Coakley, T. J. (1993), "Turbulence Modeling for Complex Hypersonic Flows," AIAA Paper 93-0200, Reno, NV.
- Huang, P. G., Bradshaw, P., and Coakley, T. J. (1993), "Skin Friction and Velocity Profile Family for Compressible Turbulent Boundary Layers," *AIAA J.*, Vol. 31, No. 9, pp. 1600 - 1604.
- Huang, P. G., Bradshaw, P., and Coakley, T. J. (1994), "Turbulence Models for Compressible Boundary Layers", *AIAA J.*, Vol. 32, No. 4, pp. 735-740.
- Huang, P. G., and Coleman, G.N. (1994), "On the van Driest Transformation and Compressible Wall-Bounded Flows", to be published in the *AIAA J.*
- Kim, K.-S., Lee, Y., Alvi, F. S., Settles, G. S., and Horstman, C. C. (1991, "Skin Friction Measurements and Computational Comparison of Swept Shock/Boundary-Layer Interactions," *AIAA J.*, Vol. 29, No. 10, pp. 1643-1650.
- Knight, D. D., Narayanswami, N., and Horstman, C.C. (1991), "A Numerical Investigation of the Interaction Between Crossing Oblique Shocks and a Turbulent Boundary Layer in Hypersonic Flow," 44th APS Annual Meeting, Tempe, AZ.
- Knight, D. D., Settles, G. S., and Horstman, C. C. (1991), "Three-Dimensional Shock Wave Turbulent Boundary Layer Interactions Generated by a Sharp Fin at Mach 4," AIAA Paper 91.-0648, Reno, NV.
- Knight, D. D., Horstman, C. C., and Monson, D. J. (1992), "The Hypersonic Shock Wave-Turbulent Boundary Layer Interaction Generated by a Sharp Fin at Mach 8.2," AIAA Paper 92-0747, Reno, NV.
- Knight, D. D., Badekas, D., Horstman, C. C., and Settles, G. S. (1992), "On the Quasi-conical Flowfield Structure of the 3-D Single Fin Interaction," *AIAA J.*, Vol. 30, No. 12, pp. 2809-2816.
- Knight, D. D., Horstman, C. C., and Bogdonoff, S. (1992), "Structure of a Supersonic Turbulent Flow Past a Swept Compression Corner," *AIAA J.*, Vol. 30, No. 4, pp. 890-896.
- Kussoy, M. I., and Horstman, C. C. (1975), "An Experimental Documentation of a Hypersonic Shock-Wave Turbulent Boundary Layer Interaction Flow - with and without Separation," NASA TM X-62412.
- Kussoy, M. I., and Horstman, C. C. (1989), "Documentation of Two- and Three-Dimensional Hypersonic Shock Wave/Turbulent Boundary Layer Interaction Flows," NASA TM 101075.

- Kussoy, M. I., and Horstman, C. C. (1991), "Documentation of Two and Three-Dimensional Shock-Wave/Turbulent-Boundary-Layer Interaction Flows at Mach 8.2," NASA TM 103838.
- Kussoy, M. I., Kim, K-S., and Horstman, C. C. (1991), "An Experimental Study of a Three-Dimensional Shock Wave/Turbulent Boundary-Layer Interaction at a Hypersonic Mach Number," AIAA Paper 91-1761, Honolulu, HI.
- Kussoy, M. I., and Horstman, C. C. (1992), "Intersecting Shock-Wave/Turbulent Boundary-Layer Interactions at Mach 8.3," NASA TM 103909.
- Kussoy, M. I., and Horstman, K. C. (1993), "Three-Dimensional Hypersonic Shock Wave/Turbulent Boundary-Layer Interactions," *AIAA J.*, Vol. 31, No. 1, pp. 8-9.
- Kussoy, M. I., Horstman, K. C., and Horstman, C. C. (1993), "Hypersonics Crossing Shock-Wave/Turbulent-Boundary-Layer Interactions," *AIAA J.*, Vol. 31, No. 12, pp. 2197-2203; also in AIAA Paper 93-0781, Reno, NV.
- Jones, W.P., and Launder, B.E. (1972), "The Prediction of Laminarization with a Two Equation Model of Turbulence," *Int. J. of Heat and Mass Transfer*, Vol. 15, pp. 301-304.
- Launder, B.E., and Sharma, B.I. (1974), "Application of the Energy-Dissipation Model of Turbulence to the Calculation of Flow Near a Spinning Disk," *Letters in Heat and Mass Transfer*, Vol. 1, pp. 131-138.
- Lee, Y., Settles, G. S., and Horstman, C. C. (1992), "Heat Transfer Measurements and CFD Comparison of Swept Shock Wave/Boundary-Layer Interactions," AIAA Paper 92-3665, Nashville, TN.
- Marvin, J. G. (1987), "Wind Tunnel Requirements for Computational Fluid Dynamics Code Verification," Paper 34, AGARD Symposium on Aerodynamic Data Accuracy and Quality, Requirements and Capabilities in Wind Tunnel Testing, Naples, Italy; also in NASA TM 100001.
- Marvin, J. G. (1990), "Progress and Challenges in Modeling Turbulent Aerodynamic Flows," *Engineering Turbulence Modeling and Experiments*, editors W. Rodi and E. N. Genic, Elsevier, pp. 3-12; also in NASA TM 102811.
- Marvin, J. G., and Coakley, T. J. (1990), "Turbulence Modeling for Hypersonic Flows," 2nd Joint Europe-US Short Course in Hypersonics, Air Force Academy, Colorado Springs, CO; also in NASA TM 101079, Jun. 1989, and 3d Joint US/Europe Short Course in Hypersonics, Aachen, W. Germany.

- Marvin, J. G., Horstman, C. C., Lockman, W. K., and Strawa, A. W. (1991), "CFD Validation Experiments for NASP (U)," Tenth NASP Symp., Monterey, CA.
- Marvin, J. G. (1992), "A CFD Validation Roadmap for Hypersonic Flows," AGARD 70th Fluid Dyn. Panel Meeting, Torino, Italy.
- Marvin, J. G. (1992), "CFD Validation Experiments for Hypersonic Flows," AIAA Paper 92-4024, Nashville, TN.
- Menter, F.R. (1993), "Zonal Two Equation  $k-\omega$  Turbulence Models for Aerodynamic Flows," AIAA Paper 93-2906, Orlando, FL.
- Narayanswami, N., Knight, D. D., Bogdonoff, S. M., and Horstman, C. C. (1991), "Crossing Shock Wave-Turbulent Boundary Layer Interactions," AIAA Paper 91-0649, Reno, NV.
- Narayanswami, N., Knight, D. D., Bogdonoff, S. M., and Horstman, C. C. (1992), "Interaction Between Crossing Oblique Shocks and a Turbulent Boundary Layer," *AIAA J.*, Vol. 30, No. 8, pp. 1945-1952.
- Narayanswami, N., Knight, D. D., and Horstman, C. C. (1992), "Investigation of a Hypersonic Crossing Shock Wave/Turbulent Boundary Layer Interaction Shock Waves," *AIAA J.*, Vol. 2, No. 4.
- Narayanswami, Horstman, C. C., and Knight, D. D. (1993), "Computation of Crossing Shock/Turbulent Boundary Layer Interaction at Mach 8.3," AIAA Paper 93-0779, Reno, NV.
- Prabhu, D. K., Tannehill, J. C., and Marvin, J. G. (1986), "Hypersonic Nonequilibrium Flow Fields over Wedges and Cones," NASP Tech. Symposium, Johns Hopkins Univ., Laurel, MD.
- Prabhu, D. K., Tannehill, J. C., and Marvin, J. G. (1987), "A New PNS Code for Chemical Nonequilibrium Flows," AIAA Paper 87-0284, Reno, NV.
- Prabhu, D. K., Tannehill, J. C., and Marvin, J. G. (1993), "A New PNS Code for Three-Dimensional Chemically Reacting Flows," AIAA 87-1472, Honolulu, HI.
- Samimy, M., and Elliot, G.S. (1990), "Effects of Compressibility on the Characteristics of Free Shear Layers," *AIAA J.*, Vol. 28, No. 3, pp. 439-445.
- Sarkar, S. (1991), "Modeling the Pressure-Dilatation Correlation," ICASE Report 91-42, NASA Langley Research Center.

- Settles, G. S, and Dodson, L. J. (1991), "Hypersonic Shock/Boundary-Layer Interaction Database," NASA CR 177577.
- Settles, G. S., and Dodson, L. J. (1993), "Hypersonic Turbulent Boundary-Layers and Free-Shear Layer Database," NASA CR 1776.
- Settles, G. S, and Dodson, L. J. (1993), "Hypersonic Shock/Boundary-Layer Interaction Database: New and Corrected Data," Dept. of Mech. enrg., Penn State Univ., University Park, PA; also to be published as NASA CR.
- Spaid, F. W., and Keener (1993), "Hypersonic Nozzle/After body CFD Code Validation Part 1: Experimental Measurements," AIAA Paper 93-0607, Reno, NV.
- Viegas, J.R., and Rubesin, M.W. (1991), "A comparative Study of Several Compressibility Corrections to Turbulence Models Applied to High Speed Shear Layers," AIAA Paper 91-1783, Honolulu, HI.
- Viegas, J.R., and Rubesin, M.W. (1992), "Assessment of Compressibility Corrections to the  $k$ - $\epsilon$  Model in High-Speed Shear Layers," *AIAA J.*, Vol. 30, No. 10, pp. 2369-2370.
- Wilcox, D.C. (1991), "A Half Century Historical Review of the  $k$ - $\omega$  Model," AIAA Paper 91-0615, Reno, NV.
- Wilcox, D.C. (1991), "Progress in Turbulence Modeling," AIAA Paper 91-1785, Honolulu, HI.
- Zeman, O. (1990), "Dilatation Dissipation: The Concept and Application in Modeling Compressible Mixing Layers," *Physics of Fluids A*, Vol. 2.
- Zhelotovodov, A. A., Borisov, A. V., Knight, D. D., Horstman, C. C., and Settles, G. S. (1992), "The Possibilities of Numerical Simulation of Shock Waves/Boundary Layer Interaction in Supersonic and Hypersonic Flows," Proceedings of International Conf. on the Methods of Aerophysical Research, pp. 164-170, Novosibirsk, Russia.

GWP	DESCRIPTION
GWP 0218 CFD - Turbulence Compressibility Corrections	
1810 DEVELOP EXPERIMENTAL DATA BASE	
1811 Document Exlst. Shock Data	
1812 3.5' HWT Shock Exp. & Document	
1813 Document Exlst. Shear Layer Data	
1814 3.5' HWT Shear Layer Exp. & Document	
1820 DEVELOP COMPRESSIBLE TURBULENCE MODELS	
1821 Select Baseline Models	
1822 Implement Models in Codes	
1823 Test Models on Data Base	
1824 Recommend & Document Models	

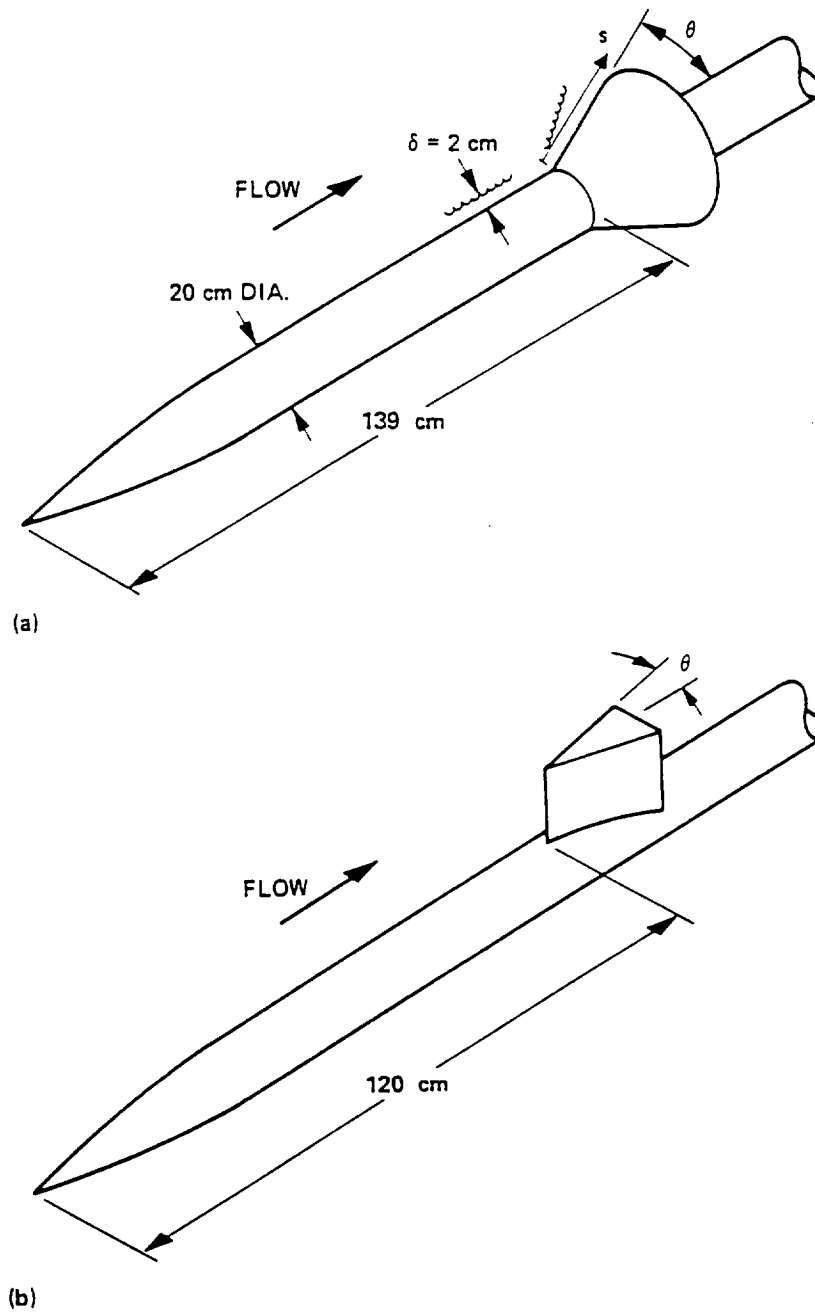


Fig. 2. Ogive-cylinder experimental configuration with (a) flare attached and (b) with fin attached of Kussoy and Horstman (1989).

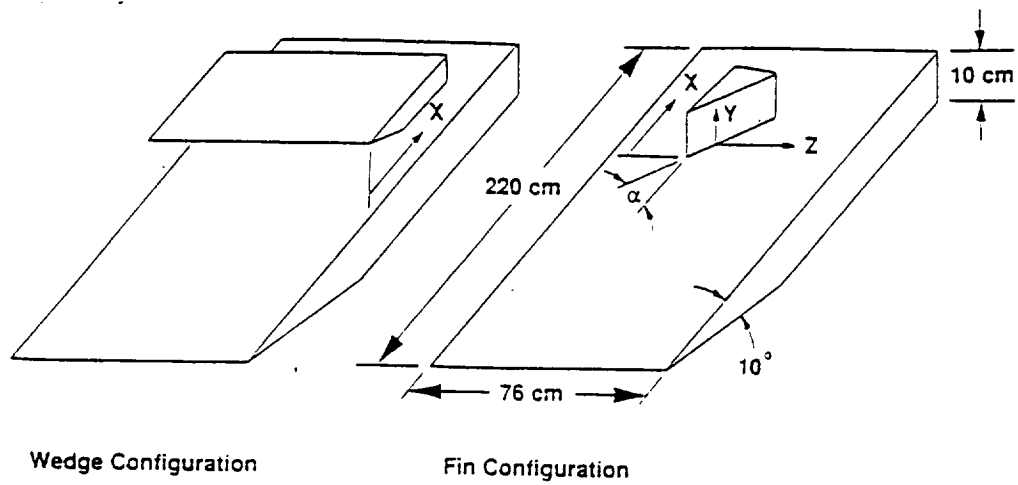


Fig. 3. 2-D wedge and 3-D vertical fin on flat plate configuration of Kussoy and Horstman (1991a)

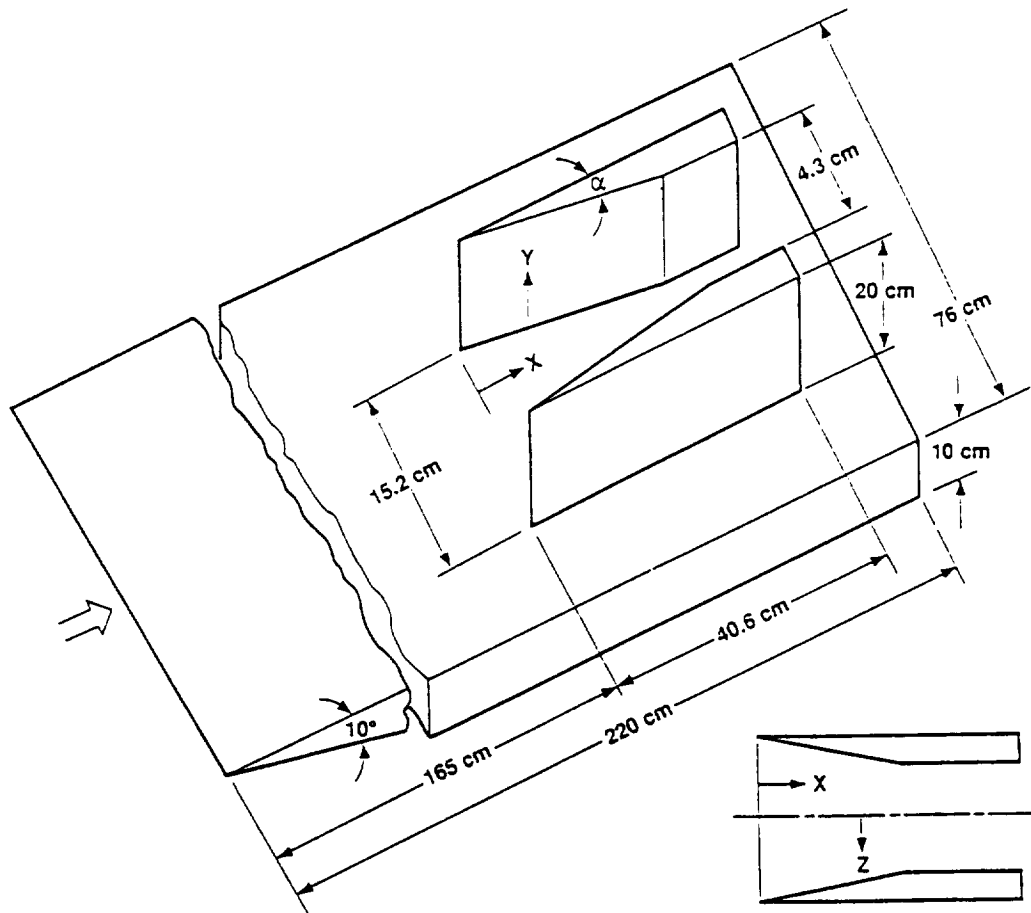
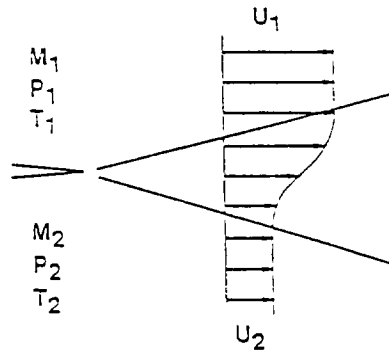


Fig. 4. Crossing shocks generated with two vertical fins on flat plate configuration of Kussoy and Horstman (1992).

Shear layer



Vorticity thickness

$$\delta_\omega = (U_1 - U_2) / (\partial U / \partial y)_{\max}$$

$$\delta'_\omega = C_\omega(M_c) \frac{1 - U_2/U_1}{1 + U_2/U_1}$$

$$C_\omega(M_c)/C_\omega(0)$$

$$M_c = \frac{M_1 \sqrt{\frac{\rho_2}{\rho_1}} - M_2}{\sqrt{\frac{\rho_2}{\rho_1}} + 1.0}$$

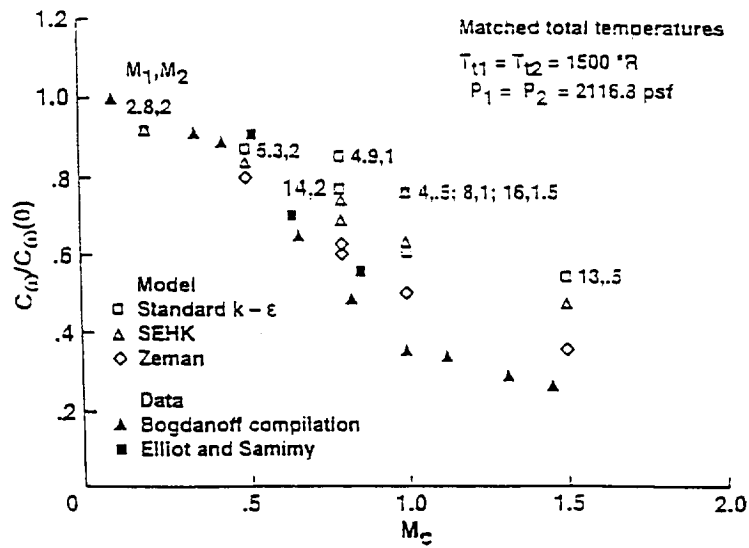


Fig. 5. Effect of compressibility on normalized vorticity thickness growth rate for mixing layer (Viegas and Rubesin (1991, 1992)).

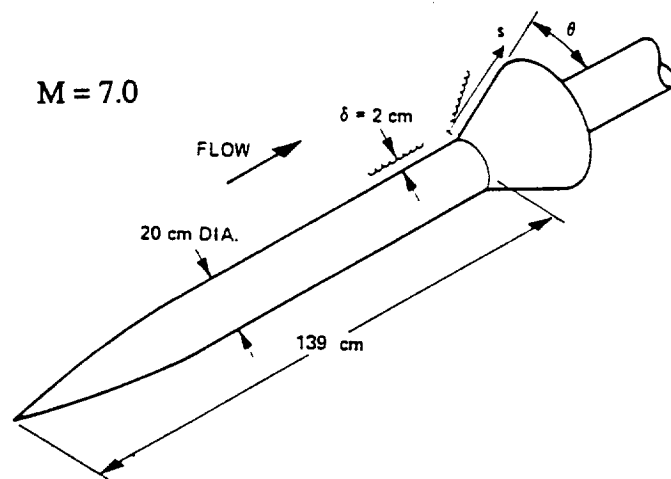


Fig. 6a. Axisymmetric compression generated with ogive-cylinder-flare configuration of Kussoy and Horstman (1989).

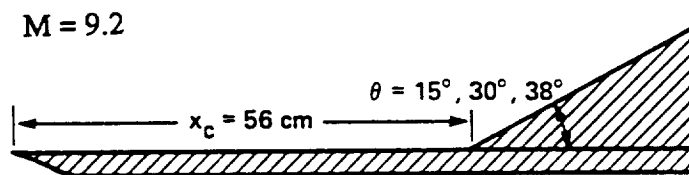


Fig. 6b. 2-D planar compression ramp configuration of Coleman and Stollery (1972).

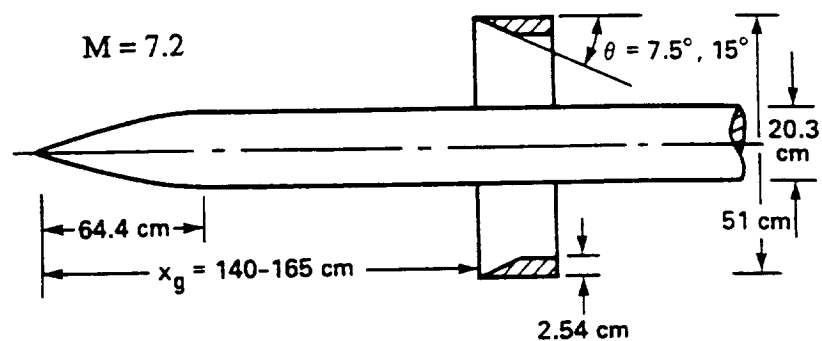


Fig. 6c. Axisymmetric impinging shock generated with a cone-ogive cylinder and an annular fin configuration of Kussoy and Horstman (1975).

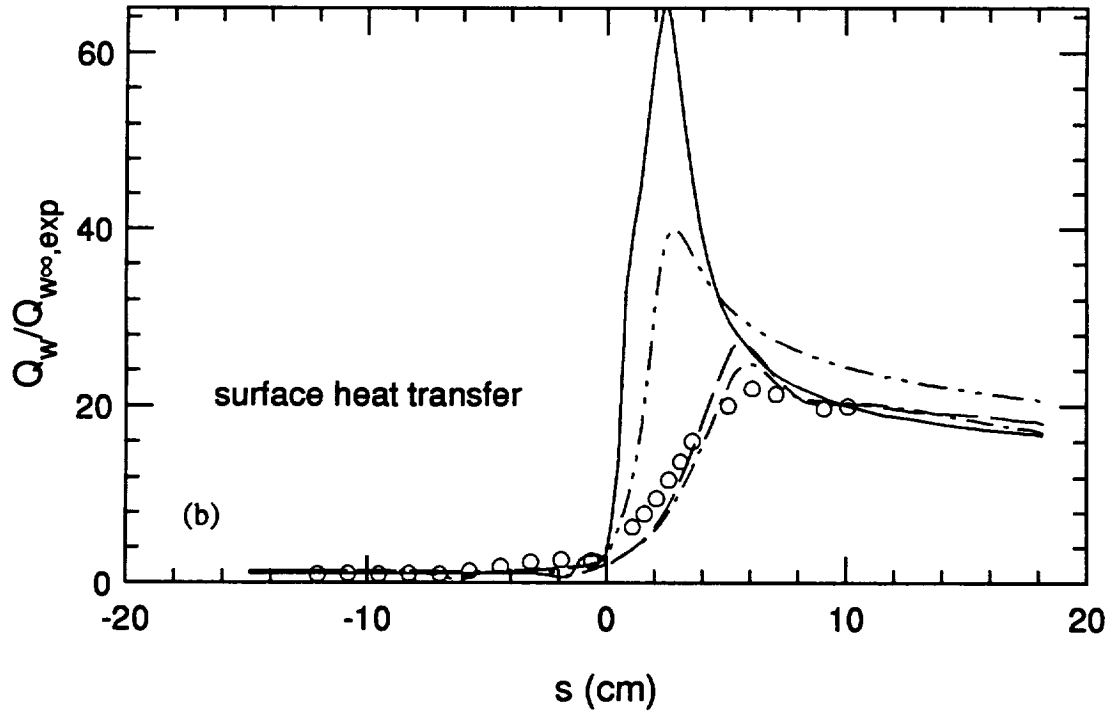
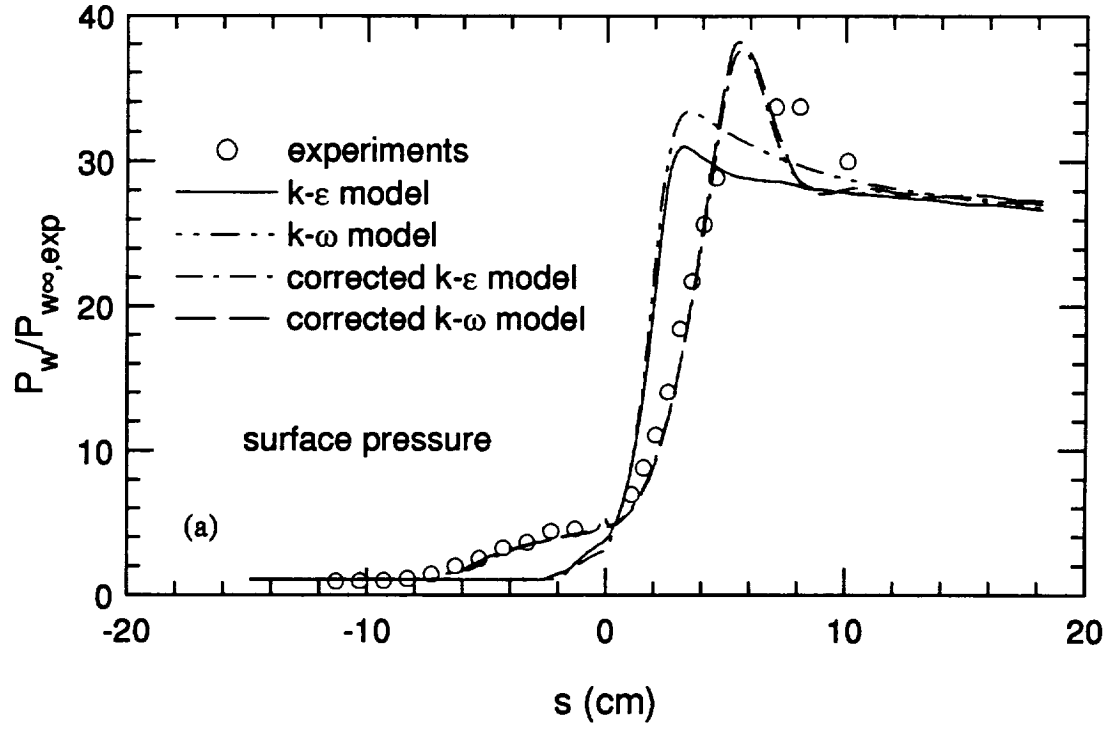


Fig. 7. Surface pressure (a) and heat transfer (b) in axisymmetric compression flow of Kussoy and Horstman (1989), geometry shown in Fig. 6a.

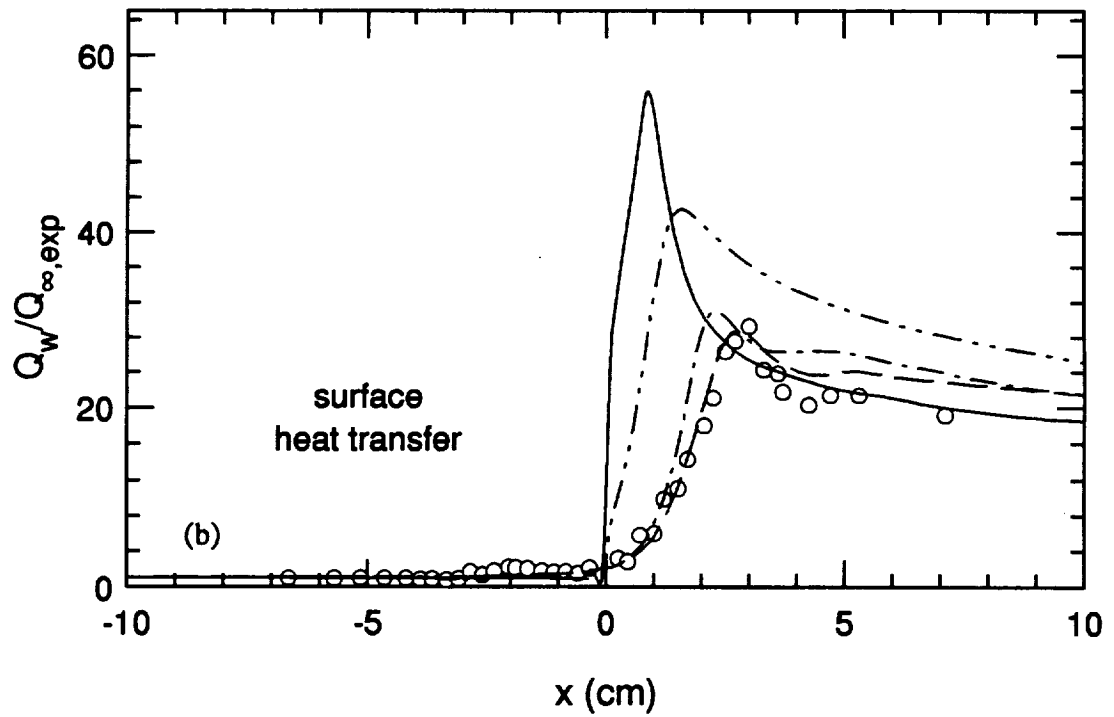
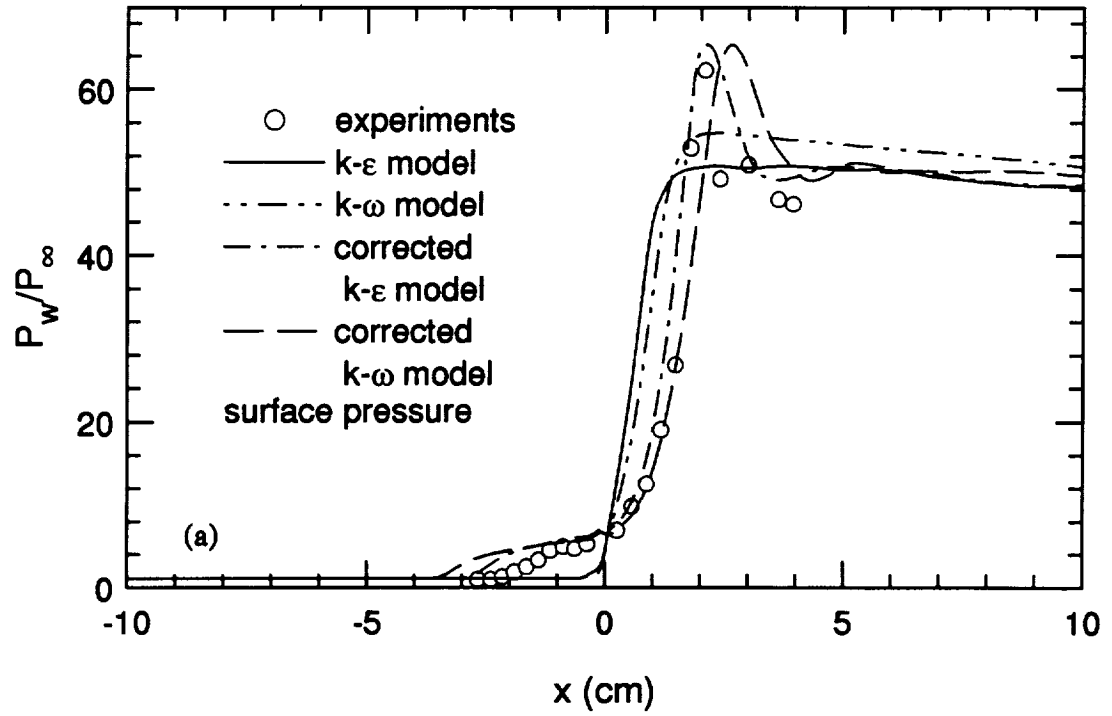


Fig. 8. Surface pressure (a) and heat transfer (b) in 2-D planar compression ramp flow of Coleman and Stollery (1972), geometry shown in Fig 6b.

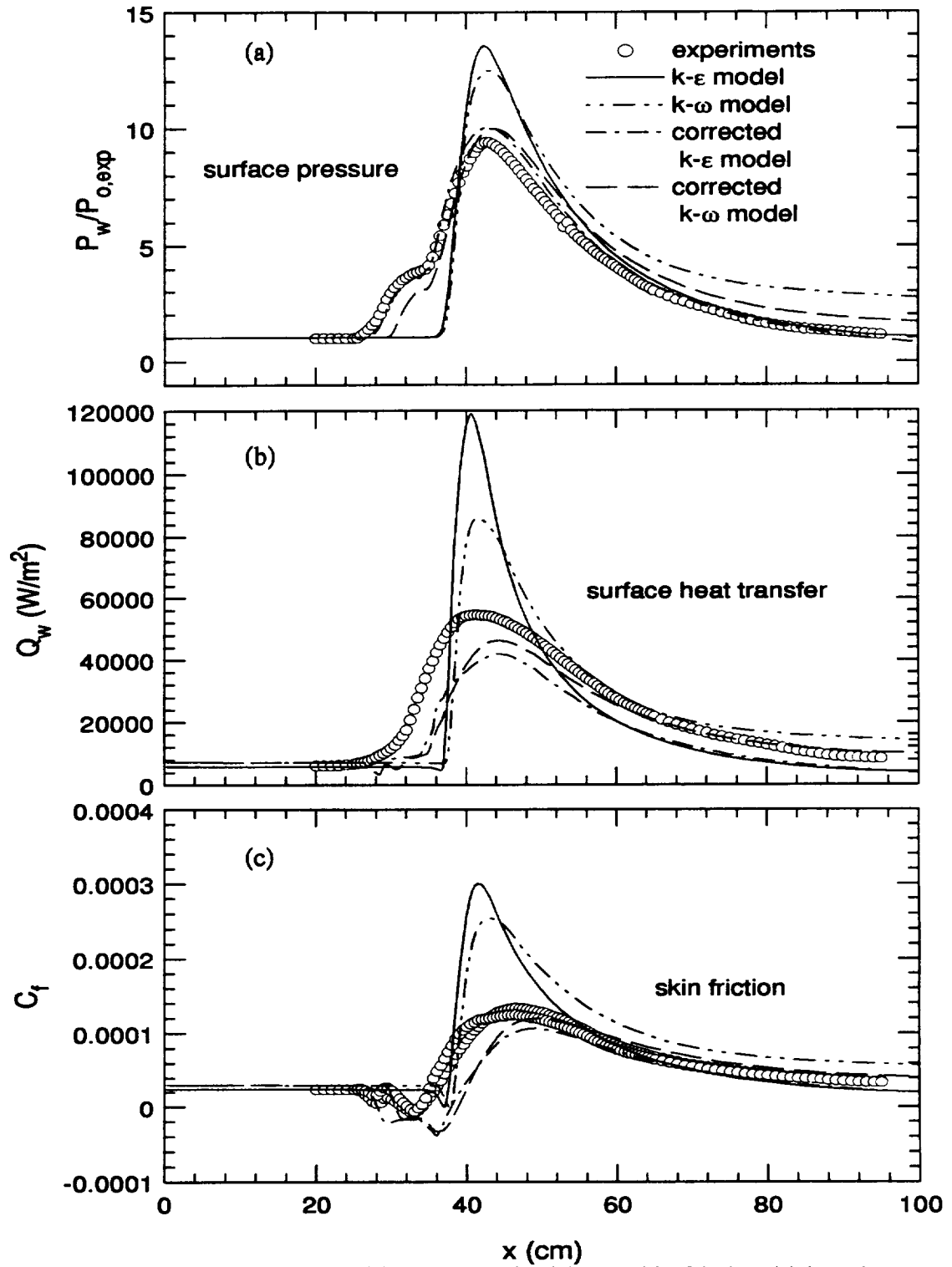


Fig. 9. Surface pressure (a), heat transfer (b) and skin friction (c) in axisymmetric impinging shock flow of Kussoy and Horstman (1975), geometry shown in Fig 6c.

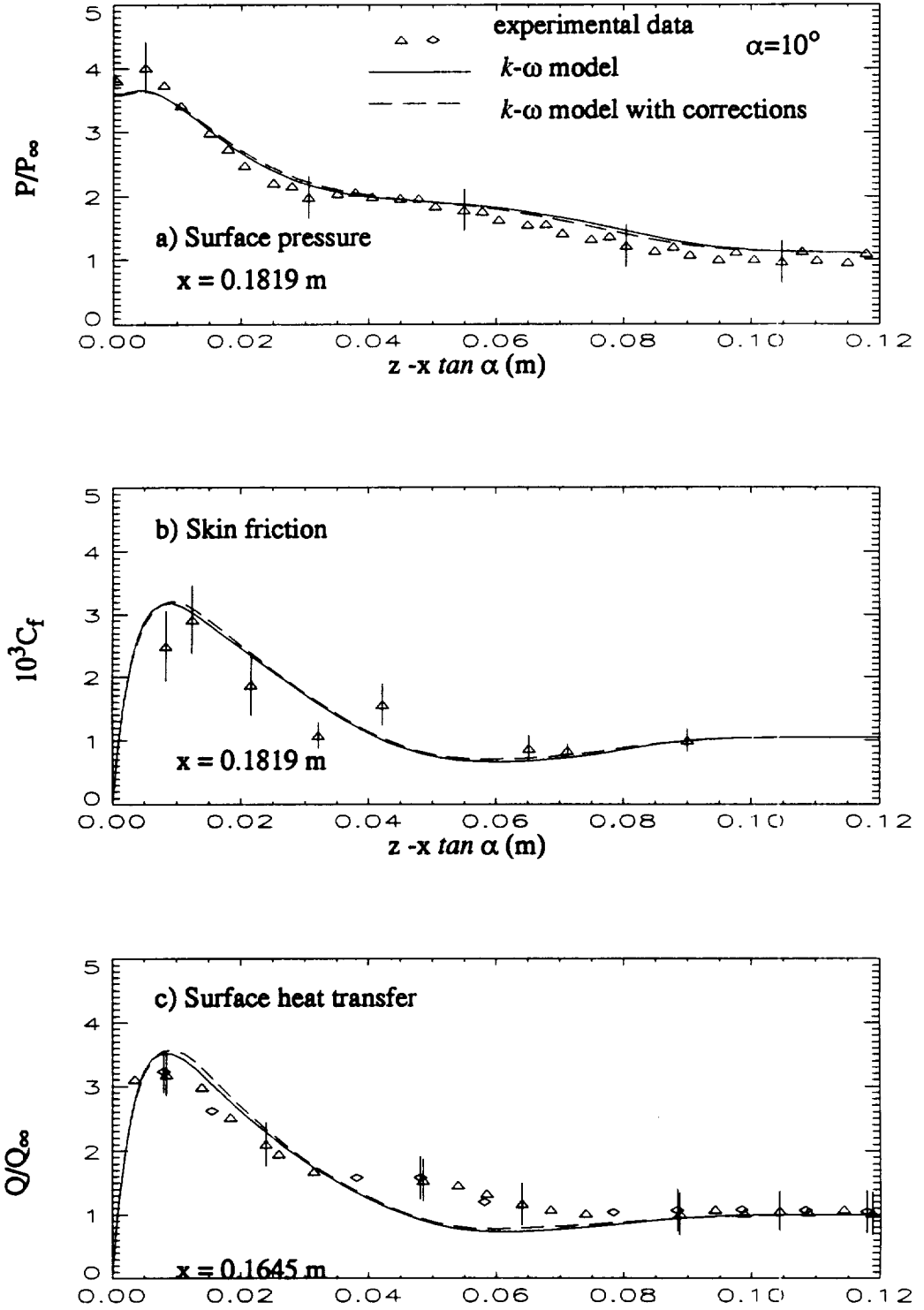


Fig. 10. Surface flow predictions in the 3-D vertical fin interaction flow ( $\alpha=10^\circ$  case) of Kussoy and Horstman (1991a), geometry shown in Fig. 3.

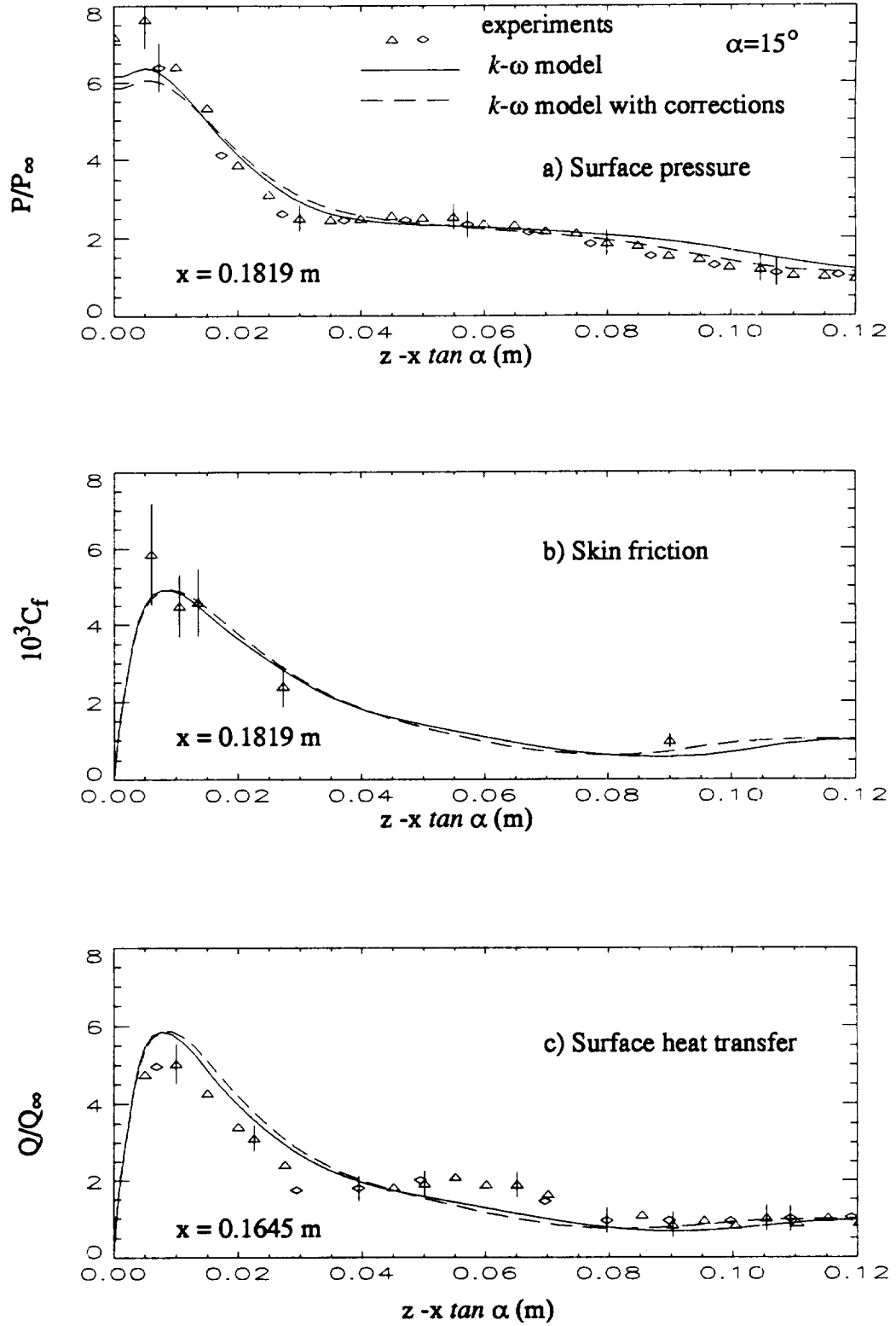


Fig. 11. Surface flow predictions in the 3-D vertical fin interaction flow ( $\alpha=15^\circ$  case) of Kussoy and Horstman (1991a), geometry shown in Fig. 3.

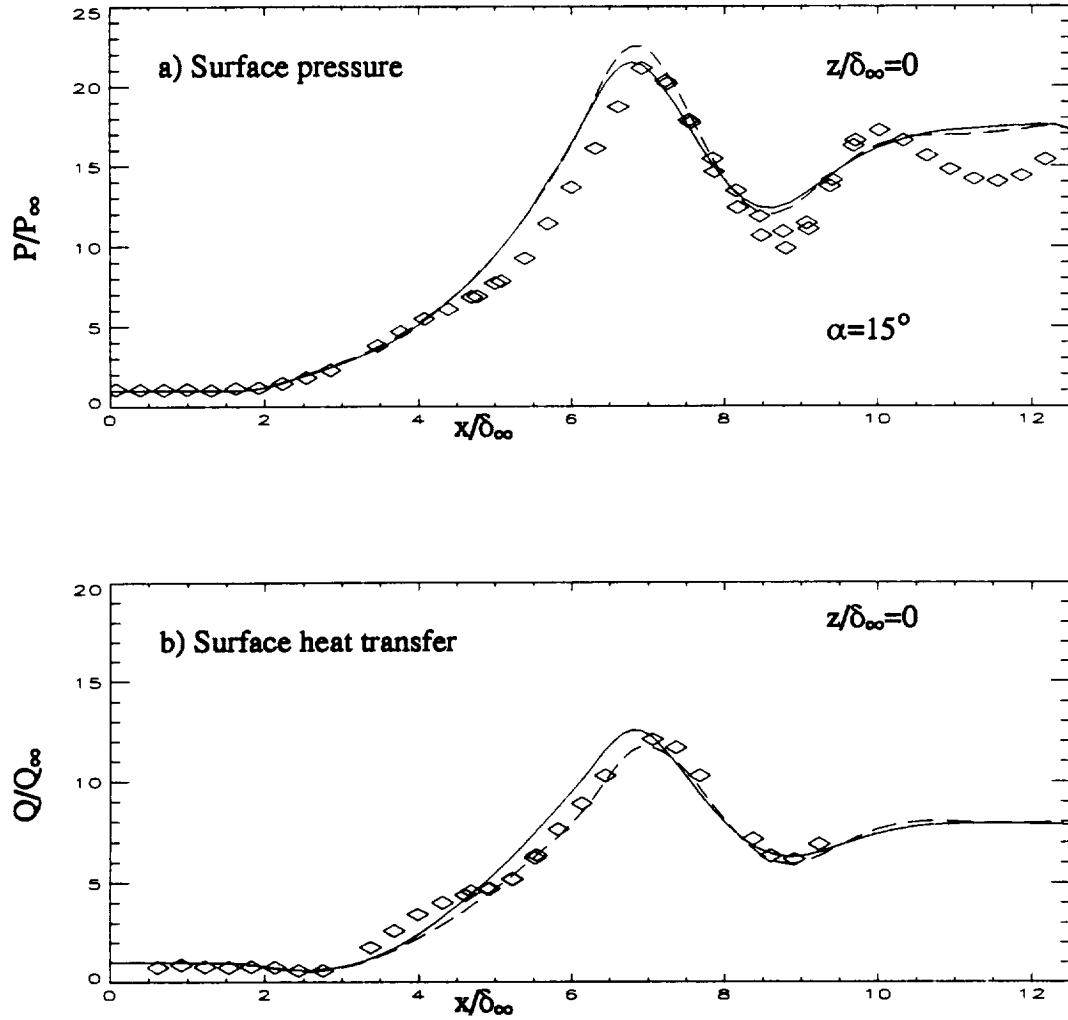
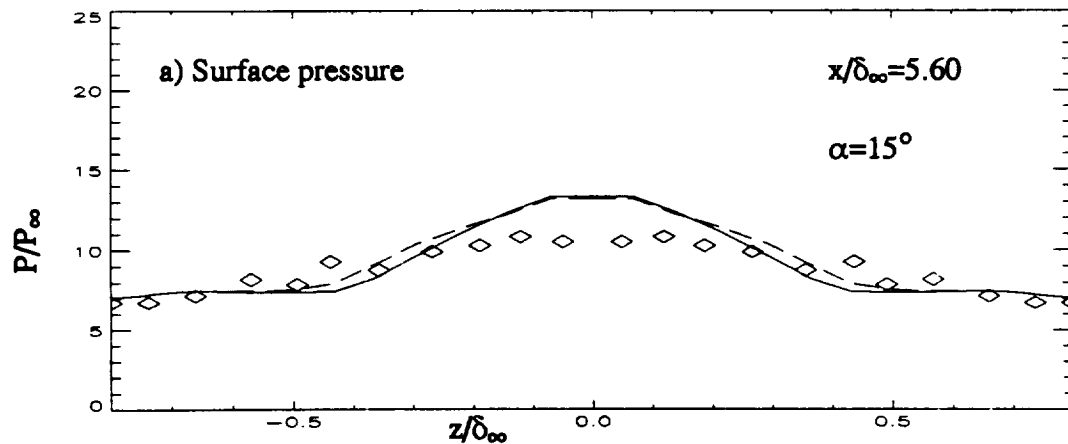


Fig. 12. Surface flow predictions in the symmetry plane of the 3-D crossing shock flow ( $\alpha=15^\circ$  case) of Kussoy and Horstman (1992), geometry shown in Fig. 4. (Symbols represent experimental data, —  $k-\omega$  model, and ---  $k-\omega$  model with corrections).



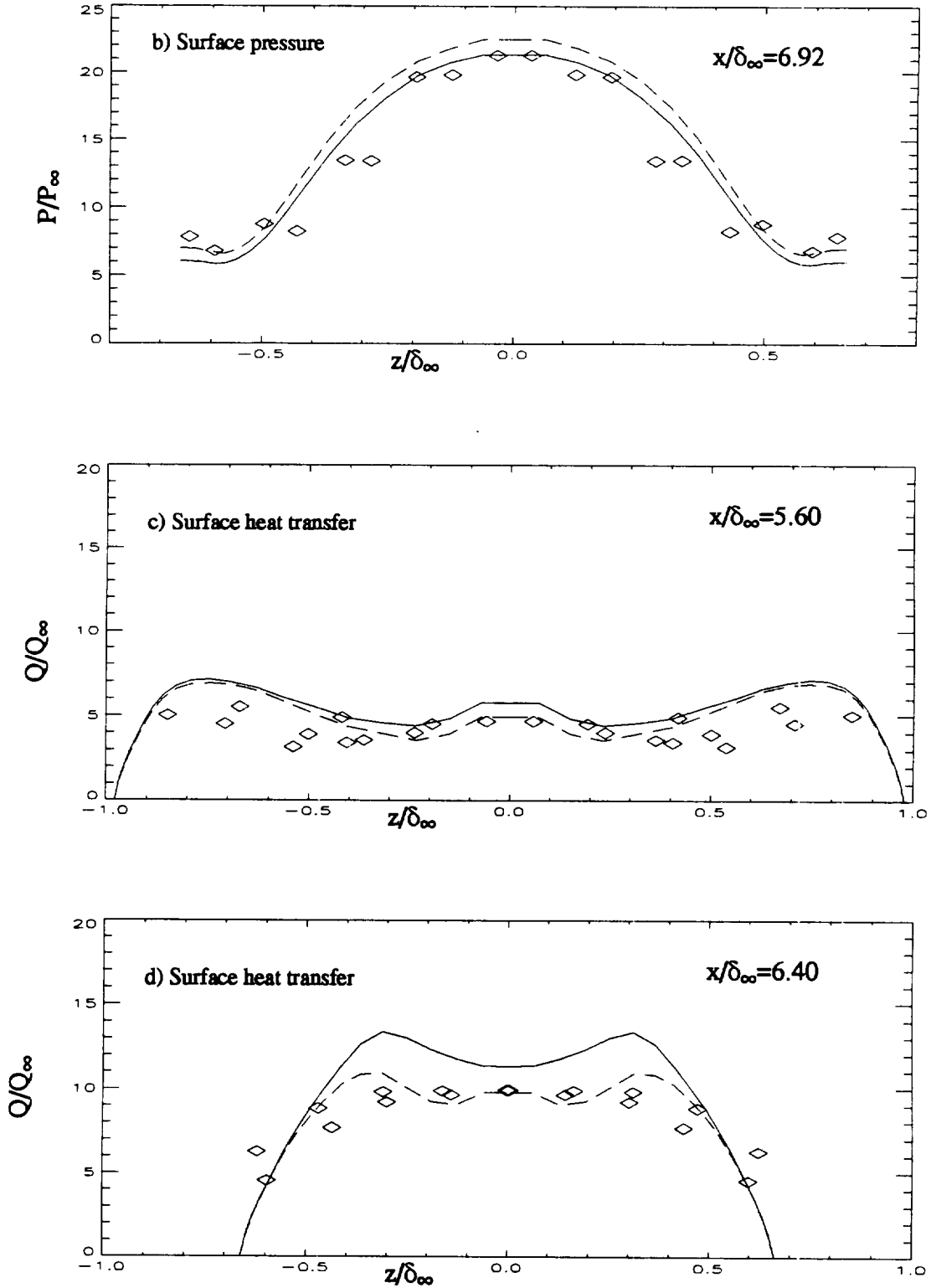
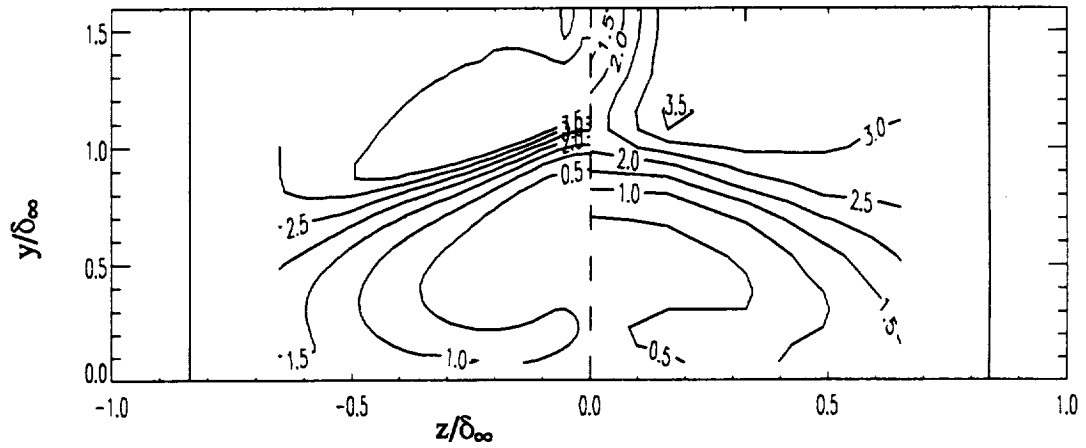
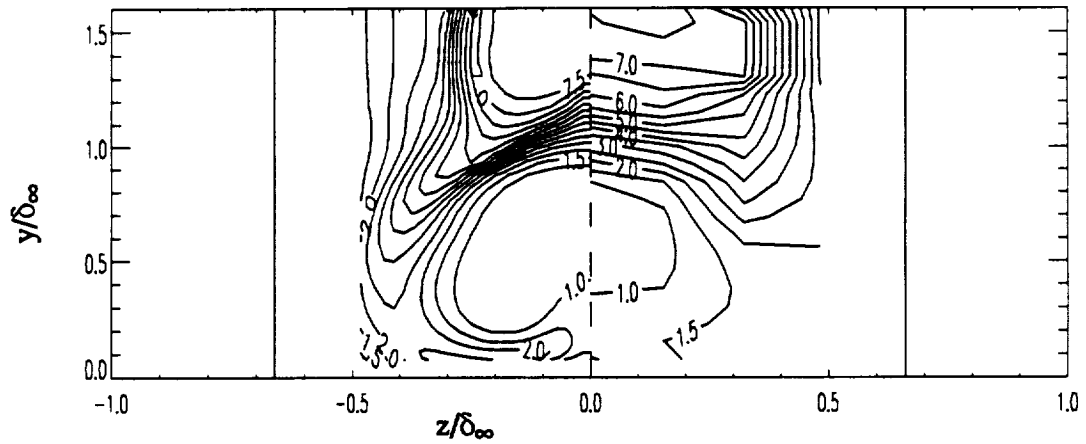


Fig. 13. Surface flow quantities in the 3-D crossing shock interaction flow ( $\alpha=15^\circ$  case) of Kussoy and Horstman (1992), geometry shown in Fig. 4. (Symbols represent experimental data, —  $k-\omega$  model, and ---  $k-\omega$  model with corrections).

SIMULATION -  $x/\delta_\infty = 5.6$  - EXPERIMENT



SIMULATION -  $x/\delta_\infty = 6.9$  - EXPERIMENT



SIMULATION -  $x/\delta_\infty = 8.3$  - EXPERIMENT

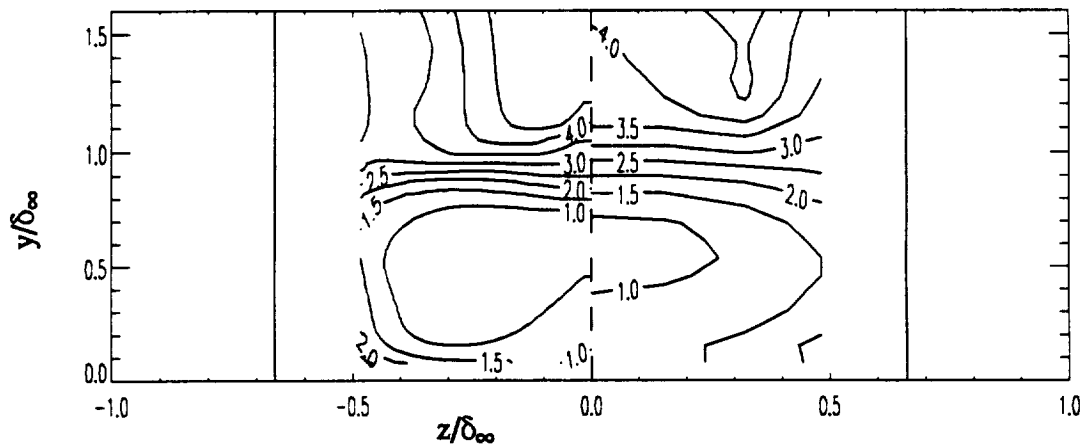


Fig. 14. Pitot pressure contours on cross-sections of 3-D crossing shock interaction flow ( $\alpha=15^\circ$  case) of Kusoy and Horstman (1992), geometry shown in Fig. 4. (The fin leading edges are located at  $x = 0$ , and  $\delta_\infty$  is the thickness of the undisturbed turbulent boundary layer at  $x = 0$ ).







100B

## **AIAA 94-1905**

# **Three-Dimensional Navier-Stokes Simulations with Two-Equation Turbulence Models of Inter- secting Shock-Waves/Turbulent Boundary Layer at Mach 8.3**

J.E. Bardina,  
MCAT Institute,  
Sunnyvale, CA  
T.J. Coakley,  
NASA Ames Research Center,  
Moffett Field, CA

**12th AIAA Applied Aerodynamics Conference**  
June 20-23, 1994/Colorado Springs, Colorado



# THREE-DIMENSIONAL NAVIER-STOKES SIMULATIONS WITH TWO-EQUATION TURBULENCE MODELS OF INTERSECTING SHOCK-WAVES/TURBULENT BOUNDARY LAYER AT MACH 8.3

J.E. Bardina\*

MCAT Institute,  
Sunnyvale, California

T.J. Coakley†

NASA Ames Research Center,  
Moffett Field, California

## **Abstract**

An investigation of the numerical simulation with two-equation turbulence models of a three-dimensional hypersonic intersecting (SWTBL) shock-wave/turbulent boundary layer interaction flow is presented. The flows are solved with an efficient implicit upwind flux-difference split Reynolds-averaged Navier-Stokes code. Numerical results are compared with experimental data for a flow at Mach 8.28 and Reynolds number  $5.3 \cdot 10^6$  with crossing shock-waves and expansion fans generated by two lateral 15 fins located on top of a cold-wall plate. This experiment belongs to the hypersonic database for modeling validation. Simulations show the development of two primary counter-rotating cross-flow vortices and secondary turbulent structures under the main vortices and in each corner singularity inside the turbulent boundary layer. A significant loss of total pressure is produced by the complex interaction between the main vortices and the uplifted jet stream of the boundary layer. The overall agreement between computational and experimental data is generally good. The turbulence modeling corrections show improvements in the predictions of surface heat transfer distribution and an increase in the strength of the cross-flow vortices. Accurate predictions of the outflow flowfield is found to require accurate modeling of the laminar/turbulent boundary layers on the fin walls.

## **Introduction**

The present investigation is a continuous research effort to develop, verify and apply two-equation turbulence models for three-dimensional compressible turbulent flows<sup>1-8</sup>. Two-equation turbulence models are simple, general, robust, and efficient for CFD applications on high speed flows. Their simplicity is mainly due to the eddy

viscosity hypothesis; their generality is built on the use of transport equations to define turbulent velocity- and length-scale instead of algebraic definitions; their robustness is based on recent advances on numerical methods; and their efficiency is based on continuous improvements of present numerical processors. There is clear evidence showing that most widely used two-equation models tend to under-predict flow separation and over-predict heat transfer near flow re-attachment regions. In hypersonic flow calculations, these model deficiencies are even more pronounced, particularly regarding their inability to predict the extent of the flow separation.

In a recent investigation, Bardina and Coakley<sup>1</sup> tested two model corrections that were designed to remedy the above mentioned difficulties for 3-D hypersonic flows. Previously, Coakley and Huang<sup>2</sup> tested these model corrections against experimental data in 2-D compressible flows. The first one limits the turbulence length scale to be no greater than the von Kármán length scale. This correction is equivalent to the use of a one-equation model in regions where the length scale of the two-equation model is larger than the von Kármán length scale. The main effect of this correction was observed to reduce the heat transfer rate near flow-reattachment in agreement with experimental observations. The second model correction, designed to increase the extend of separation, causes the length scale to decrease (or increase) when the flow undergoes rapid compression (or expansion).

The development and validation of turbulence models for hypersonic shock-wave/turbulent boundary layer interactions is based on the fundamental understanding of the turbulence physics of the flows and the availability of an acceptable experimental database. In a parallel research effort to this investigation, Settles and Dodson<sup>9-11</sup> have completed an extensive review of the available experimental data on compressible turbulent high-speed flows suitable for turbulence model validation. This research was developed for the (NASP) National AeroSpace Plane program in the Modeling and Experimental Validation Branch at NASA Ames Research Center. The review of 2-D and 3-D flows includes complex hypersonic flows with pressure profiles, skin friction, wall heat transfer, yaw

Copyright © 1994 by the American Institute of Aeronautics and Astronautics, Inc. No copyright is asserted in the United States under Title 17, U.S. Code. The U.S. Government has a royalty-free license to exercise all rights under the copyright claimed herein for Governmental purposes. All other rights are reserved by the copyright owner

\* Senior Research Scientist.

† Research Scientist. Member AIAA.

angles, pitot pressure, and turbulence statistics data. In this paper, we present comparisons of numerical simulation results and the selected experimental data of Kussoy and Horstman<sup>12</sup> on intersecting shock-waves/ turbulent boundary layer (ISWTBL) interactions. This simple geometry shows complex turbulence structures of great interest in the design of uniform high-pressure flows at the entrance of inlets.

### **Turbulence Models**

The turbulence models used in this study are the two-equation  $k-\omega$  model of Wilcox<sup>13,14</sup>, the  $k-\epsilon$  model of Launder and Sharma<sup>15</sup>, the SST ( $k-\omega/k-\epsilon$ ) model of Menter<sup>16</sup> and the algebraic eddy viscosity model formulation of Baldwin and Lomax<sup>17</sup>. The two-equation  $k-\omega$  model is also studied with the compressibility model corrections, in particular, the length-scale and the separation corrections. A detailed description of these models is found in the references, and a detailed description of these models, including the model corrections is found in references 2 and 4. The main aim of the present effort is to further study the effects of the compressibility corrections in the simulation of complex 3-D flows. Currently, research on improved compressibility corrections for turbulence modeling is being performed to account for the complex effects encountered in shock boundary layer interactions.

### **Numerical Method**

The cost-effective engineering design of aerospace vehicles encountering subsonic, transonic, supersonic and hypersonic speeds requires advanced and efficient computational fluid dynamics (CFD) technology<sup>8</sup>. Accurate aerodynamic prediction of complex full 3-D flow fields and the integration of different areas of technology and research are presently required to account for the significant nonlinear effects on aerodynamic coefficients, lift, drag, and heat load. An improved 3-D Navier-Stokes code has been further developed to efficiently validate turbulence models for high speed flows. The general methodology is found in Bardina<sup>3</sup>, and therefore only a brief description of the method is given below.

The model equations are the 3-D compressible Reynolds-averaged Navier-Stokes equations Turbulence Models in a general curvilinear coordinate system with mass-averaged and non-dimensional variables. All flux differences are treated implicitly in order to increase stability and to be able to use large increments of time or CFL numbers. The numerical scheme for the viscous fluxes is second-order central difference, while the numerical scheme for the inviscid fluxes is a higher-order TVD upwind flux-difference splitting. The higher-order TVD scheme has the capability to represent first-order upwind, second-order upwind, third-order upwind biased, second-

order Fromm scheme, and other combinations of second-order upwind and central differences.

The efficiency of the method is based on an implicit symmetric Gauss-Seidel "method of planes" relaxation scheme with alternating directional space marching sweeps along one coordinate direction, Newton-Raphson inner iteration procedure with an implicit block-tridiagonal diagonally dominant approximate factorization relaxation scheme along the other two directions. This method requires less data in central memory and less total transfer of data into central memory per iteration than implicit upwind schemes using only time-dependent approximate factorizations; therefore, the capability of processing larger and/or complex data bases and computational grids is available. The data is conveniently stored on successive planes along the streamwise coordinate, and the system of equations is solved twice in each successive plane first along the forward direction and afterwards along the backward direction. The repeated solution procedure provides an effective Newton-Raphson convergence acceleration. In each plane the solution is obtained by a two level diagonally dominant approximate factorization DDADI procedure<sup>13</sup>. The space marching alternating directional sweeps in the streamwise coordinate are von Neumann unconditionally stable for zones of subsonic and streamwise separated and reversed flows as well as supersonic flow. As the more restrictive PNS techniques, the present space marching method results in improved propagation of nonlinear effects to accelerate convergence to steady state, generally in about one order of magnitude fewer iterations than approximated factorization methods.

This method combines the best features of data management and computational efficiency of space marching procedures with the generality and stability of time dependent Navier-Stokes procedures to solve flows with mixed subsonic and supersonic zones, including streamwise separated flows. Its robust stability derives from a combination of conservative implicit upwind flux difference splitting, inner approximation procedure in grid cells where changes of eigenvalue sign are present, diagonally dominant approximate factorization and relaxation scheme, flux limiters of higher-order flux differences, and well-posed characteristic-based implicit boundary approximations. It provides the capability of predicting complex flow structures in complex geometries with good accuracy.

### **Boundary Conditions**

Mathematically well posed implicit characteristic-based boundary procedures were imposed at every boundary point. The equilibrium turbulent boundary layer was prescribed at the inflow boundary points. The inflow profile matched the experimental displacement thickness,  $\delta^*_\infty = 0.0126$  m, located at 1.62 m from the leading edge of

the flat plate. On the fin and flat plate boundary points, constant wall temperature ( $T_w=300\text{ }^\circ\text{K}$ ) and no slip conditions were imposed; the turbulent kinetic energy  $k$  and its dissipation rate  $\epsilon$  were set equal to zero;  $\omega$  was set equal to 10 times greater than the corresponding theoretical value at the first point off the wall. On the symmetry plane, no flow through and zero-gradient extrapolation of density, pressure, streamwise velocity, and turbulence variables were imposed. On the upper free-flow plane and other inflow/outflow boundary points, finite difference was imposed both along and toward the boundaries. The procedure automatically determined whether the fluid was flowing locally toward or from the boundary, and it imposed appropriate conditions accordingly. If the inflow was subsonic, no changes in entropy, tangential velocity components, enthalpy, and turbulence variables were imposed. If the outflow was subsonic, no pressure gradient was imposed since only one characteristic-based boundary approximation was required in the differences toward the boundary. If the outflow was supersonic, the solution was naturally extrapolated with the upwind scheme with no external boundary approximations. These boundary approximations have been proven to be effective in previous simulations and free stream has been effectively maintained<sup>3</sup>.

### **Code Performance**

The numerical simulations in the Cray Y-MP C90 supercomputer located at NASA Ames Research Center performed at a rate of 51 MIPS and 288 MFLOPS. Simulations studies were done with  $101 \times 61 \times 41$  and  $231 \times 81 \times 81$  grid points. Small differences between the solutions were observed in the surface pressure and heat transfer distributions, more differences were observed in the flow structures. The fine mesh solutions provided the best resolution of the turbulence structures, while the less refine mesh solutions are considered accurate for engineering purposes. Most results presented here were obtained with the  $101 \times 61 \times 41$  grid and required less than 6 hours of CPU time and less than 600 sweeps (or global iterations) to achieve convergence to steady state. The performance of this diagonal-dominant implicit upwind code shows at least one order of magnitude better efficiency than other Navier-Stokes codes based on well-known central-difference numerical methods.

### **Intersecting Shock-Waves/Turbulent Boundary Layer Interaction (ISWBLI)**

The Ames experiment of Kussoy and Horstman<sup>12</sup> on 3-D shock-wave boundary-layer interactions was used here to test the compressible turbulence models and the model corrections. This experiment studies the interactions of two intersecting hypersonic shock waves with a thick turbulent boundary layer. The experimental configurations reflect several key elements of generic hypersonic

inlets, thick turbulent boundary-layer approaching two vertical fins of varying wedge angles, crossing shock-waves, boundary-layer cross-flow vortices, and large pressure gradients. The test body for this series of experiments is shown in fig.1. Two  $15^\circ$  fins mounted on top of a 2.2 m long flat plate generated two planar oblique crossing shock waves on a thick turbulent boundary layer. The free-stream Mach number was  $M_\infty = 8.3$ , the free-stream temperature was  $T_\infty = 80\text{ }^\circ\text{K}$ , the Reynolds number was  $Re_\infty = 5.3 \cdot 10^6$  per meter, and the wall temperature was fixed at  $300\text{ }^\circ\text{K}$ .

The physics of this flow shows a pattern of intersecting shock-waves above the boundary layer and a complex set of cross-flow vortices and structures inside of the turbulent boundary layer. Previous experimental and computational analyses have provided a general description of the flow fields generated through the interaction of a single shock-wave and a turbulent boundary layer. Settles and Dolling<sup>18</sup> reviewed the early work on this class of turbulent flow interaction, while Kubota and Stollery<sup>19</sup> described the main vortical structure developed inside the boundary layer and under an oblique shock-wave. The interaction of each shock wave with the boundary layer generated a cross-flow vortex separation with a "quasi conical" shape<sup>1,20,21</sup>. Although the "quasi-conical" structure has been used in different studies of turbulence models and conical simulations<sup>21,22</sup>, this approximation has been disputed previously<sup>1</sup>. The comparison of Bardina et al<sup>1</sup> and Knight et al<sup>21</sup> shows that this approximation introduces large errors and make comparisons of turbulence models meaningless. In this particular experiment, the influence of the lateral fins in the flow structures and surface quantities imply the necessity of a full 3-D numerical simulation. This flow is further complicated by the intersection of both counter-rotating cross-flow vortices, which uplifted the flow, producing large losses of total pressure, and generating a very complex flow structure with secondary structures developed under the cross-flow vortices and on the lateral fins. The fins developed their own hypersonic laminar boundary layer with expansion fans and lateral separation. In recent numerical investigations, Narayanaswami et al<sup>23</sup> used the algebraic mixing-length model of Baldwin and Lomax, and the modified  $k-\epsilon$  model of Rodi<sup>22</sup> for the turbulent eddy viscosity. Their results showed qualitative agreement with experimental data, peak surface pressures and heat transfer data are overpredicted. Gaitonde and Shang<sup>24</sup> have used the Baldwin and Lomax turbulence model and Roe's flux-difference split upwind numerical scheme. Their results show agreement with surface pressure data, and overprediction of surface heat transfer data.

A selected comparison between experimental data and numerical simulation results is described below. In general, symbols in the figures shown below represent the experimental data points, the solid lines show solutions

obtained with two-equation turbulence models, and the dash lines show solutions obtained with two-equation turbulence models and model corrections (length-scale and rapid compression corrections).

### **Velocity vectors**

A set of velocity vector plots are shown in Figure 2. These results were obtained with the  $k-\omega$  model including the length-scale and rapid compression corrections. The fin boundary layers were treated as turbulent below and laminar above the edge of the flat-plate boundary layer. Fig. 2a shows the velocity vectors next to the flat plate surface. It shows the vortex interaction zone, the flow turning and reflections, and the wake-like structure in the downstream zone. Fig. 2b shows the velocity vectors in the symmetry plane between the lateral fins. The main results show the uplifting of the boundary layer flow due to the vortex "collision", and the secondary uplifting and reattachment below the main vortices. Fig. 2c, 2d, 2e, and 2f show velocity vectors in different crossed sections,  $x/\delta_\infty = 3, 6, 9$ , and 12, respectively. They show the formation of two cross-flow vortices as main structures, a center bubble under the main vortices, corner vortices in the fin/plate junctions, and strong flow turnings at the edge of the flat plate boundary layer. The strength of the main vortices is model dependent. Figures 2f, 2g, and 2h compared the standard  $k-\omega$  model with and without model corrections and modeling the fin boundary layer as turbulent/laminar, turbulent, and laminar, respectively. The main feature is the increase of vorticity generated by the model corrections (Fig. 2f and 2h) and the almost disappearance of the main vortices with the standard  $k-\omega$  model (Fig. 2g).

### **Pressure contours**

Figures 3a and 3b show the normalized pressure contours in two cross-section planes. It shows the well known structure of the "quasi-conical" shape, the vortex, the triple point, the slip line. In the center zone, a secondary structure on the plate surface and a pressure wave between the plate surface and the free stream are present. These features show the complexity generated by the double fin interaction, beyond the single fin case.

### **Flow-field yaw angle**

Figures 4a through 4e show the comparison of yaw-angle contours between simulation and experiment on different cross-sectional planes. The main emphasis is to differentiate between the simulations with and without model corrections, and to verify if the treatment of the fin boundary layers affect the results. The flow turning as represented by the yaw-angle is well modeled with the model corrections in Fig. 4b and 4e, especially if we consider the few measurements available in each plane. On the other hand, the absence of the model corrections in Fig. 4d shows almost no turning above the main vortices as shown in the experimental data.

### **Flow-field pitot pressure**

Figures 5a through 5e show the comparison of Pitot pressure contours between simulation and experiment on different

cross-sectional planes. The main emphasis is also to differentiate between the simulations with and without model corrections. The low Pitot pressure zone in the main vortices zone shows agreement with the experimental data, especially if we consider the few experimental measurement points in each plane. The model corrections show larger gradients in Fig. 5b than the simulations without the model corrections in Fig. 5d. The laminar treatment of the fin boundary layers shown in Fig. 5e shows large differences with the turbulent/laminar treatment shown in Fig. 5b.

### **Surface pressure**

Figure 6 shows the comparisons between prediction and experimental data of surface pressure distributions on the flat plate. Fig. 6a shows the centerline profiles between the two lateral fins. Figures 6b, 6c, and 6d show transverse surface pressure distributions at  $x/\delta_\infty = 5.6, 6.92$ , and  $8.31$  boundary layer thicknesses downstream of the fin leading edges, respectively. A wave structure with high and low peaks of static pressure are observed. The pressure rises induced by the shock waves generated by the fin leading edges, and decreases induced by the expansion fans generated by the interior fin corners. The peak pressure value is located at the reattachment zone of the secondary structure formed under the two principal counter-rotating vortices. The first transverse distribution is located in the shock-wave "collision" zone, the second one is located near the peak surface pressure zone generated by the secondary flow re-attachment, and the third one is located near the lower expansion pressure zone. The turbulence models shown here are the  $k-\omega$  model, the SST model and the Baldwin-Lomax model. The  $k-\omega$  model includes the (l) length-scale, (r) separation bubble, and/or (w) rotation corrections. All simulations show good agreement with the experimental data, and the peak values are well predicted within the experimental uncertainty of 10%. Overprediction near the outflow zone is observed when the fin boundary layer are computed as (tur) turbulent boundary layers. If the fin boundary layers are computed as (lam) laminar boundary layers, no overprediction is obtained. The best treatment is obtained when the fin boundary layer is treated as (tur/lam) turbulent below and laminar above the turbulent boundary layer on the flat plate. Different from the results observed with a single fin<sup>1</sup>, the modeling of the fin boundary layers affect the centerline pressure distribution. Since the pressure ratio in this 3-D simulations is smaller than the ones presented in the 2-D hypersonic database experiments<sup>9-11</sup>, the model corrections show only small differences in the numerical predictions.

### **Surface heat transfer rate**

Figure 7 shows the comparisons between prediction and experimental data of surface heat transfer distributions on the flat plate. Similar to the pressure distributions shown in the previous figures 6, Fig. 7a shows the centerline distributions and Figures 7b, 7c, and 7d show the transverse distributions at  $x/\delta_\infty = 5.08, 6.4$ , and  $7.78$ , respectively. A similar wave structure with high and low peaks along the centerline is also observed. The experimental data in the transverse profiles show a flatter distribution in the cross-sectional planes. Recent

simulations of Narayanswami et al<sup>23</sup> and Gaitonde et al<sup>24</sup> showed overprediction of heat transfer rate and "are thought to be associated with deficiencies in turbulence modeling." Therefore, the testing of the turbulence model corrections is of great interest here.

All models showed excellent agreement with the experimental data along the centerline distribution. The small plateau at the beginning of the interaction is not shown in this 101x61x41 grid simulations, however, they are present in the 231x81x81 simulations not shown here. In the transverse distributions, the k-w, SST, and Baldwin-Lomax models show an overprediction which seems to be associated with the cross-flow reattachment. The model corrections improve the predictions and show good agreement with the experimental data in the first two stations shown in Fig 7b and 7c. This agreement is only present when the fin boundary layers are treated as turbulent ones below the edge of the boundary layer on the flat plate. These results support the model corrections and the proper treatment of each boundary layer. Once again, best treatment is obtained when the fin boundary layer is treated as (tur/lam) turbulent below and laminar above the turbulent boundary layer of the flat plate. In the last transverse station shown in Fig. 7d, overprediction in the lateral cross-flow reattachment zone is still observed with all models, and it shows the complexity of this flow.

#### **Total pressure**

Figure 8 shows the normalized total pressure distribution along the streamwise direction. The numerical results<sup>21</sup> obtained by Horstman with Rodi's modified *k-ε* model and Knight with the Baldwin-Lomax model are also included in this figure. The results show a significant loss of about 85% in total pressure due to the boundary layer interaction with the shock-waves forming the two cross-flow vortices as a low total pressure outflow jet. The need to eliminate these inefficiencies in this kind of interaction is a subject of continuous research, including boundary layer bleeding and geometry modifications.

#### **Concluding Remarks**

In this section we summarize the research work, give our principal results and recommendations, and discuss plans for future work. The more promising turbulence model corrections for compressible flows were tested. The agreement with the experimental data is very good in surface pressure, heat transfer rates, yaw angles, and Pitot pressure. The model corrections give improved heat transfer predictions. Different than the single fin simulations, the treatment of the fin boundary layer affects the surface plate predictions. The best results are obtained with the proper turbulent/laminar boundary layer on the fin walls. Accurate and efficient aerodynamic predictions of the intersecting SWTBL interaction have been presented. The present results show that numerical solutions can be efficiently obtained in order to provide a data set for engineering design. The flow structures are well captured within a few grid points and free of oscillations. The predictions in these zones are superior and show detailed primary and secondary turbulence

structures. The physical understanding of these structures is fundamental to improve inlet designs and to improve the compressibility model corrections. This methodology provides a promising computational capability for aerospace vehicles.

#### **Acknowledgments**

This work is sponsored by NASA Ames Research Center, Modeling and Experimental Validation Branch, under Grant NCC 2-15. The authors wish to acknowledge helpful discussions with J.G. Marvin and C.C. Horstman.

#### **References**

1. Bardina, J.E., Coakley, T.J., and Marvin, J.G., "Two-Equation Turbulence Modeling for 3-D Hypersonic Flows," *AIAA-92-5064*, 4th International Aerospace Planes Conference, Orlando, Florida, December, 1992.
2. Coakley, T.J., and Huang, P.G., "Turbulence Modeling for High Speed Flows," *AIAA-92-0436*, Reno, NV, January 1992.
3. Bardina, J. E., "Three-Dimensional Navier-Stokes Method with Two-Equation Turbulence Models for Efficient Numerical Simulation of Hypersonic Flows," *AIAA-94-2950*, Indianapolis, IN, 1994.
4. Coakley, T.J., Horstman, C.C., Marvin, J.G., Viegas, J.R., Bardina, J.E., Huang, P.G., and Kussoy, M.I., "Turbulence Compressibility Corrections," to be published as NASA TM, 1994.
5. Coakley, T. J., and Marvin, J. G., "Compressibility corrections for Hypersonic Flow Turbulence Modeling," 1993 National Aero-Space Plane Technology Review, Monterey, CA, 1993.
6. Coakley, T. J., Huang, P. G., Bardina, J. E., and Viegas, J. R., "Modeling of Turbulence for Complex High Speed Flows," Second National Congress on Computational Mechanics, Washington, D. C., 1993.
7. Huang, P. G., and Coakley, T. J., "Turbulence Modeling for Complex Hypersonic Flows," *AIAA-93-0200*, Reno, NV., January, 1993.
8. Marvin, J.G., "A CFD Validation Roadmap for Hypersonic Flows," published in AGARD-CP-514, *Theoretical and Experimental Methods in Hypersonic Flows*, Reference 17, 1993.
9. Settles, G. S., and Dodson, L. J., "Hypersonic Shock/Boundary-Layer Interaction Database," *NASA CR 177577*, 1991.
10. Settles, G. S., and Dodson, L. J., "Hypersonic Turbulent Boundary-Layers and Free-Shear Layer Database," *NASA CR 1776*, 1993.
11. Settles, G. S., and Dodson, L. J., "Hypersonic Shock/Boundary-Layer Interaction Database: New and Corrected Data," Dept. of Mech. Engrg., Penn State Univ., University Park, PA; also to be published as *NASA CR*, 1993.

12. Kussoy, M.I., and Horstman, K.C., "Intersecting Shock\_Wave/Turbulent Boundary Layer Interactions at Mach 8.3," *NASA TM 103909*, 1992.
13. Wilcox, D.C., "A Half Century Historical Review of the  $k-\omega$  Model," *AIAA-91-0615*, Reno, NV, January, 1991.
14. Wilcox, D.C., "Progress in Turbulence Modeling," *AIAA-91-1785*, Honolulu, HI, June 1991.
15. Launder, B.E., and Sharma, B.I., "Application of the Energy-Dissipation Model of Turbulence to the Calculation of Flow Near a Spinning Disk," *Letters in Heat and Mass Transfer*, Vol. 1, 1974, pp. 131-138.
16. Menter, F.R., "Zonal Two Equation  $k-\omega$  Turbulence Models for Aerodynamic Flows," *AIAA-93-2906*, Orlando, FL, June 1993.
17. Baldwin, B.S., and Lomax, H., "Thin Layer Approximation and Algebraic Model for Separated Turbulent Flows," *AIAA-73-257*, 1973.
18. Settles, G.S., and Dolling, D.S., "Swept Shock/Boundary Layer Interactions: Tutorial and Update," *AIAA-90-0375*, Reno, NV, January, 1990.
19. Kubota, H., and Stollery, J., "An Experimental Study of the Interaction Between a Glancing Shock Wave and a Turbulent Boundary layer," *J. Fluid Mech.*, 116, 1982, pp. 431-458.
20. Knight, D. D., Badekas, D., Horstman, C. C., and Settles, G. S., "On the Quasi-conical Flowfield Structure of the 3-D Single Fin Interaction," *AIAA J.*, Vol. 30, No. 12, 1992, pp. 2809-2816.
21. Knight, D.D., Horstman, C.C., and Monson, D.J., "The Hypersonic Shock Wave-Turbulent Boundary Layer Interaction Generated by a Sharp Fin at mach 8.2," *AIAA-92-0747*, Reno, NV, January, 1992.
22. Rodi, W., "Experience with Two-Layer Models Combining the  $k-\epsilon$  with a One-equation Model near the Wall," *AIAA-91-0216*, Reno, NV, January, 1991.
23. Narayanswami, Horstman, C. C., and Knight, D. D., "Computation of Crossing Shock/Turbulent Boundary Layer Interaction at Mach 8.3," *AIAA-93-0779*, Reno, NV, January, 1993.
24. Gaitonde, D., and Shang, J.S., "Calculations on a Double-Fin Turbulent Interaction at High speed," *AIAA-93-3432*, Monterey, CA, August, 1993.

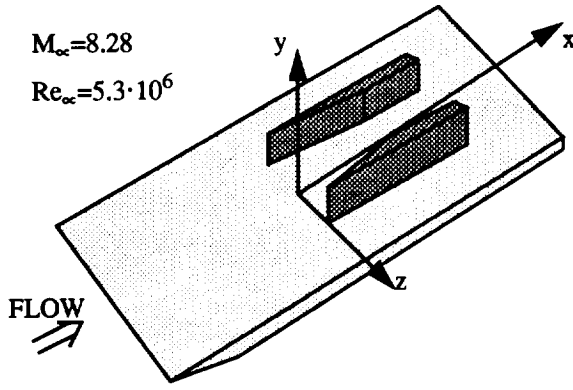


Fig. 1. Geometry of flat-plate with two 15° lateral fins.

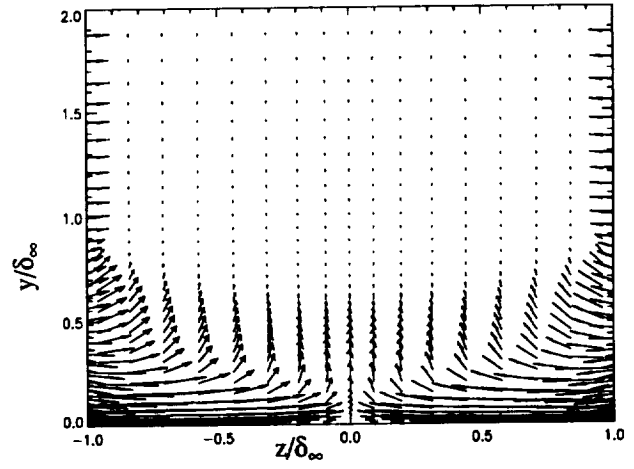


Fig. 2c. Velocity vectors on crossflow plane located at  $x/\delta_\infty = 3$ .  $k-\omega$  model with model corrections.

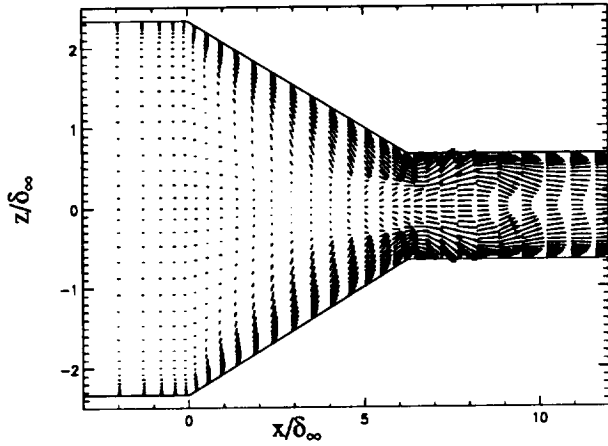


Fig. 2a. Velocity vectors on top of flat-plate surface.  $k-\omega$  model with model corrections.

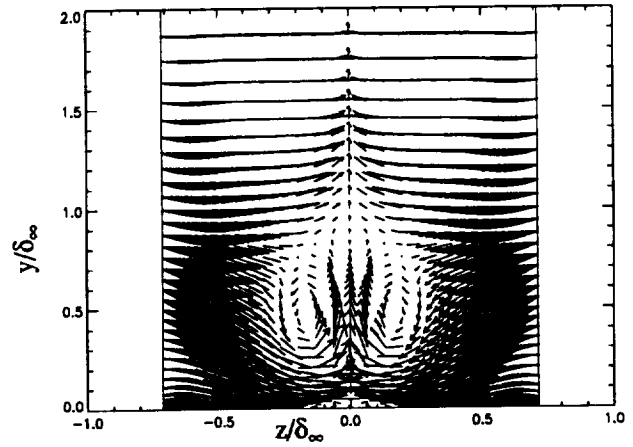


Fig. 2d. Velocity vectors on crossflow plane located at  $x/\delta_\infty = 6$ .  $k-\omega$  model with model corrections.

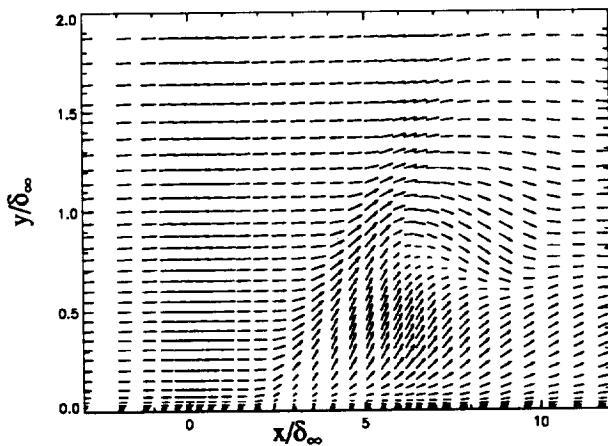


Fig. 2b. Velocity vectors on symmetry plane ( $Z = 0$ ) between lateral turbulent/laminar boundary layer fins.  $k-\omega$  model with model corrections.

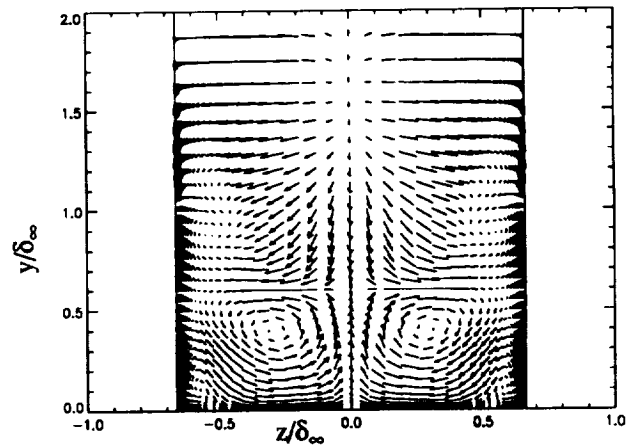


Fig. 2e. Velocity vectors on crossflow plane located at  $x/\delta_\infty = 9$ .  $k-\omega$  model with model corrections.

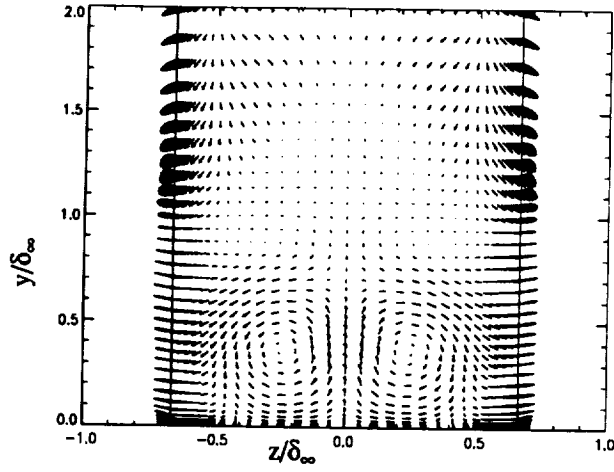


Fig. 2f. Velocity vectors on crossflow plane located at  $x/\delta_\infty = 12$  and turbulent/laminar fin.  $k-\omega$  model with model corrections.

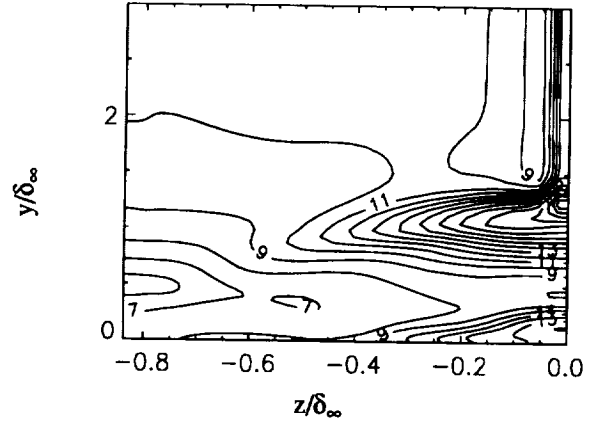


Fig. 3a. Normalized pressure contours on crossflow plane located at  $x/\delta_\infty = 6$  and turbulent/laminar fin.  $k-\omega$  model with model corrections.

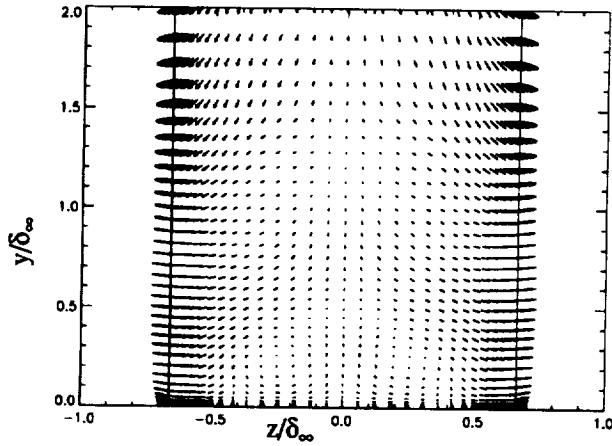


Fig. 2g. Velocity vectors on crossflow plane located at  $x/\delta_\infty = 12$  and turbulent fin.  $k-\omega$  model with no model corrections.

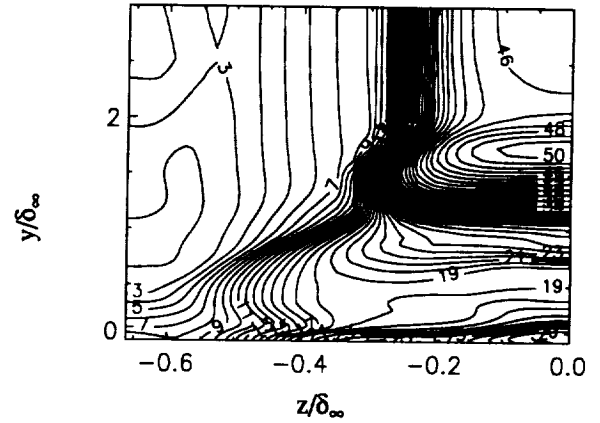


Fig. 3b. Normalized pressure contours on crossflow plane located at  $x/\delta_\infty = 9$  and turbulent/laminar fin.  $k-\omega$  model with model corrections.

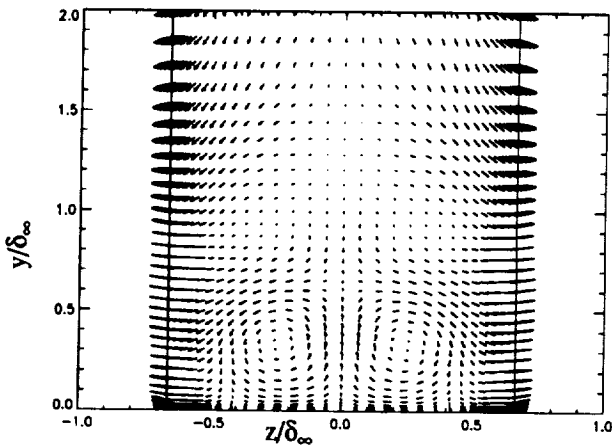


Fig. 2h. Velocity vectors on crossflow plane located at  $x/\delta_\infty = 12$  and laminar fin.  $k-\omega$  model with model corrections.

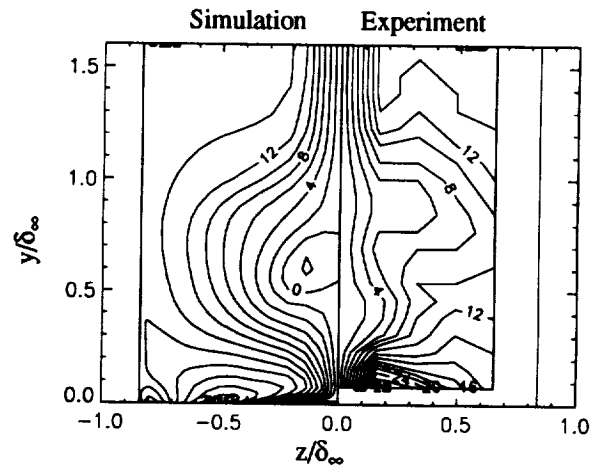


Fig. 4a. Yaw angle contours on crossflow plane located at  $x/\delta_\infty = 5.6$  and turbulent/laminar fin with  $k-\omega$  model and model corrections.

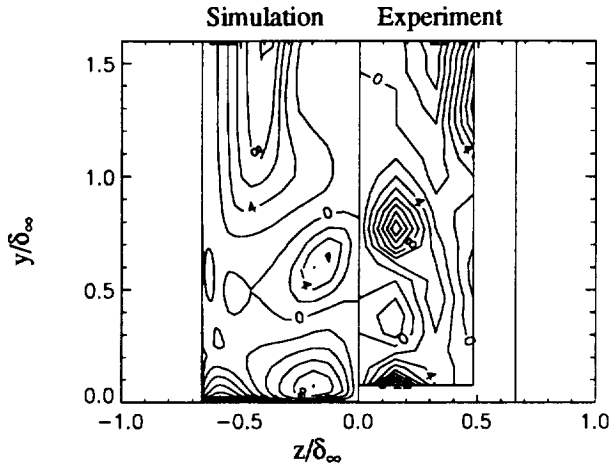


Fig. 4b. Yaw angle contours on crossflow plane located at  $x/\delta_\infty = 6.92$  and turbulent/laminar fin with  $k-\omega$  model and model corrections.

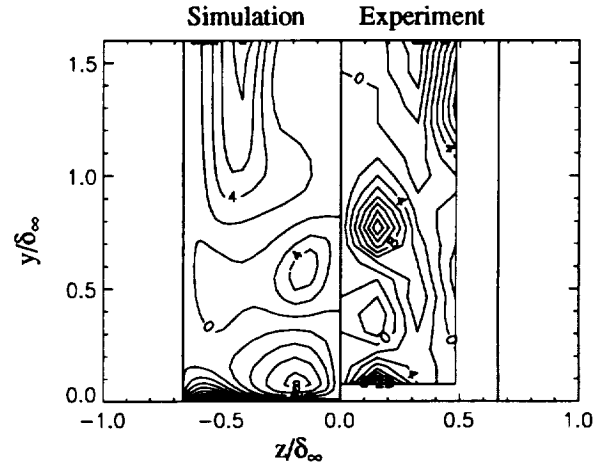


Fig. 4e. Yaw angle contours on crossflow plane located at  $x/\delta_\infty = 6.92$  and laminar fin with  $k-\omega$  model and model corrections.

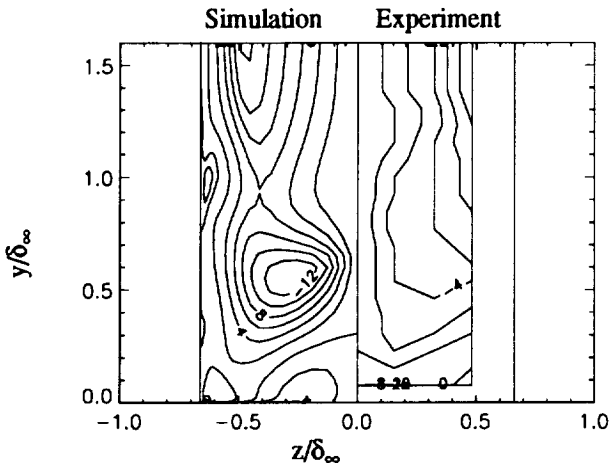


Fig. 4c. Yaw angle contours on crossflow plane located at  $x/\delta_\infty = 8.3$  and turbulent/laminar fin with  $k-\omega$  model and model corrections.

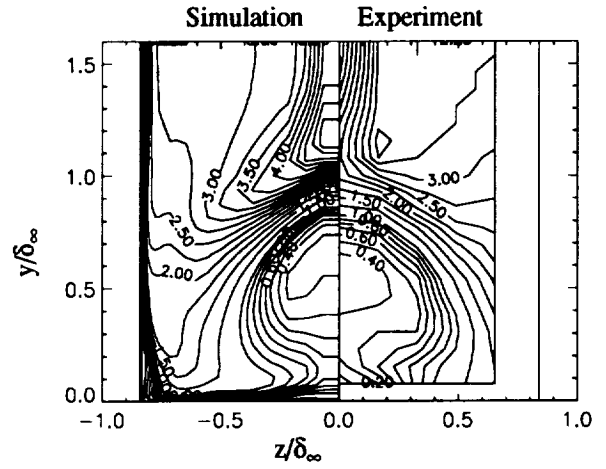


Fig. 5a. Pitot pressure contours on crossflow plane located at  $x/\delta_\infty = 5.6$  and turbulent/laminar fin with  $k-\omega$  model and model corrections.

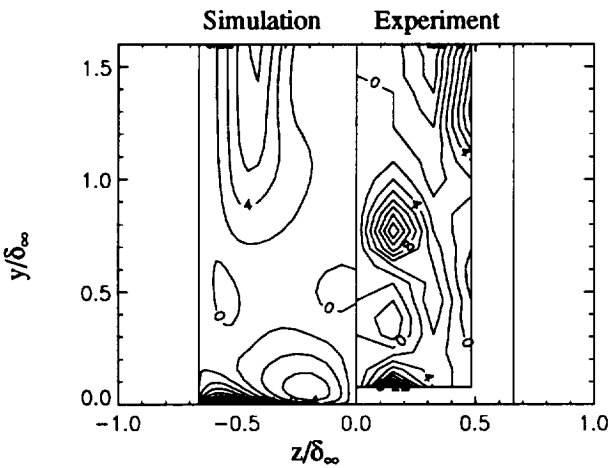


Fig. 4d. Yaw angle contours on crossflow plane located at  $x/\delta_\infty = 6.92$  and turbulent fin with  $k-\omega$  model and no model corrections

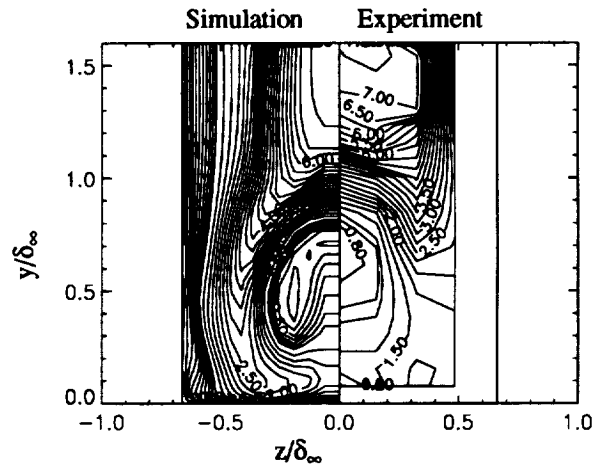


Fig. 5b. Pitot pressure contours on crossflow plane located at  $x/\delta_\infty = 6.92$  and turbulent/laminar fin with  $k-\omega$  model and model corrections.

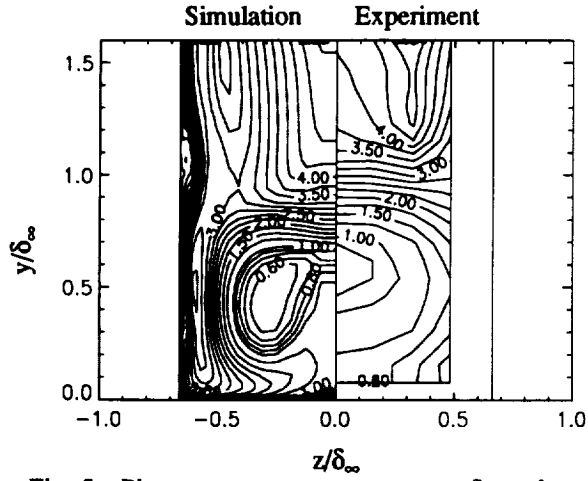


Fig. 5c. Pitot pressure contours on crossflow plane located at  $x/\delta_\infty = 8.3$  and turbulent/laminar fin with  $k-\omega$  model and model corrections.

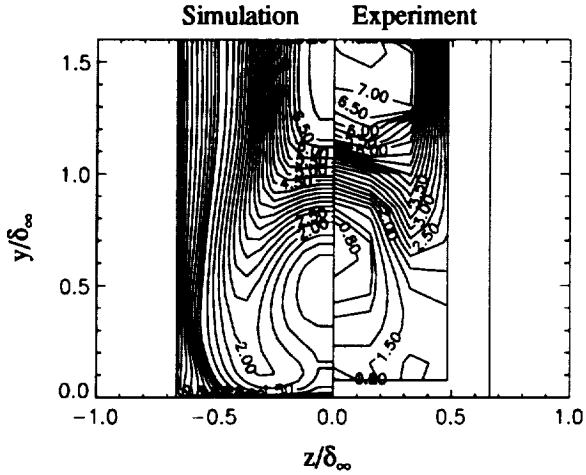


Fig. 5d. Pitot pressure contours on crossflow plane located at  $x/\delta_\infty = 6.92$  and turbulent fin with  $k-\omega$  model and no model corrections.

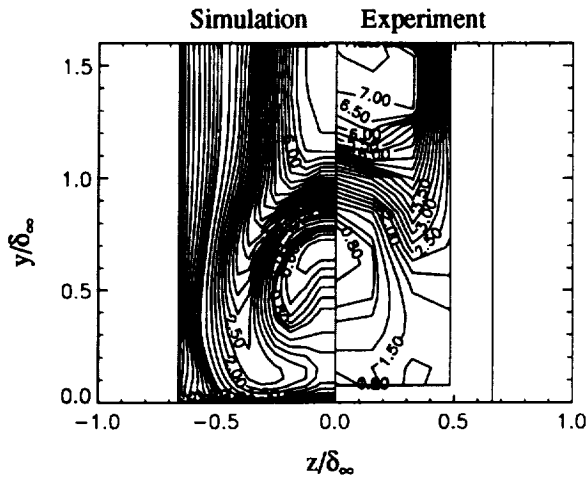


Fig. 5e. Pitot pressure contours on crossflow plane located at  $x/\delta_\infty = 6.92$  and laminar fin with  $k-\omega$  model and model corrections.

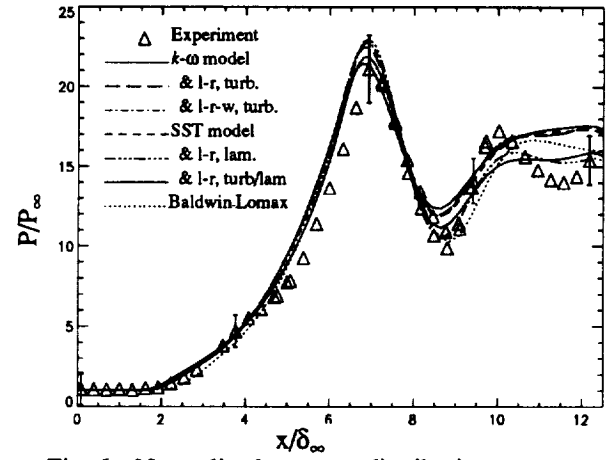


Fig. 6a. Normalized pressure distribution on centerline plane,  $z/\delta_\infty = 0$  and  $y/\delta_\infty = 0$ .

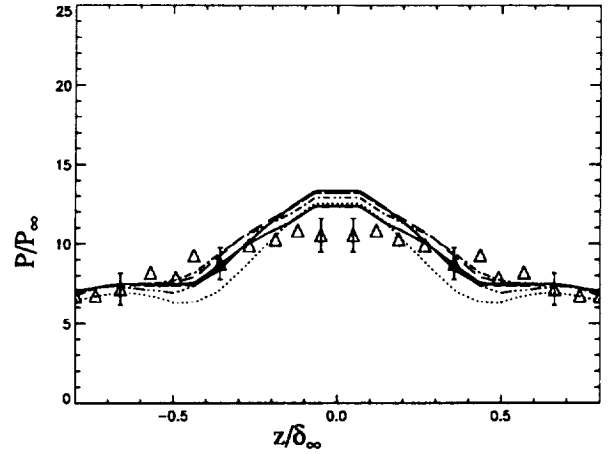


Fig. 6b. Normalized pressure distribution on crossflow plane located at  $x/\delta_\infty = 5.6$  and  $y/\delta_\infty = 0$ .

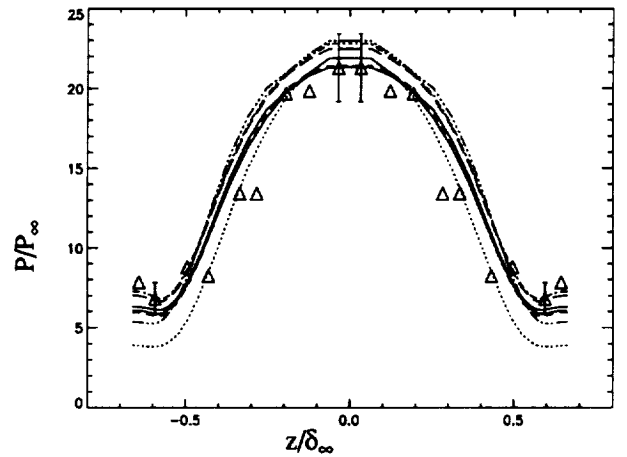


Fig. 6c. Normalized pressure distribution on crossflow plane located at  $x/\delta_\infty = 6.92$  and  $y/\delta_\infty = 0$ .

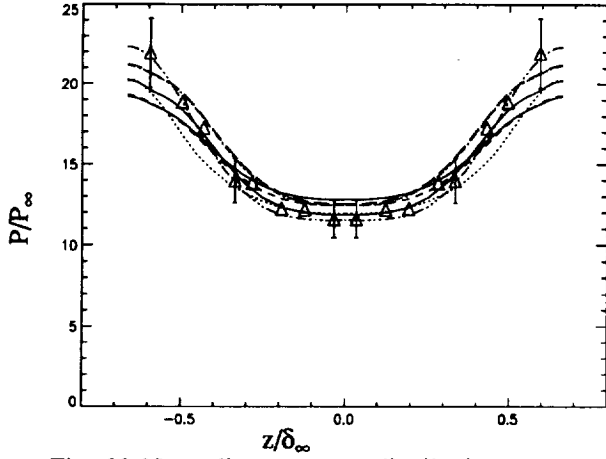


Fig. 6d. Normalized pressure distribution on cross-flow plane located at  $x/\delta_\infty = 8.3$  and  $y/\delta_\infty = 0$ .

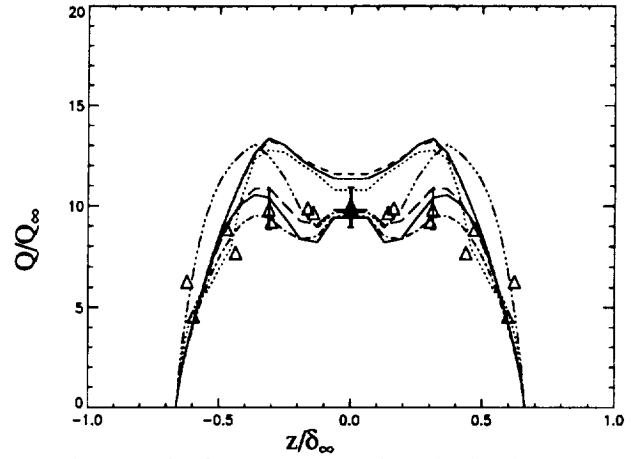


Fig. 7c. Surface heat transfer distribution on crossflow plane located at  $x/\delta_\infty = 6.4$  and  $y/\delta_\infty = 0$ .

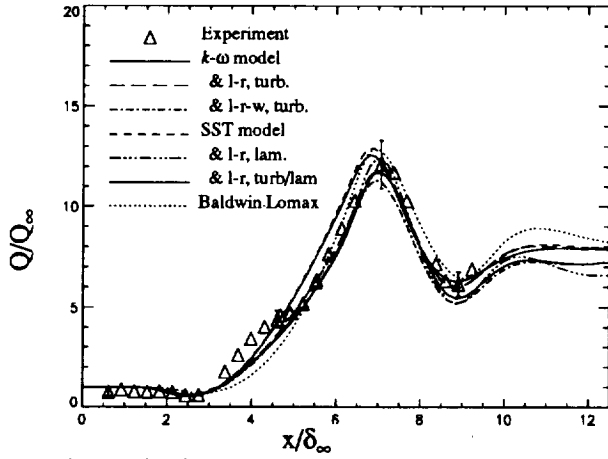


Fig. 7a. Surface heat transfer distribution on center-line plane,  $z/\delta_\infty = 0$  and  $y/\delta_\infty = 0$ .

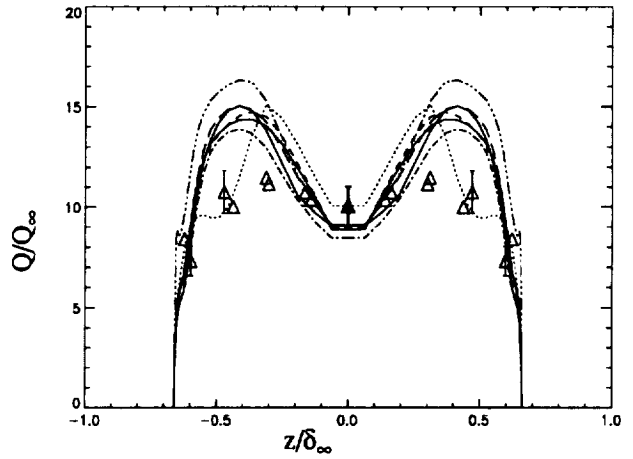


Fig. 7d. Surface heat transfer distribution on crossflow plane located at  $x/\delta_\infty = 7.78$  and  $y/\delta_\infty = 0$ .

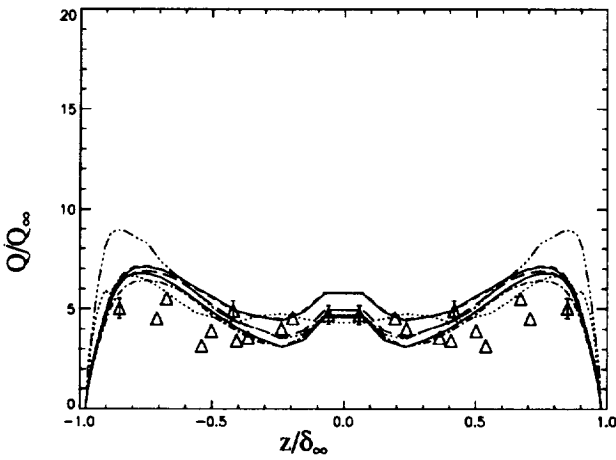


Fig. 7b. Surface heat transfer distribution on cross-flow plane located at  $x/\delta_\infty = 5.08$  and  $y/\delta_\infty = 0$ .

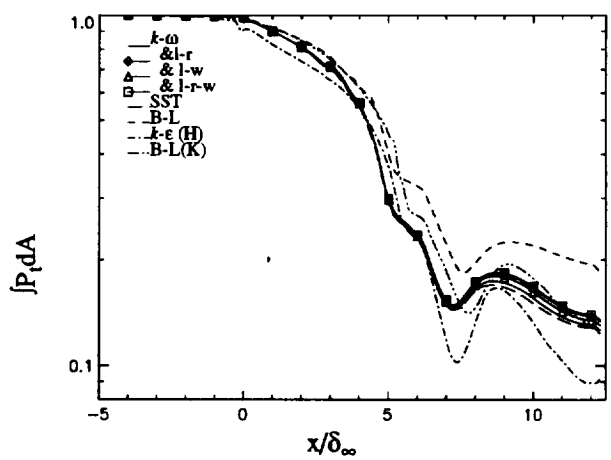


Fig. 8. Normalized integrated total pressure distribution.

## ***NOTES***



NDB

**AIAA 94-2950**

**Three-Dimensional Navier-Stokes Method with  
Two-Equation Turbulence Models for Efficient  
Numerical Simulation of Hypersonic Flows**

J.E. Bardina,  
MCAT Institute,  
Sunnyvale, CA

**30th AIAA/ASME/SAE/ASEE  
Joint Propulsion Conference and Exhibit**  
June 27-29, 1994/Indianapolis, Indiana



# THREE-DIMENSIONAL NAVIER-STOKES METHOD WITH TWO-EQUATION TURBULENCE MODELS FOR EFFICIENT NUMERICAL SIMULATION OF HYPERSONIC FLOWS

J.E. Bardina\*  
MCAT Institute,  
Sunnyvale, California

## **Abstract**

A new computational efficient 3-D compressible Reynolds-averaged implicit Navier-Stokes method with advanced two-equation turbulence models for high speed flows is presented. All convective terms are modeled using an entropy satisfying higher-order Total Variation Diminishing (TVD) scheme based on implicit upwind flux-difference split approximations and arithmetic averaging procedure of primitive variables. This method combines the best features of data management and computational efficiency of space marching procedures with the generality and stability of time dependent Navier-Stokes procedures to solve flows with mixed supersonic and subsonic zones, including streamwise separated flows. Its robust stability derives from a combination of conservative implicit upwind flux-difference splitting with Roe's property U to provide accurate shock capturing capability that non-conservative schemes do not guarantee, alternating symmetric Gauss-Seidel "method of planes" relaxation procedure coupled with a three-dimensional two-factor diagonal-dominant approximate factorization scheme, TVD flux limiters of higher-order flux differences satisfying realizability, and well-posed characteristic-based implicit boundary-point approximations consistent with the local characteristics domain of dependence. The efficiency of the method is highly increased with Newton-Raphson acceleration which allows convergence in essentially one forward sweep for supersonic flows.

The method is verified by comparing with experiment and other Navier-Stokes methods. Here, results of adiabatic and cooled flat plate flows, compression corner flow, and 3-D hypersonic shock-wave/turbulent boundary layer interaction flows are presented. The robust 3-D method achieves a better computational efficiency of at least one order of magnitude over the CNS Navier-Stokes code. It provides cost-effective aerodynamic predictions in agreement with experiment, and the capability of predicting

complex flow structures in complex geometries with good accuracy.

## **Introduction**

A new improved 3-D Navier-Stokes code<sup>1,2</sup> has been developed to efficiently validate turbulence models for high speed flows. The cost-effective engineering design of aerospace vehicles encountering subsonic, transonic, supersonic and hypersonic speeds requires advanced and efficient computational fluid dynamics (CFD) technology<sup>3</sup>. Accurate aerodynamic prediction of complex full 3-D flow fields and the integration of different areas of technology and research are presently required to account for the significant nonlinear effects on aerodynamic coefficients, lift, drag, and heat load.

In this last decade, a substantial research effort has been conducted on the development of upwind methods for the numerical treatment of the convective terms of the Navier-Stokes equations<sup>4-18</sup>. Three generations of numerical methods can be differentiated. The first generation is represented by McCormack's predictor-corrector method<sup>4</sup> for aerodynamic predictions. The second generation is represented by implicit central-difference approximation schemes<sup>5,6</sup> with dimensionally split approximated factorizations, explicit and implicit artificial viscosity terms, and explicit boundary approximations. Although these methods have been shown not to be von Neuman unconditionally stable<sup>14,16,17</sup> in the absence of smoothing procedures, they have been proven effective in transonic flow-field predictions in respective time and space marching implementations. In highly nonlinear and rapidly varying flow fields, performance has not been as satisfactory. The predictions are largely governed by the sensitive upstream movements of shocks with increasing Mach number, and the computational accuracy and numerical stability become of major importance<sup>8-17</sup>. Intimately related to the shocks are precursor expansions which are equally difficult and important to treat accurately. A final computational detail available for improvement is the ability to accurately compute flow in the vicinity of contact discontinuities which appear in streamwise and cross-flow separations, for example.

The third generation of numerical methods is represented by upwind split-difference approximation schemes

---

Copyright © 1994 by the American Institute of Aeronautics and Astronautics, Inc. No copyright is asserted in the United States under Title 17, U.S. Code. The U.S. Government has a royalty-free license to exercise all rights under the copyright claimed herein for Governmental purposes. All other rights are reserved by the copyright owner.

\*Senior Research Scientist.

with diagonally-dominant relaxation procedures<sup>16</sup>. Different procedures are available to formulate these methods. Major differences are found in flux-vector splitting methods<sup>8-11</sup> and flux-difference splitting methods<sup>12,14-17</sup>. The larger dissipation errors in both inviscid and viscous calculations associated with flux-vector splitting methods have led to further implementations of flux-difference methods<sup>12,16</sup>. No major differences are observed between solutions of finite-volume and finite-difference procedures once convergence is achieved, although there are differences in the formulation and/or the location of the cell areas of the Jacobian matrix of the generalized coordinate transformation<sup>10,15,16</sup>.

Solutions based on first-order difference approximations contain too much numerical dissipation. Higher-order methods are formulated based on interpolation and/or extrapolation procedures of fluxes or dependent variables (MUSCL approach)<sup>11</sup>. Total variation diminishing schemes (TVD) are upwind or symmetric high-resolution schemes within smooth regions with first-order accuracy at local extrema<sup>10</sup>. The aim of adding the least amount of numerical dissipation over the physical dissipation to avoid spurious oscillations in shock regions is bounded by the need to obey the second law of thermodynamics and avoid entropy violations.

The present method represents an advance in the third generation of flux-difference splitting methods. It is based on the mathematical well-posed discrete-approximation of the Jacobian matrix of the flux-difference vectors.

### Governing Equations

The governing equations of motion are the 3-D compressible Reynolds-averaged Navier-Stokes and turbulence model equations for the conservation laws of mass, momentum, and energy of a perfect gas with mass-averaged and non-dimensional variables. The conservation laws are written in general curvilinear coordinates  $\xi_i(x_i)$  and compressed vector notation as

$$\frac{\partial}{\partial t} (J \vec{U}) + \frac{\partial}{\partial \xi_i} (J \xi_{ij} \vec{F}_j) = 0 \quad (1)$$

where repeated sub-indices in any term imply summation over the index range ( $j=1,2,3$ ); sub-index  $j$  following a comma imply partial differentiation with respect to the respective Cartesian spatial coordinate direction  $x_j$ ;  $J$  is the Jacobian of the spatial-coordinate transformation

$$J = \varepsilon_{ijn} \frac{\partial x_1}{\partial \xi_i} \frac{\partial x_2}{\partial \xi_j} \frac{\partial x_3}{\partial \xi_n} \quad (2)$$

and  $\varepsilon_{ijn}$  is the third-order isotropic alternating tensor.

The conservative dependent-variable vector  $\vec{U}$  and flux vectors  $\vec{F}_j$  are written in terms of non-dimensional mass-averaged variables.

$$\vec{U} = \begin{bmatrix} \rho \\ \rho u_1 \\ \rho u_2 \\ \rho u_3 \\ e \end{bmatrix}; \vec{F}_j = \begin{bmatrix} \rho u_j \\ \rho u_1 u_j + p \delta_{1j} \\ \rho u_2 u_j + p \delta_{2j} \\ \rho u_3 u_j + p \delta_{3j} \\ (e + p) u_j \end{bmatrix} + \begin{bmatrix} 0 \\ \tau_{1j} \\ \tau_{2j} \\ \tau_{3j} \\ -u_i \tau_{ij} - q_j \end{bmatrix} \quad (3)$$

where  $\rho$ ,  $p$  and  $T$  are the fluid density, pressure and temperature, respectively;  $u_i$  are the Cartesian velocity components;  $p = \rho T$  is the non-dimensional equation of state;  $e = p/(\gamma-1) + 0.5 \rho u_i u_i + \rho k$  is the total specific energy;  $k$  is the turbulent kinetic energy;  $\tau_{ij}$  is the stress tensor;  $q_j$  is the heat flux vector;  $\gamma$  is the ratio of specific heats at constant pressure and volume; and  $\delta_{ij}$  is the second-order isotropic Kronecker delta. The first term of the flux vectors  $\vec{F}_j$  in Eq. 3 represents the inviscid hyperbolic conservation law terms, and the second term represents the laminar and turbulent viscous stresses and heat fluxes.

The viscous stress tensor  $\tau_{ij}$  and the heat-flux vector  $q_j$  include both molecular and (Reynolds averaged) turbulent contributions. These variables are modeled using the Boussinesq approximation in terms of an eddy viscosity as

$$\tau_{ij} = 2(\mu + \mu_T)(S_{ij} - \delta_{ij} S_{nn}/3) - 2\rho k \delta_{ij}/3 \quad (4)$$

$$q_j = -\frac{\gamma}{\gamma-1} \left( \frac{\mu}{Pr} + \frac{\mu_T}{Pr_T} \right) T_j - \left( \mu + \frac{\mu_T}{Pr_k} \right) k_j \quad (5)$$

where  $\mu$  and  $\mu_T$  are the molecular and turbulent (eddy) viscosities,  $Pr = c_p \mu / \kappa$  and  $Pr_T = 0.9$  are the molecular and turbulent Prandtl numbers (assuming air),  $Pr_k$  is a turbulence model parameter,  $S_{ij} = (u_{ij} + u_{ji})/2$  is the strain rate tensor. Both last terms of Eq. 4 and Eq. 5 require the turbulent kinetic energy  $k$ , they are neglected in zero-equation turbulence models (for example, Baldwin-Lomax and Cebeci-Smith models), and usually included in two-equation turbulence models (for example,  $k$ - $\omega$  and  $k$ - $\varepsilon$  models).

### Two-Equation Eddy Viscosity Models

The turbulent eddy viscosity in two-equation models is here expressed in terms of the turbulent kinetic energy,  $k$ , and either the dissipation rate,  $\varepsilon$ , or the specific dissipation rate,  $\omega$ , depending on the model. This expression is

$$\mu_T = C_\mu f_\mu \rho k^2 / \varepsilon = C_\mu f_\mu \rho k / \omega \quad \varepsilon = \omega k \quad (6)$$

where  $C_\mu$  is a modeling constant, and  $f_\mu$  is a damping function depending on the specific model used.

The two transport equations are expressed in terms of the generic variables  $k$ - $\vartheta$  (where  $\vartheta = \varepsilon$  or  $\vartheta = \omega$  depending on the model) by the following formulas given below

$$\begin{aligned} \frac{\partial}{\partial t}(J\rho k) + \frac{\partial}{\partial \xi_i} \left( J\xi_{ij} \left( \rho k u_j - \left( \mu + \frac{\mu_T}{\sigma_k} \right) \frac{\partial k}{\partial x_j} \right) \right) &= S_k \\ \frac{\partial}{\partial t}(J\rho\vartheta) + \frac{\partial}{\partial \xi_i} \left( J\xi_{ij} \left( \rho\vartheta u_j - \left( \mu + \frac{\mu_T}{\sigma_\omega} \right) \frac{\partial \vartheta}{\partial x_j} \right) \right) &= S_\vartheta \end{aligned} \quad (7)$$

The source terms are defined as

$$S_k = P_k - \rho\omega k - L_k \quad (8)$$

$$S_\vartheta = (C_{\vartheta 1} P_k - f_2 C_{\vartheta 2} \rho\omega k + C_{\vartheta 3} \rho k S_{ij})(\vartheta/k) + L_\vartheta \quad (9)$$

and the production of turbulent kinetic energy is

$$P_k = 2\mu_T (S_{ij}S_{ij} - S_{ii}S_{jj}/3) - 2S_{ij}\rho k/3 \quad (10)$$

The model parameters for Wilcox  $k$ - $\omega$  model and Launder-Sharma  $k$ - $\varepsilon$  model are shown in the following Tables 1 and 2.

Table 1: Wilcox  $k$ - $\omega$  Model,  $\vartheta \equiv \omega = \varepsilon/k$

$C_{\omega 1} = 5/9$	$C_\mu = 0.09$	$f_\mu = f_2 = 1$
$C_{\omega 2} = 5/6$	$\sigma_k = \sigma_\omega = 2$	$L_k = L_\omega = 0$

Table 2: Launder-Sharma  $k$ - $\varepsilon$  Model,  $\vartheta \equiv \varepsilon = \omega k$

$C_{\varepsilon 1} = 1.45$	$f_\mu = \exp(-3.4/(1+R_T^2/50))$
$C_{\varepsilon 2} = 1.92$	$f_2 = 1 - 0.3\exp(-R_T^2)$
$\sigma_k = 1$	$L_k = 2\mu (\partial\sqrt{k}/\partial x_n)^2$
$\sigma_\varepsilon = 1.3$	$L_\varepsilon = 2(\mu\mu_T/\rho) (\partial^2 u/\partial x_n \partial x_n)^2$
$C_\mu = 0.09$	$R_T = \rho k^2/\mu\varepsilon$

At present, different turbulence models have been implemented in the numerical code for validation studies. These models include two-equation turbulence models<sup>19</sup> ( $k$ - $\omega$ , transitional  $k$ - $\omega$ , BSL, SST,  $k$ - $\varepsilon$ ) and the algebraic Baldwin-Lomax eddy viscosity model<sup>20</sup>. Compressibility corrections for the two-equation turbulence models have also been incorporated into the code<sup>1,19</sup>.

### Numerical Method

The present method is a model of the three-dimensional, implicit, flux-difference split upwind Navier-Stokes equations expressed in Favre-averaged variables and generalized curvilinear coordinates. It provides the capability of predicting complex flow structures in complex geometries with good accuracy.

This method combines the best features of data management and computational efficiency of space marching procedures with the generality and stability of time dependent Navier-Stokes procedures to solve flows with mixed subsonic and supersonic zones, including streamwise separated flows. Its robust stability derives from a combination of conservative implicit upwind flux difference

splitting, inner approximation procedure in grid cells where changes of eigenvalue sign are present, three-dimensional diagonally dominant approximate factorization and relaxation scheme, flux limiters of higher-order flux differences, and well-posed characteristic-based implicit boundary approximations.

The efficiency of the method is based on an implicit symmetric Gauss-Seidel "method of planes" relaxation scheme with alternating directional space marching sweeps along one coordinate direction, Newton-Raphson inner iteration procedure, together with an implicit block-tridiagonal diagonally dominant approximate factorization relaxation scheme along the other two directions. This method requires less data in central memory and less total transfer of data into central memory per iteration than implicit upwind schemes using only time-dependent approximate factorizations; therefore, the capability of processing larger and/or complex data bases and computational grids is available. The data is conveniently stored on successive planes along the streamwise coordinate, and the system of equations is solved twice in each successive plane along the forward direction, firstly, and along the backward direction, afterwards. The repeated solution procedure provides an effective Newton-Raphson convergence acceleration. In each plane the solution is obtained by a two level diagonally dominant approximate factorization DDADI procedure<sup>16</sup>. The space marching alternating directional sweeps in the streamwise coordinate are von Neumann unconditionally stable for zones of subsonic and streamwise separated and reversed flows as well as supersonic flow. Much as the more restrictive PNS techniques, the present space marching method results in improved propagation of nonlinear effects to accelerate convergence to steady state, generally in about one order of magnitude less iterations than two level linearized implicit methods. The method requires only a few 2-D cross-flow data planes in core at any marching step and thus with fast data transfer, such as is available on supercomputers, can efficiently treat complex problems requiring very large numbers of mesh points.

### Flux-Difference Jacobian Matrix $A$

All flux differences are treated implicitly in order to increase stability and to be able to use large increments of time or CFL numbers. The differentiation of each flux-difference term of the transport equations the inviscid along each curvilinear coordinate is defined as a product of a discrete Jacobian matrix  $A$  and the conservative dependent-variable vector  $\delta U$ ,

$$\delta F \equiv A \cdot \delta U \quad (10)$$

For simplicity, the vector notation and the sub-index  $j$  are omitted. The Jacobian matrix  $A$  is decomposed using a similarity transformation as

$$A = (MNT) \Lambda (MNT)^{-1} \quad (11)$$

where  $\Lambda$  is a diagonal matrix whose coefficients are the eigenvalues of the Jacobian matrix, and  $(MNT)$  is the column-eigenvector matrix of  $A$ . The  $M$  matrix represents the transformation between conservative and primitive variable differences. The matrix  $N$  represents the transformation between Cartesian and curvilinear coordinates. The matrix  $T$  represents the transformation between primitive and characteristic variable differences.

A major difference between most numerical methods is the definition of the coefficients of the Jacobian matrix  $A$ . All well-posed methods converge to the exact Jacobian  $\partial F/\partial U$  in the continuous space, however, they have truncation-error differences in the discrete space of finite-differences or finite-volume. In the discrete space, there are infinite number of matrices that obey the identity of Eq. 10. The general solution is obtained from

$$A = A_p + cA_h \quad (12)$$

the sum of a particular solution that obeys Eq. 10 and an homogeneous solution which may be multiplied by any factor  $c$ . A simple observation is one particular solution given by Roe's method<sup>12</sup>, another particular solution is the one shown below in the present method, and the difference between both of them is an homogeneous solution. The main difference between all these methods is not the identity of Eq. 10, but the differences in each coefficient of the Jacobian matrix  $A$ , furthermore, they represent different flux changes due to particular dependent variable differences. Mathematically, the best approximation is the one provided by the discrete representation of the partial derivative  $\partial F/\partial U$ , which is close to the one described below.

In the present method, the arithmetic averaging is used to define the matrix  $A$ . The conservation property of all flux-difference split methods requires the discrete identity

$$\delta(ab) \equiv \bar{b}\delta a + \bar{a}\delta b \quad (12)$$

between any two quantities  $a$  and  $b$ . The overbar represents a monotonous averaging procedure between two extreme quantities. In the present method, the overbar represents arithmetic averaging (in Roe's method,  $\bar{p}$  represents geometric averaging).

$$M = \begin{bmatrix} 1 & 0 & 0 & 0 & 0 \\ \bar{u}_1 & 1 & 0 & 0 & 0 \\ \bar{u}_2 & 0 & 1 & 0 & 0 \\ \bar{u}_3 & 0 & 0 & 1 & 0 \\ \bar{S}^2 & \bar{u}_1 & \bar{u}_2 & \bar{u}_3 & 1 \end{bmatrix}, M^{-1} = \begin{bmatrix} 1 & 0 & 0 & 0 & 0 \\ -\bar{u}_1 & 1 & 0 & 0 & 0 \\ -\bar{u}_2 & 0 & 1 & 0 & 0 \\ -\bar{u}_3 & 0 & 0 & 1 & 0 \\ \bar{u}_j\bar{u}_j - \bar{S}^2 & -\bar{u}_1 & -\bar{u}_2 & -\bar{u}_3 & 1 \end{bmatrix} \quad (13)$$

where  $\bar{S}^2 = \frac{\bar{u}_j\bar{u}_j}{2}$  and the primitive variable differences are defined as

$$M^{-1} \cdot \delta U = (\delta\rho, \bar{p}\delta u_1, \bar{p}\delta u_2, \bar{p}\delta u_3, \delta(p/(\gamma-1))) \quad (14)$$

The coordinate transformation matrices for the flux differences in the  $\xi$  coordinate direction are

$$N = \begin{bmatrix} 1 & 0 & 0 & 0 & 0 \\ 0 & \bar{x}_{1,\xi_2} & \bar{x}_{1,\xi_3} & \bar{\xi}_{1,1} & 0 \\ 0 & \bar{x}_{2,\xi_2} & \bar{x}_{2,\xi_3} & \bar{\xi}_{1,2} & 0 \\ 0 & \bar{x}_{3,\xi_2} & \bar{x}_{3,\xi_3} & \bar{\xi}_{1,3} & 0 \\ 0 & 0 & 0 & 0 & 1 \end{bmatrix}, N^{-1} = \begin{bmatrix} 1 & 0 & 0 & 0 & 0 \\ 0 & \bar{x}'_{1,\xi_2} & \bar{x}'_{2,\xi_2} & \bar{x}'_{3,\xi_2} & 0 \\ 0 & \bar{x}'_{1,\xi_3} & \bar{x}'_{2,\xi_3} & \bar{x}'_{3,\xi_3} & 0 \\ 0 & \bar{\xi}'_{1,1} & \bar{\xi}'_{1,2} & \bar{\xi}'_{1,3} & 0 \\ 0 & 0 & 0 & 0 & 1 \end{bmatrix} \quad (15)$$

where each vector is normalized as

$$\begin{aligned} \bar{\xi}'_{1,i} &= \bar{\xi}_{1,i} / \sqrt{\bar{\xi}_{1,i}\bar{\xi}_{1,i}} \\ \bar{x}'_{i,\xi} &= \bar{x}_{i,\xi} / \sqrt{\bar{x}_{i,\xi}\bar{x}_{i,\xi}} \end{aligned} \quad (16)$$

The  $\bar{x}$  symbol is used to denote the inverse matrix coefficients of the non-orthogonal matrices, i.e.,

$$\begin{aligned} \bar{x}_{1,2'} &= (\hat{x}_{1,2'} - \hat{x}_{1,3'}(\bar{x}_{1,2'}\bar{x}_{1,3'})) \cdot \left( \frac{|\bar{\xi}_2||\bar{\xi}_3|}{J|\bar{\xi}_1|} \right)^2 \\ \bar{x}_{1,2'} &= (\hat{x}_{1,2'} - \hat{x}_{1,3'}(\bar{x}_{1,2'}\bar{x}_{1,3'})) \left( 1 - (\bar{x}_{1,2'}\bar{x}_{1,3'})^2 \right) \end{aligned} \quad (17)$$

$$\bar{x}_{1,2'} = \left( \hat{x}_{2,3'}\bar{\xi}_{1,3} - \hat{x}_{3,3'}\bar{\xi}_{1,2} \right) \left( \frac{|\bar{\xi}_2||\bar{\xi}_3|}{J|\bar{\xi}_1|} \right)$$

which are all equivalent expressions.

$T$  is a transformation matrix between primitive and characteristic variables

$$T = \begin{bmatrix} -\bar{p} & 0 & 0 & \bar{p}/2 & \bar{p}/2 \\ 0 & 1 & 0 & 0 & 0 \\ 0 & 0 & 1 & 0 & 0 \\ 0 & 0 & 0 & \frac{\bar{p}\bar{c}'}{2} \left( 1 - \frac{\bar{d}}{\bar{c}} \right) & -\frac{\bar{p}\bar{c}'}{2} \left( 1 + \frac{\bar{d}}{\bar{c}} \right) \\ 0 & 0 & 0 & \frac{\bar{\gamma}\bar{p}}{2(\gamma-1)} & \frac{\bar{\gamma}\bar{p}}{2(\gamma-1)} \end{bmatrix} \quad (17)$$

$$T^{-1} = \begin{bmatrix} -1/\bar{p} & 0 & 0 & 0 & (\gamma-1)/\bar{\gamma}\bar{p} \\ 0 & 1 & 0 & 0 & 0 \\ 0 & 0 & 1 & 0 & 0 \\ 0 & 0 & 0 & \frac{1}{\bar{p}\bar{c}'} \frac{(\gamma-1)}{\bar{\gamma}\bar{p}} \left( 1 + \frac{\bar{d}}{\bar{c}} \right) \\ 0 & 0 & 0 & \frac{-1}{\bar{p}\bar{c}'} \frac{(\gamma-1)}{\bar{\gamma}\bar{p}} \left( 1 - \frac{\bar{d}}{\bar{c}} \right) \end{bmatrix} \quad (18)$$

and the characteristic variable differences (19) are

$$(MNT)^{-1} \cdot \delta U = \begin{pmatrix} -\frac{\delta p}{\bar{p}} + \frac{\delta p}{\gamma \bar{p}} \\ \bar{x}_{j, \xi_2} \bar{p} \delta \bar{u}_j \\ \bar{x}_{j, \xi_3} \bar{p} \delta \bar{u}_j \\ \frac{\xi_{1,j} \delta \bar{u}_j}{\bar{c}} + \left(1 + \frac{\bar{d}}{\bar{c}}\right) \frac{\delta p}{\gamma \bar{p}} \\ -\frac{\xi_{1,j} \delta \bar{u}_j}{\bar{c}} + \left(1 - \frac{\bar{d}}{\bar{c}}\right) \frac{\delta p}{\gamma \bar{p}} \end{pmatrix}$$

The diagonal coefficients of the eigenvalue matrix  $\Lambda$  are obtained from the solution of the characteristic equation of  $A$ . For the flux-differences in the  $\xi_1$  coordinate direction are

$$\begin{aligned} \lambda_1 &= \xi_{1,j} \bar{u}_j \\ \lambda_2 &= \lambda_3 = \xi_{1,j} \bar{p} \bar{u}_j / \bar{p} \\ \lambda_4 &= \lambda_5 = 0.5 (\lambda_1 + \lambda_2) + \bar{c} \end{aligned} \quad (20)$$

where

$$\bar{c} = \sqrt{\frac{\gamma \bar{p}}{\bar{p}} (\xi_{1,j} \xi_{1,j}) + \left(\frac{\lambda_1 - \lambda_2}{2}\right)^2} \quad (21)$$

### Flux-Difference Splitting

The split of the flux-difference terms follows the sign of their respective eigenvalues as follows

$$\delta_j F = \Delta_{j-0.5} F^+ + \Delta_{j+0.5} F^- \quad (22)$$

$$\Delta F^+ = A^+ \Delta U \quad (23)$$

$$\Delta F^- = A^- \Delta U \quad (24)$$

Unconditionally stable implicit methods are constructed by forward upwind flux differences with positive eigenvalues and backward flux differences with negative eigenvalues. Splitting of the convective terms of the two-equation turbulence models is also done according to the sign of the first eigenvalue shown in Eq. 20.

### Higher-Order TVD Fluxes

Spatial higher-order TVD flux-differences in the right-hand-side of the convective terms of the conservation law equations are defined by using a general “*minmod*” limiter. It is based on tests and generalization of the limiters proposed by Yee and Harten<sup>10</sup>, and Chakravarthy and Osher<sup>15</sup>.

The flux-limited finite-differences of the transport equations for the Navier-Stokes equations, Eq. 10, and for

the two-equation turbulence model equations, Eq. 7, are expressed as

$$\Delta_{j-0.5} F^+ = (1 - 0.5 (q_{j-0.5} - (q/r)_{j+0.5})^+) A^+ \Delta_{j-0.5} U \quad (25a)$$

$$\Delta_{j+0.5} F^- = (1 - 0.5 (q_{j+0.5} - (q/r)_{j-0.5})^-) A^- \Delta_{j+0.5} U \quad (25b)$$

This scheme is first-order if  $q=0$ , second-order central difference if  $q=1$ , and second-order upwind difference if  $q=r$ . The limiter functions are defined as a linear blending function of upwind differences ( $\phi=-1$ ) and central differences ( $\phi=1$ ) as

$$q^\pm = 0.5 [ (1+\phi) \Psi^\pm + (1-\phi) \zeta^\pm ] \quad (26)$$

$$\text{with } r_{j+0.5}^+ = \max\{0, \Delta_{j-0.5} F^+ / \Delta_{j+0.5} F^+\} \quad (27)$$

$$r_{j-0.5}^- = \max\{0, \Delta_{j+0.5} F^- / \Delta_{j-0.5} F^-\} \quad (28)$$

where  $\Psi$  and  $\zeta$  are the flux-limiter functions of the central and upwind differences, respectively. For a second-order upwind scheme

$$r^\pm \zeta^\pm = \max\{\minmod\{1, (1+a)r^\pm\}, \minmod\{r^\pm, 1+b\}\} \quad (29)$$

with  $0 \leq (a,b) \leq 1$ . This limiter becomes Yee's symmetric limiter when  $a=b=0$ , Roe's Superbee when  $a=b=1$ , and Osher-Chakravarthy limiter when  $a=0$  and  $0 \leq b \leq 1$ . To avoid entropy violations the factor  $b$  is limited to  $0 \leq b \leq 0.5$ , otherwise, violations such as overprediction of Mach numbers in shock waves may be predicted (Superbee). The end result of the flux limiters on the second-order TVD upwind scheme is a first-order flux-difference with a factor bounded between 0.5 and 1.5.

Other limiters implemented into the code are the continuous van Leer function<sup>11</sup>

$$r^\pm \zeta^\pm = (r^\pm + |r^\pm|)(1 + |r^\pm|) \quad (30)$$

and Yee's symmetric limiters<sup>10</sup>

$$r^\pm \zeta^\pm = \minmod\{1, r^\pm, r^\mp\} \quad (31)$$

$$r^\pm \zeta^\pm = \minmod\{1, r^\pm\} + \minmod\{1, r^\mp\} - 1 \quad (32)$$

$$r^\pm \zeta^\pm = \minmod\{1, r^\pm, r^\mp, 0.5(r^\pm + r^\mp)\} \quad (33)$$

In all these limiters, the “*minmod*” function is defined as the minimum magnitude between positive or negative arguments

$$\minmod(a, b) = \text{sign}(a) \cdot \max[0, \min\{|a|, b \cdot \text{sign}(a)\}] \quad (34)$$

and returns a value of zero if the product  $ab \leq 0$ .

## **Relaxation two-factor DDADI**

The numerical method is based on an implicit “method of planes” symmetric Gauss-Seidel relaxation scheme. The data is conveniently stored on successive planes along the streamwise coordinate, and the system of equations is solved in each successive plane along the forward direction, first, and along the backward direction, afterwards. In unseparated supersonic and hypersonic flows, the system of equations may be solved along the forward direction only. In each plane, the solution is obtained by using a two-level pseudo-time-dependent relaxation procedure based on a diagonally dominant approximate factorization DDADI. The space marching method results in improved propagation of nonlinear effects to accelerate convergence to steady state, much as do the more restrictive PNS techniques.

The diagonal dominant approximate factorization of the left-hand-side of the transport equations including the implicit viscous-diffusion terms leads to the following two-factor block tridiagonal equation sequence for the  $\xi_1$  plane relaxation method

$$[-(A_{\xi_2})^+, D, (A_{\xi_2})^-] \cdot \delta U^* = -RHS^{n,n+1} \quad (35)$$

$$[-(A_{\xi_3})^+, D, (A_{\xi_3})^-] \cdot \delta U = -D \cdot \delta U^* \quad (36)$$

The diagonally dominant matrix  $D$  involves the first-order split Jacobian matrices and the Jacobian matrices of the viscous terms of all coordinate directions

$$D = I + (A_{\xi_1} + A_{\xi_2} + A_{\xi_3})^+ - (A_{\xi_1} + A_{\xi_2} + A_{\xi_3})^- \quad (37)$$

and the solution is updated from time step  $n$  to time step  $n+1$

$$U^{n+1} = U^n + \delta U^n \quad (38)$$

Observe that the  $RHS$  of equation 35 has an exponent  $n, n+1$  because some terms in the streamwise direction are already updated at time step  $n+1$  due to the plane relaxation procedure. A Newton-Raphson acceleration procedure is obtained by solving each plane twice or more times in each relaxation sequence. This procedure updates the nonlinear coefficients of the Jacobian matrix  $A$  and produces significant improvement in the propagation of the nonlinear waves.

## **Boundary Conditions**

Mathematically well posed implicit boundary point procedures are imposed in every boundary plane. The

characteristic-based numerical procedure imposes implicit boundary conditions, the code automatically determines appropriate numerical boundary approximations based on the input parameters of the 3-D program and whether the flux-difference splitting indicates that the information is propagated from the boundary toward the interior domain. If the inflow is supersonic, the equilibrium turbulent boundary layer is prescribed. If the inflow is subsonic, no variation of entropy, enthalpy, and tangential velocity are imposed. If the outflow is supersonic, the solution is computed naturally with the upwind scheme without imposed external boundary conditions. If the outflow is subsonic, one characteristic-based boundary approximation is required and no pressure variation is imposed in the differences toward the boundary. At inflow/outflow boundary points, finite difference is done both along and toward the boundary, the procedure automatically determines whether the fluid is locally flowing inside or outside off the boundary and imposes appropriate conditions accordingly. On cooled walls, prescribed wall temperature and no slip conditions are imposed; the turbulent kinetic energy  $k$  and its dissipation rate  $\epsilon$  are set equal to zero;  $\omega$  is set equal to its theoretical value at each first point off the wall boundary and equal to 10 times that value at each boundary point. On symmetry planes, no flow through and zero-gradient extrapolation of density, pressure, streamwise velocity, and turbulence variables are imposed. These boundary approximations have been proven to be effective in previous simulations and free stream has been effectively maintained<sup>3</sup>.

## **Numerical Convergence**

All simulations were done in the Cray C-90 at NASA Ames Research center.

In the following numerical convergence cases, the free stream is assumed to be air obeying the perfect gas law with effective specific heat ratio 1.4, molecular Prandtl number 0.72, turbulent Prandtl number 0.9. The laminar viscosity is specified by using Sutherland's law.

Fig. 1 shows the comparison of the convergence given by the energy residuals between the CNS code<sup>21</sup> and the present code in the numerical simulation of a free-stream flow and an adiabatic flat plate flow at Mach 4 and Reynolds number of  $6 \cdot 10^5$ . Convergence to machine accuracy is achieved within one order of magnitude of less iterations with the new method.

Fig. 2 shows the convergence history of the energy residual in the present code for three different flows, a Mach 4 and Reynolds number  $6 \cdot 10^6$  free-stream flow, a Mach 5 and Reynolds number  $2.2 \cdot 10^7$  adiabatic flat plate flow, and a Mach 8 and Reynolds number  $5 \cdot 10^6$  cooled flat

plate flow with  $T_w/T_{aw}=0.3$ . Convergence is achieved within 30 sweeps in the first two cases and within 100 sweeps in the last case.

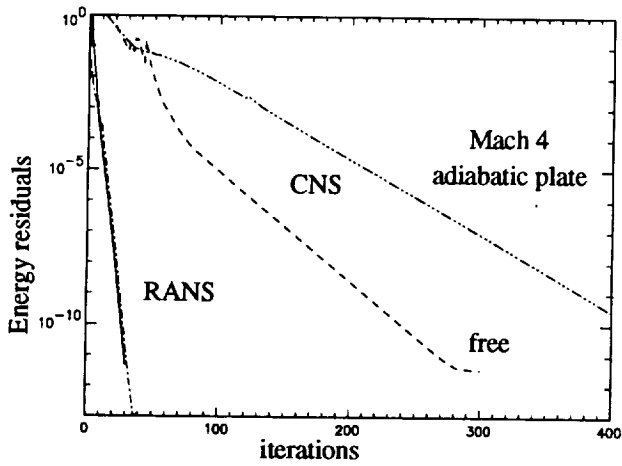


Fig. 1. Comparison of energy residual history between CNS code and new RANS code.

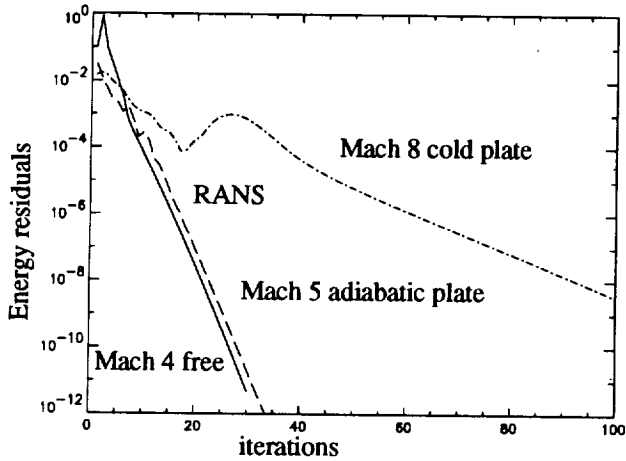


Fig. 2. Energy residual history of new RANS code.

### Mach 5 Adiabatic Flat Plate

The mean flow conditions of this flow on the adiabatic flat plate are Mach 5 and Reynolds number of  $2.2 \cdot 10^7$  per unit length. Fig. 3a shows the comparison of compressible skin friction and Reynolds number based on momentum thickness with the experimental correlation of van Driest II. The predictions with the  $k-\omega$  and the modified  $k-\omega$  models agree with the theoretical correlation. Fig. 3b shows the comparison of the velocity profile at  $Re_\theta=10^4$  with the numerical results of Coakley et al<sup>19</sup> obtained with

a well proven 2-D finite-volume flux-difference splitting Navier-Stokes code.

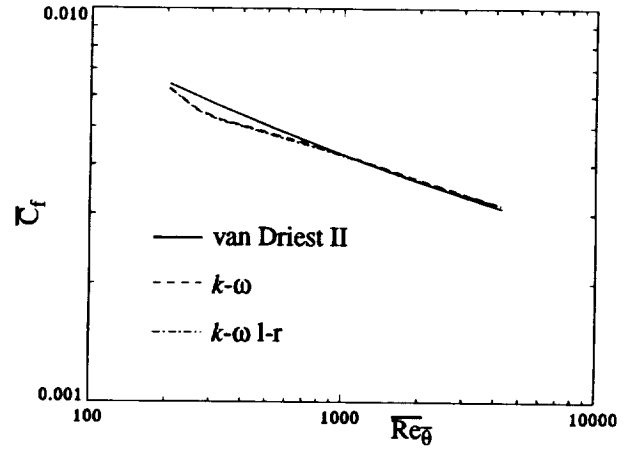


Fig. 3a. Skin friction on adiabatic flat plate with free-stream Mach number 5 and Reynolds number  $2.2 \cdot 10^7$ .

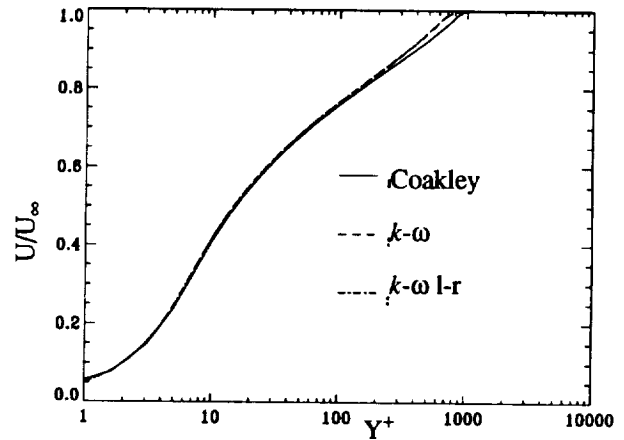


Fig. 3b. Comparison of velocity profile on flat plate.

### Mach 8 Inviscid Shock Reflection

The inviscid shock reflection of a Mach 8 flow is used here to test the flux limiters described in Eq. 29. Several simulations were run to machine convergence of residuals down to  $10^{-14}$ . Fig. 4a and 4b show the Mach number plotted as a surface plot on the reflection plane of a  $30^\circ$  shock wave, the upper surface correspond to the free stream Mach 8, the other two lower surfaces correspond to the Mach number levels after the incident shock and reflected shock, respectively. The main objective is to test the least

diffusive flux limiter (Superbee) and to check the amount of numerical dissipation needed to avoid entropy violations.

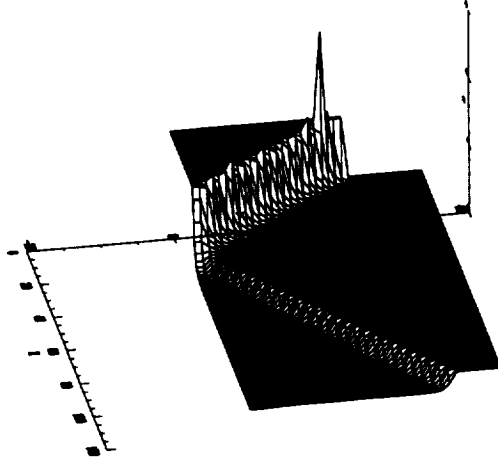


Fig. 4a. Mach number with  $a=1$  and  $b=1$  in Eq. 29.

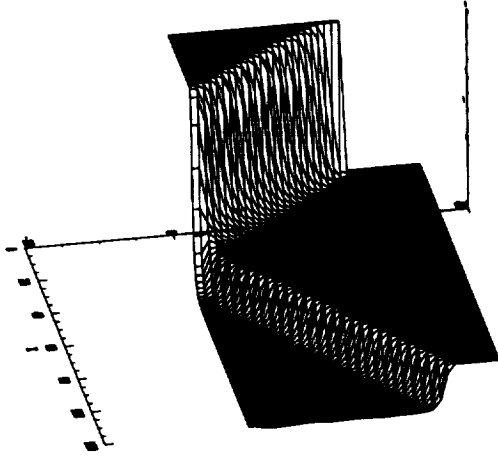


Fig. 4b. Mach number with  $a=1$  and  $b=0.5$  in Eq. 29.

The results with the least diffusive Superbee scheme shown in Fig. 4a develops local Mach number peaks upstream of the incident shock wave. If the amount of second-order central-difference is increased, as it is shown in Fig. 4b, these local peaks vanish and the solution is smooth. The test show that  $b$  should be no larger than 0.5 in Eq. 29, otherwise entropy violations will occur. This effect is very important in turbulent flows because the model variables,  $k$  and  $\omega$  or  $\epsilon$ , also develop strong fluctuations in the presence of local Mach number peaks. This is an effect observed in 3-D simulations of inlets.

#### Mach 2.84 24° Compression Corner

The experimental data on the separated turbulent boundary layer of Settles et al<sup>22,23</sup> on a 24° compression corner with a free-stream Mach number of 2.84 is com-

pared with numerical results obtained with the present method and the  $k-\omega$  turbulence model.

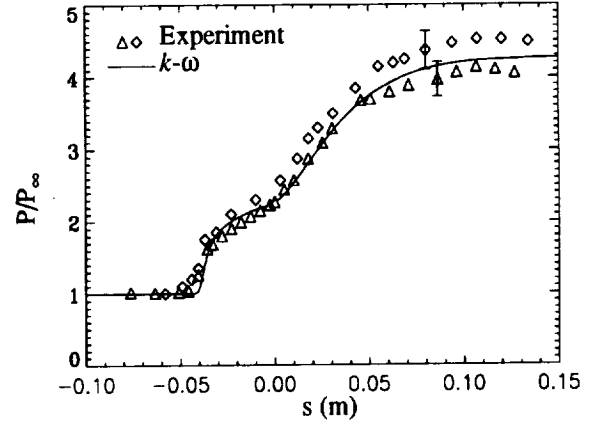


Fig. 5a. Comparison of surface pressure on 24° compression corner flow with free-stream Mach number 2.84.

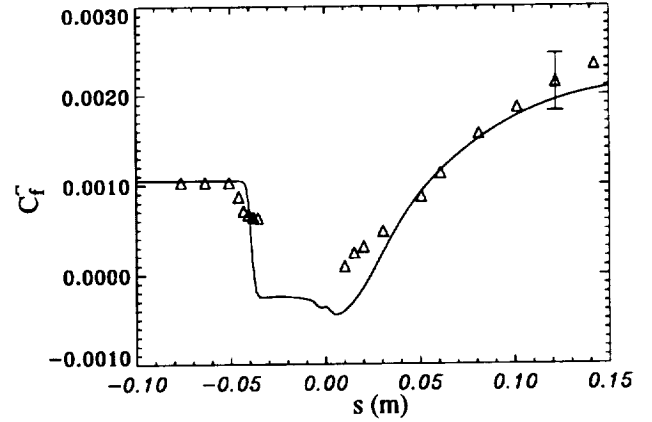


Fig. 5b. Skin friction comparison.

The agreement between the numerical results and the experimental data is very good with small underprediction of separation due to the turbulence model.

#### Mach 8.3 Intersecting Shock-Waves/Turbulent Boundary Layer Interaction

Figs. 6 show the comparison of a complex 3-D intersecting shock-waves/turbulent boundary layer interaction flow with free stream Mach number 8.3, free stream Reynolds number  $5 \cdot 10^6$ , and wall temperature 0.3 times the adiabatic wall temperature. The experimental data of Kusoy et al<sup>24</sup> belongs to the compressible database developed for model validation<sup>22</sup>. The experiment consists of a turbulent boundary layer on a flat plate with two 15° fins generating two oblique shocks with cross-flow separation within the boundary layer and a very complex vortex

interaction. Figs. 6a and 6b show the surface pressure and the heat transfer profiles, respectively, on the flat plate along the symmetry plane between the two fins. Fig. 6c and 6d show the surface pressure and heat transfer profiles on a crossed plane 7 boundary layer thicknesses downstream of the fin edges. The numerical predictions obtained with different two-equation turbulence models and the algebraic Baldwin-Lomax eddy viscosity model are compared with experimental data showing excellent agreement with experimental data.

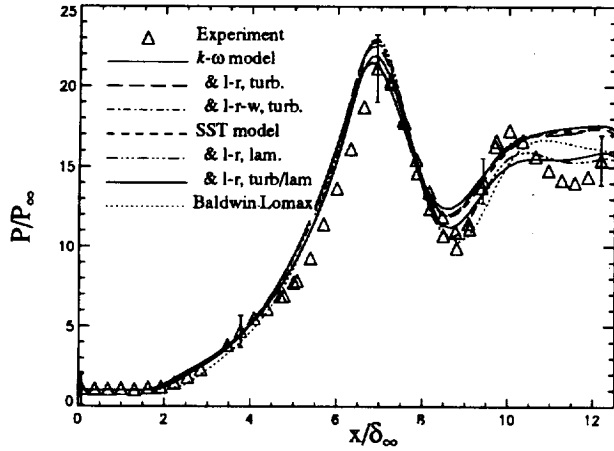


Fig. 6a. Normalized pressure distribution on center-line plane,  $z/\delta_\infty = 0$  and  $y/\delta_\infty = 0$ .

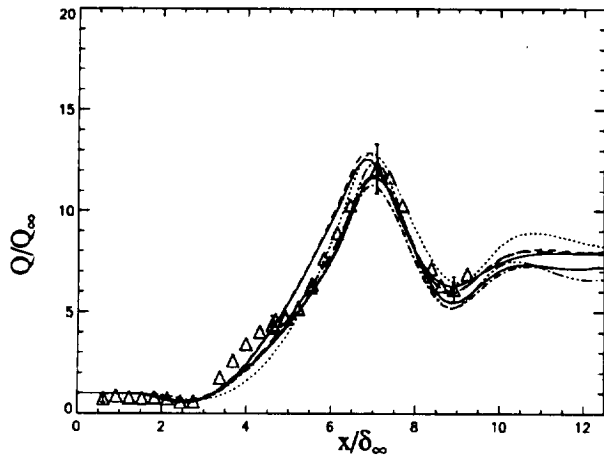


Fig. 6b. Surface heat transfer distribution on center-line plane,  $z/\delta_\infty = 0$  and  $y/\delta_\infty = 0$ .

The centerline profiles show an increase in surface pressure and heat transfer in the collision zone between the cross-flow vortices generated under the oblique shock waves. Peak values are obtained in the reattachment zone behind the collision zone. Lateral expansion waves

decrease the magnitude of the profiles, and a wave structure develops due to the intersecting shocks.

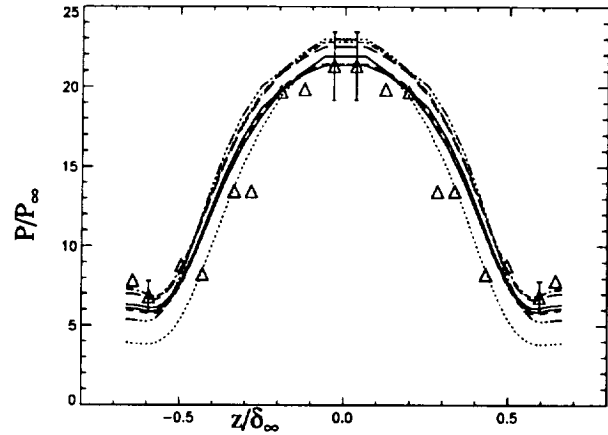


Fig. 6c. Normalized pressure distribution on cross-section plane located at  $x/\delta_\infty = 6.92$  and  $y/\delta_\infty = 0$ .

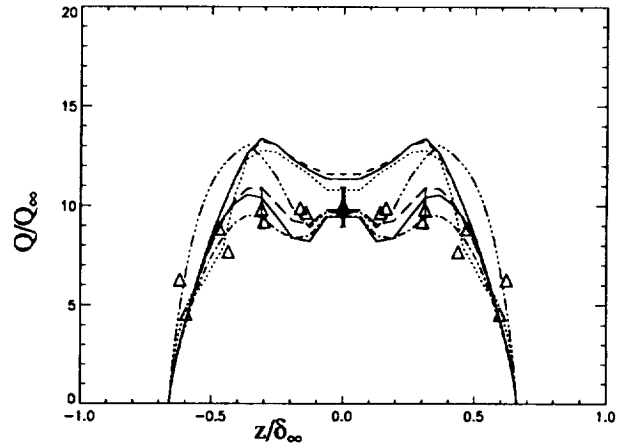


Fig. 6d. Surface heat transfer distribution on cross-section plane located at  $x/\delta_\infty = 6.4$  and  $y/\delta_\infty = 0$ .

### Concluding Remarks

Accurate and efficient aerodynamic numerical simulations have been presented. The results show the robustness and stability of the 3-D method and code including different two-equation turbulence models. Validation is shown with predictions of turbulent flows on a Mach 5 adiabatic flat plate, Mach 3 compression corner, and 3-D Mach 8 intersecting shock-waves/turbulent boundary layer interaction. The results are in quite good agreement with a well validated 2-D code, correlations, and experiment.

The present results show that numerical solutions of turbulent high speed flows can be efficiently obtained in order to provide a data set for engineering design. The flow structures are generally well captured within a few

grid points and are free of oscillations, especially the oblique shocks, as well as, the expansion and compression waves in the different complex flow zones. This method provides a promising computational capability to simulate turbulent flows in complex flow fields of aerospace vehicles.

### **Acknowledgments**

This work is sponsored by NASA Ames Research Center, Modeling and Experimental Validation Branch, under Grant NCC 2-15. The author wishes to acknowledge helpful discussions on numerical methods and turbulence models with T.J.Coakley, J.G. Marvin, and P.G. Huang.

### **References**

1. Bardina, J.E., and Coakley, T.J. "Three-Dimensional Navier-Stokes Simulations with Two-Equation Turbulence Models of Intersecting Shock-Waves/Turbulent Boundary Layer at Mach 8.3," *AIAA-94-1905*, Colorado Springs, CO, June, 1994.
2. Bardina, J.E., Coakley, T.J., and Marvin, J.G., "Two-Equation Turbulence Modeling for 3-D Hypersonic Flows," *AIAA-92-5064*, Orlando, FL, December, 1992.
3. Marvin, J.G., "A CFD Validation Roadmap for Hypersonic Flows," published in AGARD-CP-514, *Theoretical and Experimental Methods in Hypersonic Flows*, Reference 17, 1993.
4. McCormack, R.W., "The Effect of Viscosity in Hypervelocity Impact Cratering," *AIAA-69-354*, 1969.
5. Beam, R.M. and Warming, R.F., "An Implicit Factored Scheme for the Compressible Navier-Stokes Equations," *AIAA J.*, Vol. 16, No. 4, 1978, pp. 393-402.
6. Briley, W.R., and McDonald, H., "Solution of the Multi-dimensional Compressible Navier-Stokes Equations by a Generalized Implicit Method," *J. of Comp. Physics*, Vol. 24, No. 4, 1977, pp.372-397.
7. Steger, J.L., and Warming, R.F., "Flux-Vector Splitting of the Inviscid Gasdynamics Equations with Application to Finite-Difference Methods," *J. of Comp. Physics*, Vol. 40., No. 2, 1981, pp. 263-293.
8. van Leer, B., "Flux-Vector Splitting for the Euler Equations," *Lecture Notes in Physics*, Vol. 170, 1982.
9. van Leer, B., Thomas, J.L., Roe, P.L., and Newsome, R.W., "A Comparison of Numerical Flux Formulas for the Euler and Navier-Stokes Equations," *AIAA-87-1104*, 1987.
10. Yee, H.C., and Harten, A., "Implicit TVD Schemes for Hyperbolic Conservations in Curvilinear Coordinates," *AIAA J.*, Vol. 25, No. 2, 1987, pp. 266-274.
11. van Leer, B., "Flux Vector Splitting for the 1990's," Invited Lecture, *CFD Symposium on Aeropropulsion*, Cleveland, Ohio, 1990.
12. Roe, P.L., "Characteristic-Based Schemes for the Euler Equations," *Ann. Rev. of Fluid Mech.*, Vol. 18, 1986, pp. 337-365.
13. Harten, A., "High Resolution Schemes for Hyperbolic Conservation Laws," *J. Comp. Physics*, Vol 49, 1983, pp. 363.
14. Chakravarthy, S. R., "Relaxation Methods for Unfactored Implicit Upwind Schemes," *AIAA 84-0165*, 1984.
15. Chakravarthy, S. R., and Osher, S., "A new Class of High Accuracy TVD Scheme for Hyperbolic Conservation Laws," *AIAA-85-0363*, 1985.
16. Bardina, Jorge and Lombard, C.K.: "Three Dimensional CSCM Method for the Compressible Navier-Stokes Equations with Application to a Multi-Nozzle Exhaust Flowfield," *AIAA-85-1193*, 1985.
17. Lombard, C.K., Bardina, J., Venkatapathy, E., and Olinger, J., "Multi-Dimensional Formulation of CSCM - An Upwind Flux Difference Eigenvector Split Method for the Compressible Navier-Stokes Equations," *AIAA-83-1895*, 1983.
18. Bardina, J., Venkatapathy, E., and Lombard, C.K., "Two Dimensional and Axisymmetric Heat Transfer Results with the CSCM-S Upwind Implicit Algorithm," published in *Thermophysical Aspects of Re-entry Flows*, ed. by J.N. Moss and C.D. Scott, Vol. 103 of Progress in Astronautics and Aeronautics Series, AIAA, 1986.
19. Coakley, T.J., and Huang, P.G., "Turbulence Modeling for High Speed Flows," *AIAA-92-0436*, 1992.
20. Baldwin, B.S., and Lomax, H., "Thin Layer Approximation and Algebraic Model for Separated Turbulent Flows," *AIAA-73-257*, 1973.
21. Ryan, J.S., Flores, J., and Chow, C.Y., "Development and validation of CNS (Compressible Navier-Stokes) for Hypersonic Applications," *AIAA-89-1839*, Buffalo, NY, June, 1989.
22. Settles, G.S., and Dodson, L.J., "Hypersonic Shock/Boundary Layer Interaction Database," *NASA CR 177577*, April, 1991.
23. Settles, G.S., Gilbert, R.B., and Bogdonoff, S.M., "Data Compilation for Shock Wave/Turbulent Boundary layer Interaction Experiments on Two-Dimensional Compression Corners," *Princeton University report 1489-MAE*, Princeton Univ., 1980.
24. Kussoy, M.I., and Horstman, K.C., "Intersecting Shock-Wave/Turbulent Boundary Layer Interactions at mach 8.3," *NASA TM 103909*, 1992.



